2011

Quantification of Model-Form, Predictive, and Parametric Uncertainties in Simulation-Based Design

Matthew E. Riley
Wright State University

Quantification of Model-Form, Predictive, and Parametric Uncertainties in Simulation-Based Design

A dissertation submitted in partial fulfillment of the
requirement for the degree of
Doctor of Philosophy

By

MATTHEW E. RILEY
B.S., Wright State University, Dayton, OH, 2007

2011
Wright State University

WRIGHT STATE UNIVERSITY

WRIGHT STATE GRADUATE SCHOOL

July 19, 2011

I HEREBY RECOMMEND THAT THE DISSERTATION PREPARED UNDER MY SUPERVISION BY **Matthew E. Riley** ENTITLED **Quantification of Model-Form, Predictive, and Parametric Uncertainties in Simulation-Based Design** BE ACCEPTED IN PARTIAL FULFILLMENT OF THE REQUIREMENTS FOR THE DEGREE OF **Doctor of Philosophy**.

_____
Ramana V. Grandhi, Ph.D.
Dissertation Director

_____
Ramana V. Grandhi, Ph.D.
Director, Ph.D. in Engineering Program

Committee on Final Examination:

_____
Andrew Hsu, Ph.D.
Dean of Graduate School

_____
Ramana V. Grandhi, Ph.D.

_____
Erwin Johnson, Ph.D.

_____
Raymond Kolonay, Ph.D.

_____
Donald Kunz, Ph.D.

_____
Ravi Penmetsa, Ph.D.

_____
Joseph Slater, Ph.D.

ABSTRACT

Riley, Matthew E. Ph.D. College of Engineering and Computer Science, Wright State University, 2011. Quantification of Model-Form, Predictive, and Parametric Uncertainties in Simulation-Based Design.

Traditional uncertainty quantification techniques in simulation-based analysis and design focus upon on the quantification of parametric uncertainties—inherent natural variations of the input variables. This is done by developing a representation of the uncertainties in the parameters and then efficiently propagating this information through the modeling process to develop distributions or metrics regarding the output responses of interest. However, in problems with complex or newer modeling methodologies, the variabilities induced by the modeling process itself—known collectively as model-form and predictive uncertainty—can become a significant, if not greater source of uncertainty to the problem. As such, for efficient and accurate uncertainty measurements, it is necessary to consider the effects of these two additional forms of uncertainty along with the inherent parametric uncertainty. However, current methods utilized for parametric uncertainty quantification are not necessarily viable or applicable to quantify model-form or predictive uncertainties. Additionally, the quantification of these two additional forms of uncertainty can require the introduction of additional data into the problem—such as experimental data—which might not be available for particular designs and configurations, especially in the early design-stage. As such, methods must be developed for the efficient quantification of uncertainties from all sources, as well as from all permutations of sources to handle problems where a full array of input data is unavailable. This work develops and applies methods for the quantification of these uncertainties with specific application to the simulation-based analysis of aeroelastic structures.

TABLE OF CONTENTS

List of Figures:

List of Tables:

Acknowledgements

I would like to thank my advisor Dr. Ramana V. Grandhi for his help and guidance in my graduate career. I would also like to thank my committee members Ravi Penmetsa, Joseph Slater, Ray Kolonay, Donald Kunz, and Erwin Johnson for their valuable feedback and input on my work. Additionally, I would like to extend my thanks to the sponsor of this work: the Dayton Area Graduate Studies Institute fellowship program and the United States Air Force through contract FA8650-09-2-3938, Collaborative Center for Multidisciplinary Sciences.

Additionally, I would like to thank fellow students and researchers in CEPRO for their help, advice, criticism, and feedback throughout my research career, as well as sitting through my numerous presentations and short courses. I would also like to extend a special thanks to my family and friends for the encouragement and support they provided me along the way.

1. Introduction

The simulation-based design of air vehicles is a complex process that draws upon approaches and models across many disciplines to create an efficient and robust design. To design a vehicle capable of stable, efficient, and reliable flight, contributions from multiple disciplines such as structures, aerodynamics, controls, propulsion, and materials must be analyzed concurrently and the coupling among each discipline must be carefully examined. Due to the high cost of full-scale simulation and testing at the conceptual design phase of a vehicle, where hundreds to thousands of configurations are analyzed concurrently, these analyses are done through the construction of computational or simulation models that capture the relative physics driving the design within each discipline. However, multiple uncertainties arise from this modeling process that must be considered to develop a robust and efficient design of these air vehicles.

As a result of the uncertainty that exists in the simulation-based design and analysis of air vehicles, the safety of the aircraft being designed can sometimes come into question. As there are so many uncertain aspects to the design problem, there exists concurrent uncertainty in the performance of the aircraft within its flight regime. To account for this uncertainty, safety factors are often used in the design process as a

pseudo-heuristic method for accounting for potential variance in the parameters of the system (1). These safety factors—the values of which are set by the Federal Aviation Administration (FAA)—apply adjustments to the expected loads and conditions experienced by the aircraft. These safety factors will often result in an over-conservative design due to the deterministic measure in which they are applied (2).

Due to the adverse effects of this conservative design methodology, there has been much research in the past 30 years at looking into replacing the use of safety factors in aircraft design with probabilistic methods of analysis (2-4). This research intends to no longer handle the uncertainty in the aircraft design problem through deterministic measures, such as safety factors, but to instead utilize stochastic measures to be able to accurately quantify system reliability and performance. The approaches and definitions used to handle this uncertainty in such a way will be introduced and discussed in further detail in Chapters 4 and 5. The ultimate aim of these new approaches is to be able to represent the potential variability in the aircraft design problem through stochastic measures such as system reliabilities, or in the best possible case, full probability distribution functions that represent the variability in a systems performance metrics as a result of the natural variability of the problem as well as the uncertainty in the modeling of the problem itself.

Representing the response of an air vehicle stochastically will allow for risk-quantified design in which the reliability of the system can be calculated given the

variability of the system. By being able to first quantify this reliability, it can then be used as an additional design metric. That is to say, aircraft can then be designed with a desired performance reliability in mind, rather than by simply applying larger safety factors in order to achieve a purported higher reliability. There are two beneficial results from a design method of this sort. The first, and perhaps most important result, is that the reliability of the aircraft will be quantified in the design process. As a result, the reliability of the system will be known--meaning that the safety of the aircraft will also be known. This will result in the design of safer air vehicles by considering reliability measures during the design process, rather than through deterministic safety factors. The second benefit is that the result of a stochastic design is often more efficient than one using safety factors (2, 52). As was mentioned before, safety factors can often result in over-conservative designs that contain extra weight or other components that are redundant or unnecessary. This is because the safety factors are applied uniformly across the design, even in areas that are not as sensitive to variations within the design. A stochastic approach, on the other hand, will only add additional components or weight in areas that would beneficial to the performance of the design. As a result, the designs produced through a stochastic approach often are much more efficient than those that are produced when large safety factors are used for the design process (4, 52).

As detailed in Chapters 4 and 5, traditional stochastic focus primarily upon quantifying the uncertainty in input parameters to a model and propagating that

uncertainty through the analysis to develop a stochastic representation of the output response of interest. Approaches in this field have matured to the point that this stochastic representation is very accurate and can be achieved at an acceptable computational cost for most problems. However, a caveat to this approach is that it ignores two large sources of uncertainty in the computational modeling and simulation of aeroelastic phenomena: model-form and predictive uncertainty.

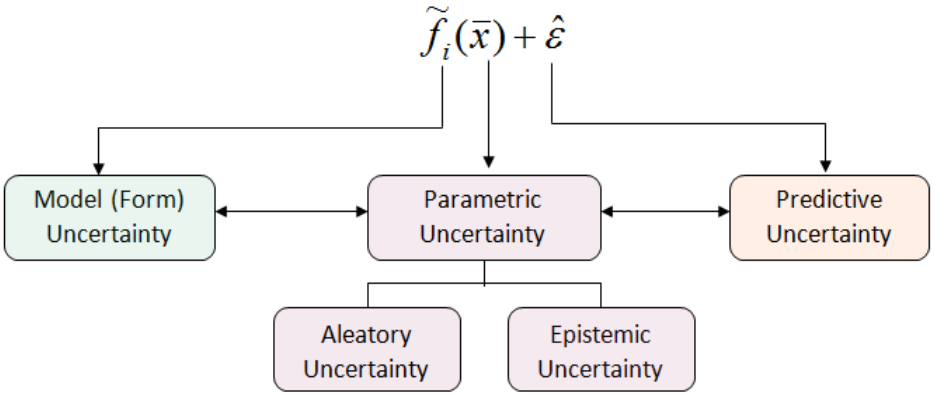

Figure 1.1: Complete Uncertainty Breakdown

These two other forms of uncertainty, shown in Figure 1.1, are related to the uncertainties that result from the modeling process itself. The formal definitions of these types of uncertainty are introduced in Chapter 4. However, in short, model-form uncertainty is the uncertainty that arises in the selection of the proper or most accurate model to use in the evaluation of the output response of interest. This uncertainty could refer to the selection of the proper fidelity of model or modeling assumptions—such as linear, quasi-linear, or non-linear assumptions—or the selection of model forms

or boundary conditions—such as full span or semi-span models used to calculate the flutter velocity of a wing design. The predictive uncertainty associated with a model, is the discrepancy between the model's prediction of the output response of interest and the actual physical value for the output. In short, predictive uncertainty can be thought to be related directly to the accuracy of a model. The more representative that a model is of the true physical scenario of interest, the smaller its predictive uncertainty will be. This predictive uncertainty that exists with a model is directly related to the assumptions that are made in the formation of the model itself, and can only be quantified if a representation of the true physical scenario, such as experimental data is available.

In the aeroelastic literature, the predictive uncertainty associated with a model is commonly only considered during the construction of a model, through a process referred to as verification and validation (76). The verification and validation process is often an intrusive process that tweaks and adjusts model parameters to reduce the predictive uncertainty of a model at a series of parameters—the benchmark validation cases. Once a model is deemed to have been reduced to an acceptable level for the validation cases used, the model is considered validated. After a model is considered validated, the predictive uncertainty associated with the model is often either ignored—with the assumption that the verification and validation process has reduced said uncertainty to an acceptable level—or is handled with a deterministic correction factor, analogous to a safety factor. For problems with parameters near the benchmark

validation cases, this method is often sufficient. However, since the benchmark validation cases used in the verification and validation process are often unable to encompass the entire potential design space, at parameter values further from the benchmark cases the predictive uncertainty inherent to a model can become significant and should be quantified in order to present a complete representation of the uncertainty in the modeling process.

Model-form uncertainty is currently seldom considered in aeroelastic design and analyses. Often, a best model is selected and used for the simulation process without 100% certainty that it is the best choice among the model set that can be considered. This approach ignores the possibility that at the given data set, or at different sets of parameters, that the model selected is not the “best” model among the model set that could be considered.

To address the uncertainty that arises from multiple sources in the aeroelastic modeling process, numerous approaches must be developed and implemented to accurately and efficiently quantify the uncertainty. In an ideal case, given the availability of the distributions of the uncertain parameters, all possible modeling choices are available and feasible, and experimental data points are available and plentiful at numerous design points, the uncertainty from all three sources can be efficiently quantified (Section 5.1.2). However, for many cases, the ideal case cannot be met and portions of the complete data approach are unavailable. A classic example of

this lack of available information occurs in the early design stage of a configuration. At this stage of design, multiple configurations of parameters are to be evaluated concurrently and experimental data for most, if not all of these parameters is unavailable. In the absence of any experimental data, the predictive uncertainty associated with each model cannot be quantified. Instead, one can only hope to quantify the parametric and model-form uncertainty associated with the design. As this process occurs in the early design stage where multiple configurations are analyzed concurrently, this evaluation of uncertainty must be done quickly and efficiently, without the necessity of numerous cost-intensive computational simulations. As such, it would be beneficial to have an approach that could efficiently quantify the model-form and parametric uncertainties in a design without the necessity for experimental data.

Once this initial model-form and parametric uncertainty has been quantified, the next step would be to determine whether it was reducible through either the introduction of additional data, or the improvement of some of the models. If the time, money, and effort were to be expended to obtain experimental results to validate configurations or models, one would want to ensure that the addition of this data could provide a certain level of reduction in the uncertainty in the prediction of the output response. Additionally, one must have a method to integrate all of this information together efficiently to quantify all three forms of uncertainty concurrently to give a complete representation of the variability in the predictions from the computational model.

This work develops, adapts, and implements numerous uncertainty quantification approaches for the aeroelastic design problem for all possible information configurations—from simple model-form uncertainty quantification to the quantification of model-form, predictive, and parametric uncertainties concurrently within an analysis framework. These uncertainty quantification techniques are coupled with advanced and novel surrogate modeling techniques to reduce the computational time required for the multiple model evaluations required. The key contributions and novel methods developed in this work are detailed below:

1. A Weighted Stack Response Surface Method (w-StackRSM) was developed and validated against the traditional least-squares response surface method. The w-StackRSM method utilizes *k*-fold sampling techniques to develop *k* individual, cross-validated response surface models. Based upon the residual error of these models, weights are assigned and a composite response surface model can be developed. It is shown in this work that utilizing the w-StackRSM approach yields approximately a *3-5%* decrease in residual error when compared to a traditional least-squares response surface approach. This response surface model is then used within the parametric uncertainty quantification techniques—specifically Fast Fourier Transforms—to efficiently and accurately quantify the parametric uncertainties associated with the models being considered. The details of this approach are included in Chapter 3 and were published in Riley and Grandhi (5).

2. The Probabilistic Adjustment Factors Approach (PAFA) was developed and validated for the quantification of parametric and model-form uncertainties in problems with computational simulations in the absence of any experimental data. This approach was an adaptation of the original Adjustment Factors Approach, which was developed and derived for use in deterministic models with no parametric uncertainties. This approach was derived for general distributions regarding the outputs of each model and demonstrated for Gaussian and Beta distributions. The details of this approach are included in Section 5.2.2 and were published in Riley and Grandhi (6).

3. The Modified Adjustment Factors Approach (MAFA) was developed in this work to estimate the sensitivity of the adjusted models developed using the traditional Adjustment Factors Approach and the Probabilistic Adjustment Factors Approach to the individual model probabilities that were assigned to the models in the analysis. This approach consists of two stages: estimating the sensitivity of the adjusted model to the model probability set as a whole, and estimating the sensitivity of the adjusted model to each of the model probabilities individually. The first stage of the approach determines the approximate reduction in model-form uncertainty that can be expected through the introduction of additional data into the problem. If additional data cannot be added, the second stage of the approach identifies which models contribute most significantly to the overall variance in the adjusted model. This identifies these models as potential outliers or erroneous models that are deserving of additional review or analysis. It also

states that an improvement in the models with the highest sensitivity will have the greatest reduction in the variance in the adjusted model. The details of this approach are discussed in Section 5.2.3 and were published in Riley et.al (7).

4. The application of Bayesian Model Averaging (BMA) as a tool to quantify parametric, predictive, and model-form uncertainties in an engineering application, specifically the aeroelastic analysis of a wing design, is demonstrated in this work. BMA was originally developed as a statistical forecasting tool for producing probabilistic forecasts given a set of prior models and results. Its use in the last ten years or so has been prevalent in the fields of economics, geology, and meteorology. However, the approach was not implemented for use with aerospace engineering models and simulations until the last two or three years with the work of Park and Grandhi (8) and Riley and Grandhi (9). BMA utilizes a given data set to update individual model predictions to quantify the predictive uncertainty associated with the model and, in conjunction with Bayes' Theorem, the data to update model probabilities given their relative capability of predicting the limited data set introduced into the problem. This work provides a novel application of the Bayesian Model Averaging approach in the field of aeroelastic design by integrating the results of aeroelastic models among multiple fidelities to quantify the uncertainty in selecting the appropriate level of fidelity needed for an analysis. The details of the BMA approach are included in this work in Section 5.3.1, and the initial application to the aeroelastic analysis problem was first presented in Riley and Grandhi (9).

The breakdown of this dissertation is as follows. Chapter 2 will introduce the concept of aeroelasticity, as well as introduce the modeling packages that will be used for modeling of aeroelastic behaviors. Chapter 3 will discuss surrogate modeling techniques for use in reducing the computational simulation time that is required for subsequent evaluations of the design space using the models discussed in Chapter 2. A novel surrogate modeling approach—the weighted Stack Response Surface Method (w-StackRSM)—is introduced in the chapter and is validated against benchmark surrogate modeling problems in the literature. Chapter 4 will define the three forms of uncertainty as they are implemented in this work. Chapter 5 will then discuss the methods that are used in the literature and that have been developed in this work to quantify the three forms of uncertainty. Two novel methods developed in this work—the probabilistic adjustment factors approach (PAFA) and modified adjustment factors approach (MAFA)—are introduced, as well as a novel implementation of Bayesian Model Averaging. Chapter 6 will then demonstrate the application of these uncertainty quantification tools to a simple closed-form spring-mass example. Chapter 7 will expand upon this application to a low-fidelity flutter analysis of a two degree of freedom airfoil subject to unsteady aerodynamics. The penultimate demonstration of these methods will be shown in Chapter 8 with the full aeroelastic simulation of the flutter velocity of the AGARD 445.6 wing using three different commercial aeroelasticity packages. Chapter 9 will then summarize the results and research contributions of this work.

2. Aeroelasticity

2.1 Introduction

Aeroelasticity is the field of science defined by Arthur Collar in 1947 as "the study of the mutual interactions that take place within the triangle of the inertial, elastic, and aerodynamic forces acting on structural members exposed to an airstream, and the influence of this study on design" (10). This breakdown is displayed in Figure 2.1.

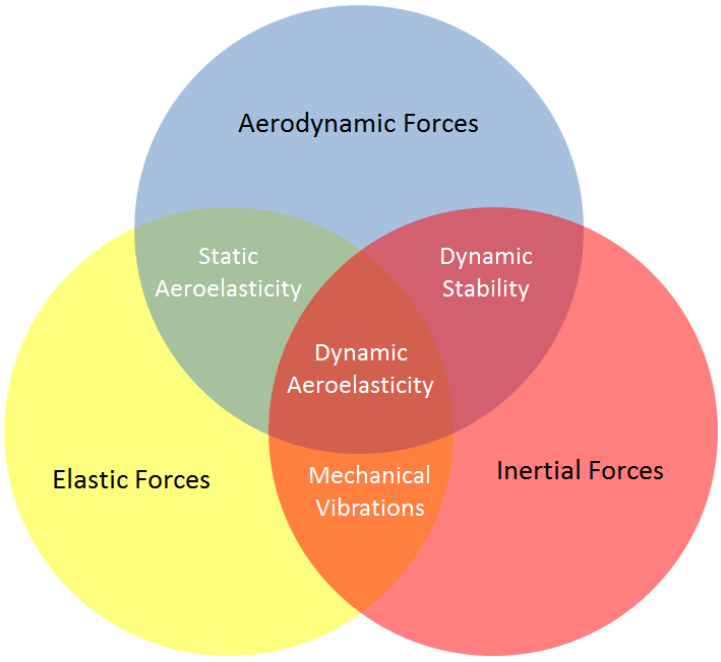

Figure 2.1: Aeroelastic Triangle of Forces (11)

In general, aeroelasticity is the study of the effects of the coupling of aerodynamics and structures in the analysis and design of a structure subject to aerodynamic loadings, often an aircraft. In operation, aircraft are subject to a wide range of loading conditions as a result of multiple phenomena such as flight maneuvers, dynamic responses, or gust loads. These loads, produced by the aircraft maneuver, are ultimately transferred to the structural components of the aircraft, which must bear the load. This results in a coupling of both the static and dynamic response of the structure to the applied loads. This coupling can be treated as static—obtaining aerodynamic loads and applying them to the structure in an instantaneous time-step, or dynamic—a continued coupling of the aerodynamic loads and the resulting structural response that is carried out for a specified period of time. As such, in the case of fixed wing aircraft, aeroelasticity can be broken down into two distinct disciplines of analysis: static and dynamic aeroelasticity.

2.1.1 Static Aeroelasticity

Static aeroelasticity is defined as the study of the deflection of flexible aircraft structures—such as wings—under the aerodynamic loads of the structure (12). Static aeroelastic problems feature several simplifying characteristics to approximate a static response. The first assumed, as denoted by the term static, is that these analyses are

independent of time, and are assumed to occur instantaneously. With this assumption, inertial forces related to the vibration of the aircraft structure are ignored. In general, most of the inertial forces in the equilibrium equation of motion are largely ignored—with a few exceptions such as the inclusion of rigid body accelerations in trim calculations—as they are time-dependent properties. A final simplification of static aeroelasticity is that only steady aerodynamic forces need be considered, as once again, unsteady aerodynamic forces are time-dependent.

In static aeroelasticity, there are multiple critical phenomena that are often analyzed: control effectiveness, lift effectiveness, induced drag, divergence and control reversal (12). Divergence is the phenomenon that occurs when the moments created by the aerodynamic forces overcome the restoring moments of the structural component due to its own structural stiffness. This phenomenon can result in catastrophic failure of the air vehicle due to structural failure (13-14). Often, the divergence dynamic pressure of a configuration can be solved for relatively simply, through eigenvalue analysis, as a result to the assumptions made in the static analysis.

The other static aeroelastic phenomenon often analyzed is control effectiveness, or more specifically, control reversal. Control surfaces are used to maneuver an air vehicle through its flight path. As such, the sizing of these control surfaces is an integral part of the design process. The effectiveness of the control surfaces changes as aerodynamic loading is changed. It has been shown that for many configurations, as the

velocity of an airfoil is increased, that the effectiveness of a control surface can decrease (15). Once the effectiveness of the control surface decreases to zero, the wing experiences what is called control reversal, where the effect of the control surface under consideration is actually reversed when compared to its intended effect. While this is not necessarily a catastrophic failure, as divergence can be, it can cause dramatic problems with controllability if not considered in the design process.

2.1.2 Dynamic Aeroelasticity

Dynamic aeroelasticity is defined as the study of the interactions among inertial, aerodynamic, and elastic forces (15). In dynamic analyses, time-dependent forces and loads are now considered, resulting in the inclusion of inertial forces to the elastic and aerodynamic forces that are considered in a static aeroelastic analysis, completing the triangle of forces shown in Figure 2.1. As a result of the inclusion of the inertial forces, the phenomena of interest for dynamic aeroelastic analyses are different than those considered in static analyses. The key phenomena that are explored in dynamic aeroelasticity are flutter, buffeting, limit-cycle oscillations, and gust response.

Aeroelastic flutter is "an unstable self-excited vibration in which the structure extracts energy from the air stream and often results in catastrophic failure" (12). This phenomenon occurs at two parameters known as the flutter speed, V_f, and frequency, ω_f. These two terms are defined, respectively, as “the lowest airspeed and the

corresponding circular frequency at which a given structure flying at given atmospheric density and temperature will exhibit sustained, simple harmonic oscillations" (15). The harmonic oscillations arise when the aerodynamic forces on the system couple with coalescing structural modes of the structure. This coupling, if undamped, can then grow unbounded to cause catastrophic forces and displacements upon the air vehicle, resulting in failure of the aircraft. Aeroelastic flutter is considered as one of the most critical and potentially catastrophic of all aeroelastic phenomenon (13-14), and details regarding the calculation of this flutter velocity for aircraft wings and structures will be detailed in the following section.

In addition to aeroelastic flutter, buffeting is another aeroelastic phenomenon that is analyzed using dynamic aeroelasticity. Buffeting refers to the transient vibrations of an aircraft surface—often in the tail of the aircraft—that are due to the aerodynamic impulses created by other components of the air vehicle further upstream, such as the wing. In general, the phenomenon can be thought of as the effect of the wake of the upstream portions of the aircraft on the downstream structural components. While buffeting can be a detrimental phenomenon if it is encountered unexpectedly, it is not always considered as a driving factor in the design of many air vehicles.

Limit cycle oscillations (LCOs) are a primary nonlinear aeroelastic response phenomenon that can be roughly considered to be a bounded form of aeroelastic flutter (16). In LCOs, instead of the harmonic oscillations of the structure growing unbounded,

as they do in flutter, they are instead bounded at an amplitude, often less than the failure point of the structure. This bounded response is a result of the fact that, as the oscillations increase in amplitude, the resisting stiffness of the structure will also increase, creating a pseudo-harmonic response, such as sinusoidal motion. Although the amplitude of the motion is bounded in LCOs and will not typically result in near-instantaneous destruction of the component, as with flutter, fatigue problems can quickly arise due to the high-frequency harmonic motion that is induced upon the structure. As such, LCOs can produce very harmful structural effects due to low or high-cycle fatigue.

2.2 Flutter Solution Methods

As aeroelastic flutter has been identified as a potentially catastrophic phenomenon in air vehicle design, the calculation and analysis of dynamic aeroelastic phenomena, namely flutter, will be discussed in this section. The flutter velocity and characteristics of a model can be calculated by first assuming simple harmonic motion of the structure, as shown in Eq. (2.1).

$$\{u(t)\} = \{u_h\} e^{i\omega t} \tag{2.1}$$

Where *u(t)* represents a vector of the displacements of the structure, often an airfoil or wing, as a function of time, and ω is the frequency of the harmonic motion. Substituting in the second order differential equation that describes the linear dynamic

behavior of a structure subject to aerodynamic forces, analogous to the fundamental equation of finite element analysis, yields Eq. (2.2).

$$\left[M_h p^2 + \left(B_h - \frac{\rho c V Q_h^I}{4k} \right) p + \left(K_h - \frac{\rho V^2 Q_h^R}{2} \right) \right] \{u_h\} = 0 \qquad (2.2)$$

In Eq. (2.2), M_h represents the modal mass matrix, B_h the modal damping matrix, and K_h the modal stiffness matrix. These three matricies represent the structural response of the model and can be obtained from a structural finite element model of the structure to be analyzed. The aerodynamic response of the structure is modeled using the other two matrices where Q_h^I represents the generalized aerodynamic damping matrix and Q_h^R represents the generalized aerodynamic stiffness matrix. The rest of the terms in Eq. (2.2) are constant flow field terms where ρ denotes the air density, c represents the mean aerodynamic chord length, V is the airspeed of the model, ω is the circular frequency, u_h is the modal displacements, and k is the reduced frequency of the model, as defined by Eq. (2.3).

$$k = \frac{\omega c}{2V} \qquad (2.3)$$

Although Eq. (2.2) represents the basic equation of motion for flutter, there are multiple methods to both obtain the values for the equation, as well as to solve the equation itself. One common method for solving this equation of motion is the 'k' Method, also known as the V-g Method (12).

'k' Method:

In the 'k' Method, the aerodynamic damping matrix, Q_h^I, and the aerodynamic stiffness matrix, Q_h^R, are both functions of the reduced frequency, *k*. The structural stiffness and mass matrices are obtained from finite element approximations. Finally, the modal damping matrix, B_{hh}, is assumed to be defined as shown in Eq. (2.4), where *g* is the structural damping coefficient.

$$B_h = igK_h \tag{2.4}$$

By modeling the damping matrix as shown in Eq. (2.4), the structural damping inherent to the structure itself is not being calculated exactly, but instead being estimated as hysteretic damping as a function of the stiffness of the model. Assuming a harmonic solution of the form $u = u_o e^{i\omega t}$ into Eq. (2.2) and dividing by ω^2, the equations of motion of the system can then be rewritten as shown in Eq. (2.5).

$$\left[M_h - i\rho\left(\frac{c}{2k}\right)Q_h^i - \rho\left(\frac{c}{2k}\right)^2 Q_h^R - \frac{1+ig}{\omega^2} K_h \right] u_o = 0 \tag{2.5}$$

As Eq. (2.5) is in terms of only the reduced frequency, *k*, it can be considered to be a generalized eigenvalue problem shown in Eq. (2.6).

$$\left(F - \lambda K_h\right) u_0 = 0 \tag{2.6}$$

Where *F* and λ are defined by Eqs. (2.7) and (2.8):

$$F = \left[M_h - i\rho\left(\frac{c}{2k}\right)Q_h^i - \rho\left(\frac{c}{2k}\right)^2 Q_h^R \right] \tag{2.7}$$

$$\lambda = \frac{1 + ig}{\omega^2} \tag{2.8}$$

From Eqs. (2.6)-(2.8), with a particular reduced frequency, *k*, selected, the frequencies and damping coefficients can be solved for as shown in Eqs. (2.9) and (2.10).

$$\omega = \frac{1}{\sqrt{\mathrm{Re}(\lambda)}} \tag{2.9}$$

$$g = \frac{\mathrm{Im}(\lambda)}{\mathrm{Re}(\lambda)} \tag{2.10}$$

The solution of Eqs (2.9) and (2.10) is then repeated across the spectrum of all possible *k* values (or in practice, a subset of *k* values), resulting in a set of values for *ω* and *g* for corresponding to different values of *k.* The formulation of this data set can be a computationally intensive process depending upon the method of development of the structural and aerodynamic matrices, as well as the discretization of the *k* values. For problems utilizing finite elements or other discretization methods, the evaluation of the equations of motion can be costly, if not computationally restrictive. In cases such as this, often a branch-and-bound method is used on *k* values where instead of discretizing the *k*-space evenly, it is only refined near the flutter point in an attempt to reduce the number of solutions of the equations of motion required.

From this data set, Vg or Vω plots can be formed by plotting *g* or *ω* against *V*. Samples of these Vg and Vω diagrams can be seen in Figures 2.2 and 2.3 respectively.

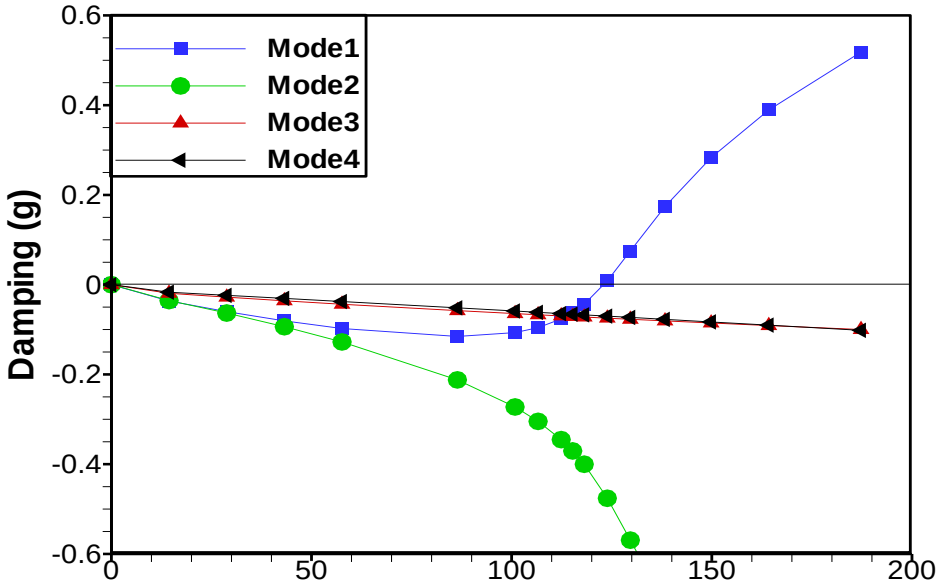

Figure 2.2: Sample Vg Plot

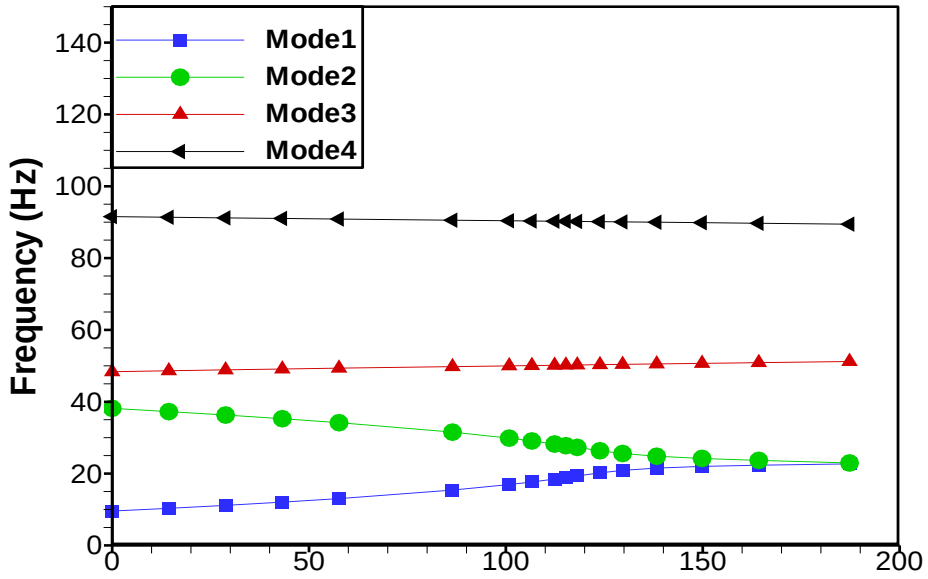

Figure 2.3: Sample Vω Plot

The data shown in Figures 2.2 and 2.3 can then be used to numerically solve for the flutter velocity of the model. In the Vg method, the Vg data and plot shown in

Figure 2.2 is utilized. Flutter is said to occur when the structural damping of the system decreases below the required damping to yield zero overall damping to the system (denoted by the value of *g* on the y-axis). Thus, the flutter velocity is defined as the free-stream air velocity corresponding to the *k* value at which the artificial damping *g* exceeds the actual structural damping of the system. Looking at the Vg plot, the onset of flutter can be shown to be at the location of the plot in which the damping value *g* for any one of the modes being plotted crosses the zero axis. In the case of Figure 2.2, this would occur where Mode 1 crosses the zero axis at approximately 130 ft/s.

A similar approach can be applied in the Vω approach using the frequencies of the modes instead of the artificial damping values. In this approach, instead of observing where a mode will cross the zero-damping axis, the flutter velocity is said to occur at the velocity where the two modes that are contributing to the flutter of the aircraft move closer to one another and eventually become equal, at which they are said to coalesce; where one of the damping ratios become increasingly positive and the other negative. Looking at the plot in Figure 2.3, this can be seen as modes 1 and 2 begin to coalesce as the velocity is increased, coming together at approximately 130 ft/s. Comparing this point to the data shown in Figure 2.2, it can be see that at the point of coalescence that the first and second models diverge from one another where mode 1's damping ratio becomes positive and mode 2's damping ratio displays asymptotic behavior, driving to large negative values.

While looking at a Vg plot might appear to give a more definitive answer, as finding the root of a mode is much more straight forward than finding where two modes coalesce, there are drawbacks to both plotting methods. The Vg plot is under the assumption that there is no structural damping inherent to the model, which is often not the case in a physical system. As such, there are two flaws with the approach. The first flaw is that, as it is assumed that there is zero structural damping, the results for the value of *g* are only valid for values of *k* that correspond to a *g* of *0*. Thus, any value of *g* off the zero-axis is inherently incorrect. However, it is assumed that for small values of *g*, the zero structural damping assumption holds true, and thus, there is an envelope around the zero-axis within which the values of *g* can be trusted. The second flaw relates to the zero damping assumption in that most physical structures have at least a small amount of natural damping, whether it be by design or due to additional effects not considered in the analysis, such as the drag encountered in the oscillatory motion. As such, using the intercept of the mode with the zero-damping axis will result in a conservative solution. Instead, a value for structural damping can be estimated, and the intersection of the modes with that line can be considered as the flutter point. There are caveats to this method though, as the estimate for structural damping must be small as to not violate the zero / small damping assumption made in the solution.

'p-k' Method (17)

The 'p-k' Method for flutter calculation uses a similar derivation to that of the 'k' Method, but has some changes in the solution process itself. First, instead of

considering all modes of the model at once, the modes are considered one at a time in a sequential manner. While it is infeasible to often consider all modes in larger models, the number of modes considered can be truncated to only include those that are expected to contribute in the flutter phenomenon. For each mode of interest, an initial guess to the frequency of the mode is made, and the corresponding reduced frequency is then calculated using Eq. (2.3). Once a reduced frequency is calculated, the aerodynamic stiffness and damping matrices can be calculated, as is done in the 'k' Method. The frequencies of the system can then be calculated at the corresponding reduced frequency using the eigenvalue solution to Eq. (2.2). The frequency solution that is closest to the initial guess is then selected and the process is repeated until convergence for the mode of interest, which is repeated for all modes of interest. This will result in a set of frequencies, damping values, and air speeds that can then be plotted in a similar manner as shown in the 'k' Method to find the flutter speed where the damping is shown to be zero.

The 'p-k' Method serves to minimize and eliminate a few of the concerns that arise with the 'k' Method. For instance, while the 'k' Method there was a zero structural damping assumption made, and instead, the structural damping matrix was modeled as a function of the structural stiffness matrix. As mentioned in the previous section, this resulted in erroneous values for damping away from the zero-damping axis. The 'p-k' Method, though, does not necessarily assume this regarding the structural damping matrix, allowing for known structural damping data to be directly included in the

calculations. In addition, as both the 'k' and 'p-k' Methods are frequency-matching techniques, there are errors in the estimates of the frequency and damping values away from the flutter speed (as mentioned before). In addition, due to the varying assumptions made, the two methods might predict different 'incorrect' values for the frequency and damping at these sub- or supercritical speeds. However, in general, at the flutter condition, the two methods will give similar estimates (12).

2.3 Simulation Packages

In small, simplified cases, the equations of motion for aerodynamic flutter (Eq. (2.2)) can be solved in closed-form. However, as the fidelity of the model of the air vehicle being considered is increased, it quickly becomes necessary to utilize a modeling package in order to obtain accurate and efficient results. There exist multiple modeling packages that are capable of modeling the aeroelastic behavior of the air vehicle in varying fidelities. Each modeling package utilizes different assumptions in the development of the package that results in each of the packages having different requirements, times required for analysis, and applicabilities in different regions of the design space. For instance, in the different Mach regimes shown in Table 2.1, different aeroelastic theories that are often applied for the simulation of aircraft performance and responses. As such, different aeroelastic packages are often utilized depending the on region of the design space interested in being analyzed.

Table 2.1: *Mach Regime Definition* ***(18)***

Regime	***Lower Bound***	***Upper Bound***
Subsonic	*0.0*	*~0.80*[a]
Transonic	*~0.80*[a]	*~1.20*[a]
Supersonic	*~1.20*[a]	*5.0*
Hypersonic	*5.0+*	

[a]Exact values are configuration dependent

While assumptions made in the construction of the model might allow that model to be valid in additional regions of the design space—such as models with non-linearity assumptions still being considered valid in more linear regions of the design space—there are often cases where particular models give significantly erroneous results if used outside of the intended region of interest. One such example of this shown in Table 2.1 is the transonic Mach regime. The transonic Mach regime is characterized by nonlinearities in the design regime due to the difficulty in the prediction of a shock-layer boundary along the profile of the wing of interest (19). As such, the solution to a transonic aeroelastic problem is often more complex and intensive than problems in the subsonic and supersonic regimes, as these nonlinearities must be accounted for by the software package, either directly or through a linearization process. Often, this complicates the solution process and can dramatically increase the simulation time required for the solution.

In this work, the transonic Mach regime will be one of great interest due to the uncertainties surrounding the modeling process and the selection of appropriate models to utilize. In the subsonic and supersonic regimes, multiple commercial software packages are available that often yield similar representations of the output response due to the relatively uniform assumptions made among the different models. Thus, as a result of the linear nature of these regimes, the results of multiple models will often show relatively good agreement with each other, meaning that the amount of uncertainty introduced into the problem through the modeling process is less than that of situations where there is significant disagreement among models being considered and can generally be considered as restricted to as parametric uncertainties (Chapter 4).

In addition, many simulation packages are incapable of solving problems in all regions of the design space, and are often designed for applicability in only one region of the Mach regime. Nonlinear solution methods, such as those commonly used in the transonic regime, can normally be used to solve problems that could be solved using linear methods, with an added expense of simulation time. However, due to the nonlinear nature of the solvers, it is possible, although remotely so, for additional numerical noise to be created that will ultimately result in an erroneous solution from the "higher" fidelity solver. However, utilizing a linear solution technique within a nonlinear region of the design space will nearly always produce erroneous results. An example of this is that linear methods, such as those implemented in many subsonic and

supersonic solvers, will give erroneous estimates for responses within the transonic region of the design space (20).

As a result when analyzing an air vehicle's performance across a wide range of Mach numbers, as must be done to determine the complete performance of a supersonic air vehicle, it is not uncommon for multiple simulation packages to be used. Although there are boundaries between the Mach regimes, these are not definitive values and are often heavily configuration dependent. As such, there exists a level of uncertainty at the transition values of the Mach regimes as to which Mach regime governs the physics driving the particular analysis. In addition, even within a particular region of the design space, there will often exist multiple simulation packages and models of varying fidelity that are created to simulate the same physical scenario at the same conditions. In cases such as this, it can be difficult for a designer to select the model that will most accurately represent the true physical scenario of interest. A simple answer to such a problem would be to select the model with the highest fidelity and assume the model to be the “truest” representation of the physical problem. However, there are three difficulties to such an approach:

1. For some problems, it could be difficult to determine the relative fidelity of different models with respect to one another. Additionally, often models can exist at similar fidelities that still yield divergent results. A simple example of this would be utilizing linear finite elements to analyze the displacement of a beam. The boundary conditions

of such a model could be represented in different manners resulting in multiple models of the same physical problem, yet all at the same fidelity. In such a case, it would be not be clear which model would be considered the "highest-fidelity" representation of the problem.

2. High fidelity models can often suffer from over-fitting issues when utilized in lower-order representations. This is best represented by looking at fitting a curve to a data set. If a large amount of data was available, a higher-order model would yield the approximation with the lowest residual in most cases. However, if that same model was then used with a significantly smaller set of data (i.e. a 10^{th} order polynomial regression model with only 10 data points), such a model can experience large over-fitting errors. As such, in the absence of data for the particular set of parameters being utilized in the model, one cannot simply assume that the highest-fidelity model will always yield the "most accurate"

3. Finally, higher fidelity models tend to have an increased computational time associated with their evaluation. This increased computational time is due to the more advanced nature of the assumptions made in the model to provide a higher-order representation of the problem. In problems that require such a representation, this increase in time is sometimes unavoidable. However, in simpler problems, it would be inefficient to use a model with such a high-order representation for a response that does not necessitate it. A classic aeroelastic example would be the excessive nature of using a full Navier-Stokes

coupled aeroelastic solution technique for a simple wing configuration at subsonic speeds. Such a model may require computational time multiple orders of magnitude larger than a linear subsonic approach even though both models should—in theory for a simple configuration—yield very similar results.

Due to the reasons listed above, fidelity and model management is a critical consideration in the design of any configuration, specifically the aeroelastic design of an air vehicle. This critical nature is not only a function of the bloated computational time that might be necessitated by inappropriate model selection, but also the uncertainties that arise in the selection of the proper model(s) to consider for the analysis of the configuration. For this work, multiple models will be considered and the impact of model selection will be discussed from the standpoint of the uncertainty that this choice introduces to the modeling process as a whole. The following sections briefly introduce the models and software packages that are utilized in this work for aeroelastic analyses.

2.3.1 V-g Solver Code

The V-g solution method, or the 'k' Method, was derived and described in detail in Section 2.2. However, the execution of the solution technique detailed in the section involves the use of numerical techniques for the evaluation of the eigenvalue problem. As such, a Matlab code has been developed in this work for the numerical solution of

the flutter velocity for a problem with an equation of motion as shown in Eq. (2.2). The code can be found in Appendix A, but will be detailed in this section.

The equation of motion shown in Eq. (2.2) is defined for an airfoil--in this case a two degree of freedom airfoil subject to unsteady aerodynamics. As the model of interest has two degrees of freedom, there are two equations of motion that define the motion of the system. By rearranging these equations and setting the determinate equal to zero, a single equation can be formed to solve for the frequencies of the system. As mentioned in Section 2.2, though, the terms in the equations of motion are functions of the reduced frequency of the system, *k*. As such, the code loops through by defining a finite number of values for *k* between two extreme values.

At each value of *k*, the code evaluates each term within the determinate equation of motion, as well as a function value known as Theodorsen's Circulation Function. Theodorsen's Circulation Function is a function consisting of both a real and an imaginary part that controls the phasing and amplitude of the lift and pitching functions with respect to the motion of the airfoil in the aerodynamic computations of the system (21). This function is represented in the code through different possible surrogate models which will be discussed in further detail in Section 6.2.

After evaluating Theodorsen's Circulation Function for a particular value of *k*, the rest of the terms in the determinate of the equations of motion are also evaluated. This

results in an equation that is quadratic with respect to ω. The two roots to this equation are then solved for using the quadratic equation root solver, as to handle potential imaginary values for the roots. Once solving for these roots, the values for g, ω_1 and ω_2 (the two frequencies of the airfoil), and V can be solved for as well for the particular k value of interest.

This process is then repeated for each of the k values defined within the range, storing the values of k, g, ω_1, ω_2, and V at each step in the process. After completing the spectrum of k's, Vg and Vω plots can then be created for the model. In addition, using a numerical interpolation technique, the flutter velocity is approximated between the sampled k values. Refinement of the k values near the flutter point would be beneficial to the accuracy of the simulation, but due to the simplicity of the numerical solution technique, a large number of k's are evaluated throughout the process, reducing the need for further iteration.

2.3.2 NASTRAN

MSC.Nastran is a MSC-supported software package that is based around its finite element method (FEM) solver. However, the scope of NASTRAN is not limited to strictly finite elements, but also contains aerodynamic solvers to construct aeroelastic analyses. NASTRAN contains a wide variety of aerodynamic methods that can be coupled with its structural FEM solver to solve problems across a wide range of Mach numbers. These

methods include subsonic doublet lattice method, strip theory, supersonic Mach box method, and supersonic piston theory (22). NASTRAN is also capable of performing both static and dynamic aeroelastic analyses, ranging from simple static trim analyses to fully dynamic responses such as flutter and modal frequency response. Concentrating upon the dynamic flutter analyses, as that will be the primary scope of this work, NASTRAN is capable of using multiple solution methodologies to solve the same problem, such as the 'k' Method, the 'P-k' Method, or the 'K-e' Method, which is a 'k' Method solution that is restricted to increase the computational efficiency of the solver.

2.3.3 ZAERO

ZAERO is a ZONA aerodynamic program that contains a wide variety of analysis techniques for flutter, static aeroelasticity, and aeroservoelasticity for subsonic, transonic, supersonic, and hypersonic Mach numbers (23). However, ZAERO does not contain an internal structural FEA module. As such, the structural modal response of the model must be imported from an external FEA solver, such as MSC.NASTRAN. Once a modal response is imported, ZAERO contains many sub modules for analysis specific to a particular phenomenon or Mach regime. The two modules that will be utilized in this work are ZONA6 and ZTAIC.

ZONA6:

ZONA6 is a ZONA developed code for use with steady and unsteady subsonic aerodynamics (i.e. M < 0.8). The module utilizes a higher-order panel formulation for the lifting surfaces of the model than what is commonly used in the conventional Doublet Lattice Method (DLM) which allows for the modeling of more complex designs (23). For the flutter case of interest in this work, the structural damping matrix is not directly available from the FE solver, and as such, is not used within the ZONA6 approach.

ZTAIC:

ZTAIC is a module developed specifically for use within the transonic Mach regime that generates unsteady transonic modal AIC provided with an externally computed steady mean pressure distribution from an aerodynamics package. Example packages used to compute this steady mean pressure distribution could include CAPTSD, a transonic small disturbance CFD code developed by NASA. Once the modal solution and steady mean pressure distributions are imported into the package, ZTAIC utilizes a transonic equivalent strip method approach to solve for both the static and dynamic aeroelastic response of a model.

2.3.4 ZEUS

ZONA's Euler Unsteady Aerodynamic Solver (ZEUS) is an aeroelastic package that incorporates dynamic structural FEM results with computational fluid dynamic (CFD)

results from an Euler solver within the program (24). Similar to ZAERO, ZEUS requires that the structural modal solution for the model be computed externally and input into the software package before performing the analysis. Once the modal solution is imported, ZEUS solves the Euler equations on a Cartesian grid system utilizing a cell-centered finite volume method with a dual-time stepping algorithm for use with unsteady solutions. To account for viscous effects in the analysis, ZEUS couples the Euler solution with a steady boundary-layer equation, reducing the computing requirement for handling viscous effects dramatically when compared to a Navier-Stokes code. Another feature of ZEUS that aids its applicability in the design process is its automated mesh generation capability, along with the ability to handle overset meshes, commonly used in the modeling of complex features.

2.4 Summary

This work will utilize the aeroelastic modeling packages listed in Section 2.3 in two problems to demonstrate the capability of the developed methodologies to quantify model-form and predictive uncertainties, as well as traditional parametric uncertainties. In the first aeroelastic problem, only the Vg Solver code will be utilized. As mentioned, the model-form uncertainty in this problem will be derived from the appropriate selection of the Theodorsen's Circulation Function approximation, as detailed in Section 6.2.

For the second aeroelastic problem of interest, the full simulation of aeroelastic flutter will be looked at for the AGARD 445.6 wing. Three packages will be used to simulate the flutter velocity of the wing—ZAERO, ZTAIC, and ZEUS. The model-form uncertainty in this problem will be derived from the selection of the appropriate modeling package and the predictive uncertainty associated with each model will be quantified as a function of how well the model predicts the "true" physical behavior of the wing—denoted by experimental data points made available in the literature.

3. Surrogate Modeling

In the simulation of the aeroelastic response of an air vehicle, the simulation time required for the evaluation of a performance metric or response of interest can often be large and restrictive. When these simulations are coupled with design approaches such as optimization or uncertainty quantification, this effect is magnified and the necessity for relaxation of simulation time is intensified. A common strategy in computationally intensive approaches is to utilize a metamodel to provide a "model of the model" being analyzed in the approach (25). These metamodels serve to reduce the computational cost associated with multiple evaluations of a full-scale model or simulation by instead using lower-order representations of the design space to repeatedly, quickly, and efficiently evaluate designs. The history of the development and implementation of metamodels in multidisciplinary design optimization was detailed in the paper by Sobieszczanski-Sobieski and Haftka (26).

Many metamodeling techniques exist and have been implemented in the literature for optimization and uncertainty quantification applications. These methods include surrogate modeling techniques such as artificial neural networks (27), kriging (28), and response surface methodology (29). Much work in the literature has been

done evaluating the relative merit and applicability of each method to a variety of problems (30). Similarly, much work has been done in comparing the relative accuracy of each of these methods to given applications or solution forms. Papila et.al compared the accuracy and efficiency of radial basis neural networks and response surface methodology for supersonic turbine applications (31). Similarly, Stander et.al looked at response surface approximations, neural networks, and kriging in the modeling of automotive crashworthiness (32). The general consensus among the research presented is that there is no single surrogate model that outperforms the others across all problems.

The inaccuracies experienced in previous surrogate models is shown by prior work in the literature to be a result of the fact that given a limited data set, it is difficult if not impossible to identify a unique surrogate model to fit said data (33). This phenomenon leads to difficulty in identifying the metamodels which best fits the set of data, referred to as model-form uncertainty. A common method used in the literature to quantify and reduce model-form uncertainty is to construct an aggregate model as the sum of the weighted individual models (7,34).

Constructing multiple surrogate models requires, in many cases, additional data points that would not necessarily be required for just a single surrogate. As such, due to the cost of obtaining additional data for the development of surrogate models, the idea of incorporating the results of multiple surrogate models into a single response has only

been recently explored in research work. Zerpa et.al detailed the potential of using multiple surrogate models in the optimization process of alkali-surfactant-polymer flooding processes (35). In this work, the authors showed that utilizing a weighted average surrogate method yields better modeling capabilities than any of the individual surrogates used alone. However, this method also required an additional number of data points to form the metamodels being considered. Goel et.al expanded upon the idea of weighted metamodels by weighing the surrogates constructed using polynomial response surfaces, kriging, and neural networks to construct a weighted surrogate (36). This idea was later demonstrated to helicopter rotor blade vibration reduction showing that at a very small additional computational cost in data collection that a more accurate surrogate can be achieved (37). This increased demand on data points was primarily driven by the more advanced surrogates such as neural networks, which often can require additional data points to train.

Work has been done on adaptive response surface methods as well to develop multiple models and integrate them into a more accurate metamodels. Das and Zheng developed a cumulative RSM approach for structural reliability estimates by using lower-order responses to drive the sampling for higher order models (38). These methods have been used in recent optimization applications (39), but they are still subject to the shortcomings of the traditional response surface methodology with respect to cross-validation and computational efficiency. These shortcomings are that, using response surface methodology, the highest computationally efficiency is obtained

using all of the available data points to form the model. However, if all data points are used to form the model, no data is available to develop a cross-validation metric. As such, there is a trade-off between efficiency and confidence in the model where a decision must be made on how many—if any—points are excluded from the model development to use as points for cross-validation.

3.1 Response Surface Methodology (RSM):

The response surface method (RSM) was developed by Box and Wilson from a simple mathematic expression to relate the input and output of experimental data points (40). The approach involves selecting an a priori functional representation of an output response of interest as a function of the *n* design variables ($\bar{x}$) and a set of parameters, $\hat{\beta}$, as shown in Eq. (3.1).

$$\tilde{y}(\bar{x}) = \beta_0 + \sum_{i=1}^{n} \beta_i x_i + \sum_{i=1}^{n} \beta_{ii} x_i^2 + \sum_{i=1}^{n} \sum_{j=1}^{n} \beta_{ij} x_i x_j + \ldots \tag{3.1}$$

The form of the surrogate shown in Eq. (3.1) is determined a priori and can vary among multiple models, as shown in the literature (41). The number of data points required to form the model is bounded below by the number of β coefficients in the equation for the surrogate. If the number of data points *n* is equal to the number of β coefficients, the unique values of β can be solved for using linear regression, as shown in Eq. (3.2):

$$\beta = (X^T X)^{-1} X^T y \tag{3.2}$$

Where *X* denotes the design matrix of data points and *y* is the response vector for the response of interest. In over-determined systems where greater numbers of data points exist than β coefficients, a numerical method such as least-squares must be used to solve for the β coefficients in Eq. (3.2). In general, equal weight is given to all data points being considered in the analysis. However, for applications such as reliability analysis, where accuracy is more important in particular regions of the design space, such as near where the limit state function is equal to zero, a weighted regression method has been used to estimate the β coefficients (42).

The RSM metamodels detailed above provide accurate representations of the data set, but do not necessarily provide a measure of the degree of accuracy. As such, validation methods in the literature have long been used to estimate the error in the metamodels through methods of cross-validation. Geisser first proposed the partitioning of the original data set into two subsets with one being used to estimate the coefficients in the response surface model, and the other subset being used to estimate the error in the model (43). One such approach for measuring the error of a model is to look at the root mean square error of the excluded subset of data (*m* x 1 vector of data), as shown in Eq. (3.3).

$$R_{ms} = \frac{1}{m}\sum_{i=1}^{m}(\tilde{y}(\bar{x}) - y_i)^2 \tag{3.3}$$

Partitioning methods such as these provide an estimate of the error in each model, but do so at the cost of an increase to the amount of data required. However,

by partitioning the original data set using *k*-fold cross validation (44), multiple metamodels and validation metrics can be developed for the same set of data.

3.2 Weighted Stack RSM (w-StackRSM):

The method of utilizing *k*-fold cross validation measures to estimate over-determined systems has been utilized in Monte Carlo Sampling approaches—referred to as StackMC—to estimate integral response in cases of excess data (45). The *k*-fold cross validation technique is applied in this work to develop multiple models and error measures. First, the original data set *y* is partitioned into *k* subsets of data, as shown in Eq. (3.4).

$$y \rightarrow [y_1; y_2; \ldots; y_k] \tag{3.4}$$

where each subset of *y* contains *m*, of the *n* original data points. With the *k* subsets of data, *k* unique, cross-validated RSM models can then be developed with a measured residual error using the *k*-fold sampling technique, as shown in Table 3.1.

Table 3.1: *k-fold Validation Models*

Model #	*Model Data*	*Validation Data*
M_1	$y_1, \ldots, y_{k-1}$	y_k
M_2	$y_1, \ldots, y_{k-2}, y_k$	y_{k-1}
…	…	…
M_k	$y_2, \ldots, y_k$	y_1

In the *k*-fold sampling technique shown above, each partition of the data set is excluded from the construction of a response surface model and used to estimate the residual error of the corresponding model, resulting in *k* individual models which make up the model set *M*, as shown in Eq. (3.5).

$$M_1, M_2, ..., M_k \in M \tag{3.5}$$

As such, there is a degree of model-form uncertainty that results in the selection of the "best" model among the model set *M*. Jin et.al explored multiple metrics and criteria for evaluating the best metamodels among a model set considered (46). However, instead of considering the results of a single model, increased accuracy and fidelity can be obtained by constructing a weighted model of the individual models constructed in the analysis. In this methodology, the weights of the models are determined through an inverse relationship among the residual errors of each of the models constructed using the *k*-fold validation—referred to as the weighted stack response surface methodology (w-StackRSM).

To calculate the weights of the individual models, two factors are considered. As a larger residual error indicates a less accurate metamodel, the weights are to be inversely related to the residual error of each model. Additionally, to ensure the proper scale of the weighted surrogate, the weights of the individual models must be normalized to a sum of *1*. The result of these two factors is Eqs. (3.6) and (3.7) which show the development and normalization of the individual model weights respectively.

$$w_{i,raw} = 1 - \frac{R_{ms}(\tilde{y}_i)}{\sum_{i=1}^{k} R_{ms}(\tilde{y}_i)} \tag{3.6}$$

$$w_i = \frac{w_{i,raw}}{\sum_{i=1}^{k} w_{i,raw}} \tag{3.7}$$

Having derived weights for each of the individual metamodels in the model set, the composite model can then be formed as shown in Eq. (3.8).

$$\tilde{y}_w = \sum_{i=1}^{k} w_i \tilde{y}_i(x_i, \beta_i) \tag{3.8}$$

This composite model consists of a linear combination of *k* independently cross-validated models weighted by their relative accuracy. This methodology stands in contrast to using all of the available data points to construct a single model in that it is validated through points not utilized in the construction of the model, providing a measure of cross-validation. As such, for the complete set of data considered, the traditional least-squares approach of considering all points results in a smaller overall residual error than this approach—as the points used to evaluate the model are the same points that are used to construct the model. However, as will be shown, when an additional set of data is used to validate the two approaches, the w-StackRSM provides a smaller residual error than the traditional least-squares approach at no increase in data cost.

3.3 Validation Cases:

The proposed methodology is first tested against conventional least-squares response surface methods using two surrogate modeling benchmark examples established in Jin et.al (46). In the validation problem, three response surface methodology approaches are considered; full least-squares estimation, cross-validation, and w-StackRSM. For the full least-squares estimation, all of the data points will be utilized to estimate the β coefficients and to estimate a residual error. Using the *k*-fold validation, *k* cross-validated models will be developed in these validation cases where the model with the lowest residual error can be considered. Finally, the accuracy of the proposed w-StackRSM method will be determined. The accuracy of these three methods will be compared for two data scenarios—only considering the initial data set used to form the models and by obtaining additional *a posteriori* points for error measures.

Case 1:

The two-variable problem shown in Eq. (3.9) is considered on the bounds $0 \leq x_1 \leq 6$ and $0 \leq x_2 \leq 10$.

$$f_1(x) = [30 + x_1 \sin(x_1)] * [4 + \exp(-x_2^2)] \tag{3.9}$$

To isolate one of the sources of model-form uncertainty, third order response surface models of the form shown in Eq. (3.10) are considered in the following analyses:

$$\tilde{y}(\bar{x}) = \beta_0 + \sum_{i=1}^{2} \beta_i x_i + \sum_{i=1}^{2} \beta_{ii} x_i^2 + \sum_{i=1}^{2} \sum_{j=1}^{2} \beta_{ij} x_i x_j + \sum_{i=1}^{2} \sum_{j=1}^{2} \beta_{iij} x_i^2 x_j \quad (3.10)$$

This surrogate results in ten β coefficients to be estimated using the response surface methodologies. Thirty data points were randomly sampled within the variable intervals specified and evaluated using Eq. (3.9) to construct the data set to be considered in the problem. Using five folds, the original data set is partitioned into five, six-point data sets to be utilized for the w-StackRSM approach. Utilizing *k*-fold validation, five individual and independent models and residual measures can be developed. Weights for these five models were then obtained from their respective residuals using Eqs. (3.6) and (3.7). Finally, the weighted response surface model was constructed using Eq. (3.8). Concurrent to the w-StackRSM approach, the traditional least-squares RSM approach was applied to the *30* data points to develop a seventh model to compare. Using the seven models constructed, the residual error of each model with respect to the complete data set was calculated (Table 3.2).

Table 3.2: *Case 1 Residuals (n=30, k=5)*

Model	*Residual*
M_1	*8.3526*
M_2	*8.9339*
M_3	*8.2792*
M_4	*8.5808*
M_5	*8.7839*
w-StackRSM	*7.2147*
LS-RSM	*7.1744*

Initially focusing on the first six models in Table 3.2, it is clear that the w-StackRSM approach yields a model with a significantly reduced residual error when compared to the individual cross-validated models that were constructed using the *k*-fold sampling technique (Models M_1-M_5). The w-StackRSM approach and the least-squares RSM approach produced nearly identical residual errors, with the LS-RSM error being slightly smaller than the w-StackRSM approach. As was noted previously, due to the fact that all of the points were used in the measurement of the residual were considered in the construction of the least-square RSM model, the least-squares RSM approach mathematically should yield the smallest residual error when only considering the data set used to construct the models. However, this is a biased result as the samples that are used for the analysis of the model are not independent of the model itself. To determine the relative impact of this bias, as well as to validate the results of these two models against *a posteriori* data, 30 additional points were then sampled at random from the design space and the average residual error of both the w-StackRSM model and the LS-RSM model was measured with respect to this new data set. This process of generating 60 data points—using 30 to construct the w-StackRSM and LS-RSM models and the other 30 to calculate each model's residual—was then repeated *100* times and the average residual for each approach is shown in Table 3.3.

Table 3.3: *Average Residuals for Additional Data Set, Case 1 (m=100)*

Model	*Avg. Residual*
w-StackRSM	*22.091*
LS-RSM	*23.392*

It can be seen in Table 3.3 that, for the problem of interest, the w-StackRSM approach yields, on average, a smaller residual error than the traditional least-squares RSM approach when calculated using an independent data set. As such, using the same original data set of *30* points, the w-StackRSM approach is able to weigh and integrate *k* independently cross-validated models to construct a superior surrogate model with no additional data cost. The only additional step when compared to a traditional least-square response surface method is the partitioning of the data into the data sets through *k*-fold sampling, and the subsequent model formulations. While this computational cost is not trivial, it pales in comparison to the cost associated with obtaining even one more data point for many models. As a frame of reference, on a personal computer with a 3.3 GHz I5 Processor and 4 GB of RAM, the LS-RSM for the above problem took 0.05s and the w-StackRSM approach took 0.09s.

The methodology validation process detailed above was then repeated on an additional problem in Jin et.al to verify the trends observed.

Case 2:

The two-variable problem shown in Eq. (3.11) is considered on the bounds $-10 \leq x_1 \leq 10$ and $-10 \leq x_2 \leq 10$.

$$f_2(x) = \sin\left(\frac{\pi x_1}{12}\right)\cos\left(\frac{\pi x_2}{16}\right) \tag{3.11}$$

Similar to the prior example, to isolate a possible source of model-form uncertainty, all response surface models considered in this case study assume the form of the model shown in Eq. (3.10). Repeating the process established before, data points were randomly sampled from the intervals given above and a data set of *30* points was acquired to construct the response surface models. Using five folds for the *k*-fold sampling process, the w-StackRSM surrogate was constructed by weighing each of the five individual models based upon their respective residuals, as shown in Eqs. (3.6-3.8). Considering the five individual models, the w-StackRSM model, and a full LS-RSM model, the residual error for each model can be determined given the *30* data points used in the model construction process (Table 3.4).

Table 3.4: *Case 2 Residuals (n=30, k=5)*

Model	*Residual*
M_1	*0.005867*
M_2	*0.006015*
M_3	*0.007162*
M_4	*0.008089*
M_5	*0.009543*
w-StackRSM	*0.004435*
LS-RSM	*0.004257*

For the second case study considered, similar results to the first problem are observed. Focusing initially on only the first six models, it is apparent that the w-StackRSM approach yields a model with a smaller residual error than its five constituent, independently cross-validated models. When comparing the performance of the w-StackRSM approach to the traditional LS-RSM approach, it is once again observed, as expected, that the LS-RSM approach will yield the smallest residual error when only the data that is utilized in the construction of the model is considered. To test the merit of these two approach to data not considered in the construction of the model, *30* additional data points are once again sampled, and only the residual of these models with respect to this *a poseriori* data is considered. Repeating this process *100* times yields the average residuals shown in Table 3.5.

Table 3.5: *Average Residuals for Additional Data Set, Case 2 (m=100)*

Model	*Avg. Residual*
w-StackRSM	*0.03969*
LS-RSM	*0.04097*

Once again, it is observed that when determined using an independent data set, the w-StackRSM approach yields a surrogate model with a smaller residual error than the traditional LS-RSM approach while still using the same original data set.

3.4. Concluding Remarks on Surrogate Modeling

From the validation cases presented above, a couple of conclusions can be developed. It is apparent from the results that, when a residual error is used as the figure of merit in evaluating the accuracy of a response surface model, the least-squares response surface methodology will yield the lowest residual error for any form of a surrogate. This accuracy is ensured through the formulation of the least-squares approach, which mathematically minimizes the residual error with the beta coefficients as the design variables. As such, the w-StackRSM approach will never yield a smaller residual than the least-squares RSM approach when only considering the points used in the construction of the model.

Proper validation and analysis of error in a surrogate model, though, should be an independent process from the model formulation itself. As such, the points that were used in the construction of a model should not be used in the evaluation of the accuracy of a model as the model will, by design, be most accurate at and near those points. Instead, to test the predictive ability of a surrogate model, an independent set of data points should be used to test the ability of the model to predict a response outside of points that were used in the construction of the model. In this case, after formulation of the models, additional samples were obtained through and independent sampling of the design space to test the predictive capabilities of both the w-StackRSM approach and the LS-RSM approach. It was observed that the w-StackRSM approach

yielded approximately a *3-6%* reduction in residual when compared with the classic LS-RSM approach. It can then be inferred—due to the comparable computational cost—that in instances where the classical least-squares response surface methodology is to be employed, that employing the w-StackRSM approach will yield a more accurate model at no increase the required simulation or data costs.

4. Uncertainty Definition

Uncertainty in the prediction of a response through a simulation-based modeling process can be thought of as taking one of three forms: parametric, predictive, and model-form uncertainty (47). For the prediction of a generic output response of interest *y*, this breakdown of uncertainty can, for a general modeling problem, be shown by the equation and definitions shown in Figure 4.1.

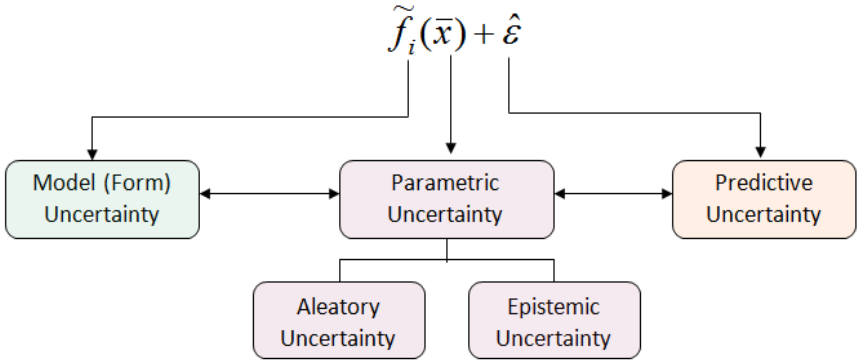

Figure 4.1: Modeling Uncertainty Breakdown

In Figure 4.1, $\tilde{f}_i(\bar{x})$ represents the result of model *i*, to a set of input parameters, $\bar{x}$. The second term in the equation, $\hat{\varepsilon}_i$, represents the discrepancy between the result of model *i*, and the true physical value of the output of interest, *y*. Given this

representation of a modeling problem, the selection of the appropriate model, $\widetilde{f}_1(\bar{x})$, is representative of the model-form uncertainty, the variation of $\widetilde{f}_1(\bar{x})$ due to uncertainties in the set of input parameters, $\bar{x}$ is representative of parametric uncertainty, and the determination of the value of $\hat{\varepsilon}_i$ represents the predictive uncertainty inherent to model *i*. The three forms of uncertainty detailed above are defined uniquely, but are often closely coupled for modeling problems of interest. As such, careful and rigorous consideration must be given to decide which uncertainties will be quantified within the modeling process and which uncertainties can be considered to be negligible with respect to the others.

4.1. Parametric Uncertainty

Parametric uncertainty refers to the uncertainty in the parameters, or inputs, into a model of interest. Simulation models require inputs into the system to represent aspects of the physical scenario such as dimensions, material properties, environmental conditions, or modeling properties. Most models require that these values be input as deterministic values for each of the parameters of interest. However, it is often possible, and likely, that the value for any parameter in the true physical scenario cannot always be known with infinite precision. As such, there is an uncertainty in the assignment of a value to any parameter within a model. This uncertainty is what is referred to as parametric uncertainty. Parametric uncertainty can commonly be defined

as taking one of two forms: aleatory and epistemic uncertainty, based upon the amount of information known regarding the uncertainty in the parameter (44,48).

Aleatory Uncertainty:

Aleatory uncertainty is defined as the uncertainty that arises as a result of natural, unpredictable variation in the performance of the system (49). This type of uncertainty is commonly thought of as an uncertainty to which enough information is known to assign probability density functions to represent the random nature of the variable. While the form of this density function could range from uniform to a complex custom density, it is assumed that the variability of the parameter is understood well enough that the density function accurately represents it without introducing additional error.

Epistemic Uncertainty:

Epistemic uncertainty is defined as any uncertainty that is due to the lack of knowledge regarding the behavior of a system that could, in theory, be resolved through the introduction of additional information (50). In terms of this definition, any type of uncertainty, including model-form and predictive uncertainty can be thought of as epistemic, as they are uncertainties which could, in theory, be reduced by the introduction of more information into the problem. However, in the scope of this work, the phrase epistemic uncertainty will be used to refer to epistemic uncertainties in the parameters of a model. Epistemic uncertainty is commonly referred to as incomplete

uncertainty; or more simply put, inherent variability of which not enough is known to accurately approximate the uncertainty through a form such as a density function. If a density function was assumed, it would introduce additional errors, and as such, additional uncertainty into the problem due to the inaccuracies in the assumptions of both the form and distribution of the parameter. This is often the case in situations where a very limited sample size is available, and no further information is known regarding the parameter.

4.2. Model-Form Uncertainty

When simulation modeling is utilized in engineering problems, there are often multiple models available to represent the same situation. Examples of this can include modeling packages among various fidelities or even differing assumptions regarding a model within the same level of fidelity, as a result of varying boundary conditions, different theories of behaviors or response, linearity assumptions, or mesh sizes. In well-understood phenomena or problems, these models are often refined through validation and verification metrics and a "best" model will often emerge. In this work, the term "best" model implies the model that most accurately represents the physical scenario being modeled. However, in many multi-physics problems, there exists a significant uncertainty in the selection of the best model, or more specifically, the assumptions made to represent a given physical scenario. As a result of this uncertainty, multiple models across different fidelities or even within the same fidelity

can produce different results for the same physical problem of interest. These discrepancies among the models are the result of the different assumptions that go into forming the individual models. As such, in order to completely quantify the uncertainty that is present in the modeling process, it is crucial that not only the parametric uncertainties be quantified, but also the uncertainty that exists in the selection of the "best" model—the model-form uncertainty.

4.3. Predictive Uncertainty

While model-form uncertainty denotes the discrepancies between multiple models of interest, predictive uncertainty denotes the difference between a model and the true physical scenario that is being represented in the model (51). The presence of predictive uncertainty is a direct result of the simplifying assumptions made in the construction of a model, such as an inviscid or incompressible flow assumption in an aerodynamic analysis. As a result, each individual model has its own unique predictive uncertainty associated with it, as the assumptions in each model are not necessarily the same. The predictive uncertainty associated with a model is often considered in the model validation process.

To quantify predictive uncertainty, information regarding the true physical scenario of interest must be known. While this information is commonly experimental data points, a couple of caveats are introduced. The experimental data that is acquired is not necessarily infallible for a couple of reasons. First, experiments are often done on

a reduced order model, or at least a model with artificial constraints--such as a full-scale wing test in a wind tunnel. As such, the experiment could technically be considered an additional model. In addition, measuring the value of parameters or outputs in an experiment is an imprecise science. As such, there is additional uncertainty introduced to the problem in that the supposed true value is also an uncertain value. To represent the complete picture of uncertainty, Kennedy and O'Hagan represent the true physical scenario as shown in Eq. (4.1) (47).

$$d_k = \gamma \Pr(M_i \mid \theta_k) + \delta(y_i) + \varepsilon_{\exp} \tag{4.1}$$

In Eq. (4.1), d_k represents the true physical value of the output response of interest—such as flutter velocity. The equation shows that this true value is actually the sum of three different terms. In the first term, γ represents an unknown regression parameter that cannot be solved for empirically. $Pr(M_i|\theta_k)$, represents the results of model *i* given the parameter set, θ_k. This could either be a probability distribution, as denoted by the equation, or a deterministic value if the model is deterministic in nature. $\delta(y_i)$ is the discrepancy term in the equation that represents the difference between the model result and the true physical scenario. This function is also referred to as the model inadequacy function (47), and it is independent of the model output, $Pr(M_i|\theta_k)$. Finally, ε_{exp} is the observation error term, and it represents the uncertainty that exists in the measurement of output d_k. This term can either be a deterministic value, or a distribution representing the uncertainty in the measurement of the experimental value. By rearranging Eq. (4.1), expressions for different representations of the

predictive uncertainty for a modeling problem can be developed, as will be shown in the following sections.

5. Uncertainty Quantification

Although the three types of uncertainty detailed in the prior section are defined uniquely, they are not necessarily independent of one another. While methods exist in the literature for quantification of one or more types of uncertainty in a simulation problem of interest, there are often multiple additional assumptions that are made in this uncertainty quantification process that restrict these approaches from being utilized to quantify the uncertainties from all possible sources. Looking at the field of simulation-based design in aerospace engineering, much of the work done in uncertainty quantification has focused upon only the quantification of the parametric uncertainties in the modeling process. Pettit summarized the approaches utilized for uncertainty quantification in aeroelastic design as well as detailed challenges facing the community--included in which quantifying the uncertainty associated with the analysis itself (52). With respect to uncertainty quantification in flutter calculations, work in the literature has primarily concentrated upon quantifying the effects of parametric uncertainties. Cheng et.al explored the effects of uncertainties in structural parameters on the quantification of the flutter velocity for suspension bridges suspect to high velocity wind loads (53). Kurdi et.al looked specifically at the AGARD 445.6 wing and the effects of parametric uncertainty on the flutter boundary of the wing through Monte Carlo Sampling (54). Similarly, Beran et.al looked at the effects of uncertain parameters

on limit-cycle oscillations using stochastic expansion methods (55). This work was expanded upon by Witteveen and Bijl to develop an Unsteady Adaptive Stochastic Finite Element (UASFE) approach for the quantification of uncertainties in the transonic flutter of a NACA0012 airfoil (56). The methods for the quantification of parametric uncertainties have been developed and matured, but are incapable of quantifying the uncertainty from all of its possible sources.

The effects of the other two forms of uncertainty—model-form and predictive—are less considered, but have not been completely ignored in the literature. Much work has focused upon intrusive methods for the quantification and eventual minimization of predictive uncertainty—often referred to in the literature as model validation and verification. Chen et al have looked at the coupling effects of parametric uncertainties in the model validation process as a preliminary approach to quantifying uncertainties induced by the modeling process, but stopped short of quantifying the predictive uncertainty (57). Numerous other researchers have looked at model validation approaches in the literature, but these approaches are often intrusive with respect to the model, and unique to each problem of interest. An additional shortcoming is that in order to quantify the predictive uncertainty of a model, a representation of the physical data—most commonly experimental data of some form—must be obtained. While the presence of this data allows for the quantification of uncertainties from all sources, it is inefficient and infeasible to obtain experimental data early in the design phase of many engineering projects. In problems such as this, it is necessary to evaluate numerous

designs quickly and efficiently, meaning that obtaining experimental data for each configuration is infeasible. As predictive uncertainty can only be quantified given experimental data, predictive uncertainty cannot be quantified in cases where the experimental data is unavailable. Instead, only model-form and parametric uncertainties can be quantified in these cases.

Additionally, the computational time involved in the evaluation of many physics-based simulations can be very large. As such, it is imperative that any technique to quantify the uncertainty in the analyses must be computationally efficient by requiring a minimal number of model evaluations. It is thus necessary to develop a method that is capable of efficiently quantifying these two forms of uncertainty in the absence of experimental data points.

5.1. Parametric Uncertainty Quantification Methods

Parametric uncertainty is the most frequently considered form of uncertainty in the literature (44). These methods, in general, follow the same basic steps. They first attempt to capture the uncertainty associated with the parameters in some form. Aleatory uncertainty quantification methods will do this by representing each variable through a probability density function of any ordinate form while epistemic uncertainty quantification methods will often use a more abstract data structure such as fuzzy logic, or basic belief assignments (58). Next, these methods will attempt to propagate this

information regarding each of the variables through the simulation-based model through either exhaustive or “fast” reliability methods. The goal of this approach is normally one of two metrics of interest: developing a distribution of a single, or set of output parameters, or determining the reliability of the system of interest. The approach that the methods take to determine the output metric of interest results in the methods being split into two different categories of approaches: exhaustive sampling methods and analytical approaches.

5.1.1 Sampling Methods

Sampling methods will, in general, utilize the developed form of each of the uncertainty variables to develop a set of deterministic parameters to be utilized in subsequent model evaluations. While methods such as this are, when compared to analytical methods, more computationally expensive, they are often much easier to implement in complex simulations or with complex designs due to their non-intrusive nature. In addition, while sampling methods began as a crude approximation tool for reliability that required a restrictive number of evaluations for adequate accuracy, as the methods have matured, the applicability and usefulness of the methods have improved as well.

In general, sampling methods are capable of approximating both metrics of interest: the distribution of a set of output parameters, or simply the probability of an

event. However, there are trade-offs to these techniques, as will be discussed in the following section.

Monte Carlo Sampling:

The Monte Carlo Sampling Method (MCS) is a numerical sampling method that was first developed by Metropolis and Ulam in 1949 (59). This method is loosely defined with a wide range of approaches that follow similar patterns. The approaches first define a domain of possible uncertain input parameters, and then generate the input values randomly from this domain utilizing a specified probability distribution function for each uncertain input parameter. After generating a vector of input values, a deterministic calculation or simulation is performed using these inputs. This process is repeated multiple times and the results of each of these individual calculations or simulations are aggregated into the final result. For example, the expected value of an arbitrary distribution function $f_x(x)$ of a variable x could be estimated through the Monte Carlo Sampling method by repeatedly sampling the distribution function of the design variable k times, and taking the mean of these values, as shown in Eq. (5.1).

$$E[f_x(x)] \approx \frac{1}{k}\sum_{t=1}^{T} x_t \tag{5.1}$$

The concept can then be extended to multi-dimensional space where multiple variables defined by vector $\bar{x}$ are assumed to be represented by distributions that can each be sampled and computed in the same way as shown in Eq. (5.1)

When the samples $\{x_t, t = 1, \dots, T\}$ are independent, as is the assumption with Monte Carlo Sampling, the laws of large numbers ensure that the approximation can be made accurate by using a sufficiently large sample size, *T*. For a problem with multiple variables, a sufficiently large sample size can range well up into the millions. While a million evaluations is not entirely cost restrictive in the evaluation of a closed-form expression, traditional Monte Carlo Sampling techniques can quickly become cost-restrictive when a computational simulation is required for each evaluation of the model of interest.

In addition to the computational cost associated with Monte Carlo Sampling methods, there are other caveats. As each of the samples drawn in Monte Carlo Sampling are independent of each other, a large amount of samples will naturally fall around the mean value of each uncertain parameter. As such, it is likely that very few samples will be drawn from the extreme tails of an input parameters' distribution. In problems where the primary interest is in the tails of the distributions--as most engineering reliability problems are--this results in very few samples being observed from the tails. In fact, even with a large amount of numbers, Monte Carlo Sampling does not guarantee that any samples would be drawn from the tails of the design. As such, it very possible for Monte Carlo Sampling to grossly misestimate values that fall in the extrema of the design envelope.

Monte Carlo Sampling is most frequently used to approximate the probability of a particular event occurring, such as the amount of output values that fall below a particular threshold given initial variable distributions. This is done by sorting the resultis through a pass / fail filter with respect to the threshold value, and then finding the frequency of a particular occurrence. However, Monte Carlo Sampling can also be used to develop a distribution for this output response as well. This is done by sorting the output data points into a histogram and then approximating a probability density function to the values of the histogram. There are many sources of potential error in a method such as this, though, as a large number of evaluations are required and the final distribution can be very sensitive to the bin size of the histogram being used.

Latin Hypercube Sampling:

In order to attempt to capture the tails of a design in the sample set to be generated, McKay et al developed Latin Hypercube Sampling (LHS) in 1979 (60). In Latin Hypercube Sampling, each distribution is broken into equally probable bins based upon the amount of samples to be considered. This is done by dividing the cumulative distribution function and dividing it into *1/k* sized intervals of equal probability, where *k* is the number of sample points of interest (Figure 5.1). By then dividing the probability distribution function into the same intervals, *k* individual bins can be formed on the pdf, as shown in Figure 5.2. These bins can then be sampled, drawing one random sample from each of the bins. These sample points are then input into the deterministic

simulation in the same way as was done with Monte Carlo Sampling, and metrics regarding the output can then be computed.

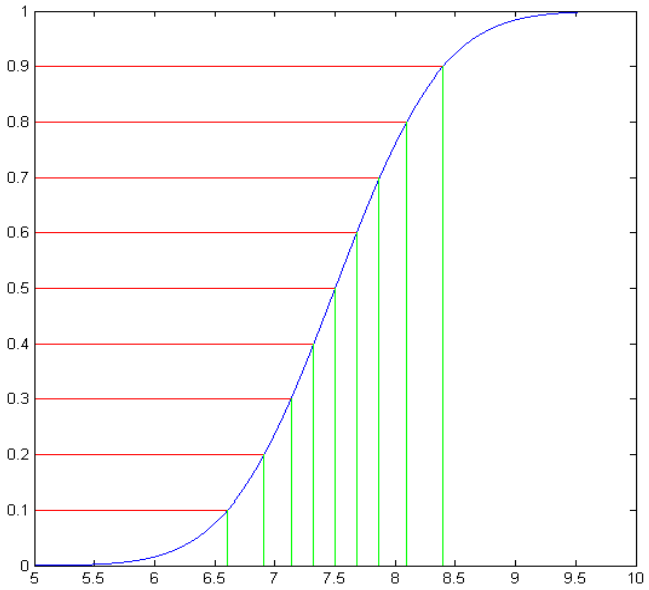

Figure 5.1: Division of CDF of a Random Variable for LHS

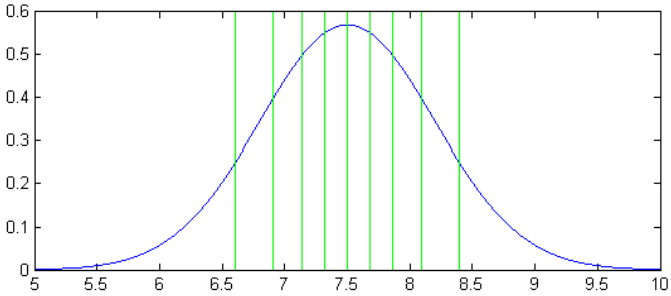

Figure 5.2: Corresponding Division of PDF of a Random Variable for LHS

Latin Hypercube Sampling provides assurance that a limited sample size will span the full range of the distribution for the variable of interest. This ensures that even with a relatively limited number of samples taken, the tails of the distributions will still be accounted for in the sample region. This idea can be extended into *n*-dimensional

space, where each variable is divided into a number of equal probability bins, and the intersections of these bins are then sampled, as shown in Figure 5.3 in a two-dimensional case.

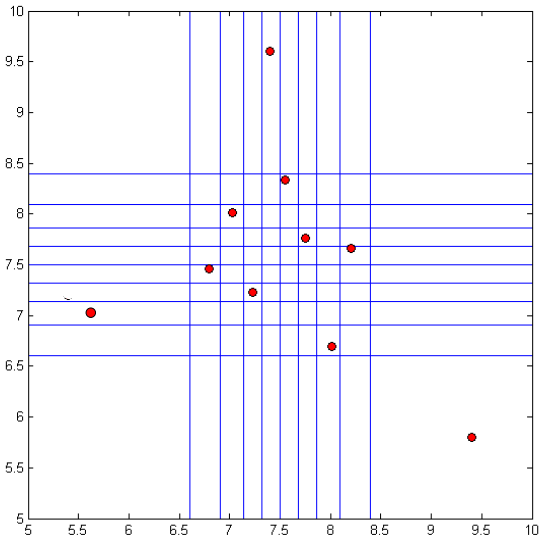

Figure 5.3: Two Dimensional LHS Sampling Scheme

Latin Hypercube Sampling still suffers from the curse of dimensionality, as more variables will require more samples to achieve the same level of confidence in the results. In addition, adding one sample to a LHS scheme after performing an analysis requires a complete restructuring of the sampling space. However, when used properly, LHS can provide a computational benefit when compared with traditional MCS in both accuracy and efficiency.

Similar to Monte Carlo Sampling, LHS can provide both the probability of a particular occurrence, or be used to approximate a distribution of the output of interest. While LHS can be more efficient at calculating the probability of a particular occurrence, it suffers from the same problems as MCS in the approximation of a distribution for an output parameter of interest.

Markov Chain Monte Carlo Sampling:

While traditional Monte Carlo Sampling generates a sequence of random variables $\{x_1, x_2, \dots, x_T\}$ where each sample, x_t, is independent of the prior states, x_{t-1}. In Markov Chain Monte Carlo Sampling (MCMCS), the next state x_{t+1} is sampled from a distribution, $f(x_{t+1}|x_t)$, which depends only upon the current state of the chain, x_t. Thus, after a sufficient break-in period of *p* iterations, points $\{x_t;\ t = p+1, \dots, T\}$ will then be dependent samples from the original data set $\{x_1, x_2, \dots, x_T\}$. After discarding the samples from the burn-in period of the chain, the expected value of the single model, $f_x(x)$, can then be calculated from Eq. (5.2).

$$E[f_x(x)] = \frac{1}{T-p}\sum_{t=p+1}^{T} x_t \tag{5.2}$$

Next, it must be determined how to construct a Markov chain such that the new state, x_{t+1} depends only upon its prior state, x_t. Many such chains have been proposed in the literature, the first by Metropolis et al. in 1953 (61). For this algorithm, the next state in the sample, x_{t+1} is determined using a proposal density $Q(x'|x_t)$, to generate a new proposed sample, x'. The proposal density $Q(x'|x_t)$ is defined based upon the

current sample x_t. Such a proposal density for a Gaussian Function can be shown in Eq. (5.3) where the distribution is centered on the current point x_t.

$$Q(x'|\,x_t) \sim Norm\left(x_t, \sigma^2\right) \tag{5.3}$$

The Metropolis algorithm defines this proposal density to be symmetric, meaning that $Q(x'|x_t) = Q(x_t|x')$. As such, the proposed next state x' is accepted as the next value (e.g. $x' = x_{t+1}$) if a value α, drawn from a *Uniform(0,1)* distribution satisfies Eq. (5.4).

$$\alpha < \frac{P(x')Q(x_t \mid x')}{P(x_t)Q(x'|\,x_t)} \tag{5.4}$$

If Eq. (5.4) does not hold true, then the future state remains the current state: $x_{t+1} = x_t$. Additional chains have been proposed in the literature by Tierney (62), Roberts (63), and Gilks (64). Due to the robust operating ability and efficiency shown in the literature (61), the original chain proposed by Metropolis et al. in 1953 will be used in this work where Markov Chain Monte Carlo Sampling is implemented.

MCMCS is different than LHS or traditional MCS in that its sampling method is biased, meaning that post-processing of the output data must be done in order to quantify any information to be extended regarding the output. Similar to the other sampling methods, MCMCS is quite adept at approximating the probability of a particular event, but can experience errors in the generation of a full distribution function to represent the potential variation in a particular output parameter.

Distribution Fitting:

All three of the sampling methods discussed above produce a set of output responses $\{y_1, y_2, \dots, y_T\}$ as a function of the *T* input parameter sets: $\{x_1, x_2, \dots, x_T\}$. If a pdf representation of the output response is needed, this can be done by fitting a distribution to the data set. A distribution form must first be assumed in this approach. In the absence of any additional information, a Gaussian form shall be assumed for the data set (Eq. (5.5)).

$$f_y(y;\mu,\sigma) = \frac{1}{\sqrt{2\pi\sigma^2}} e^{-\frac{(y-\mu)^2}{2\sigma^2}} \tag{5.5}$$

The two parameters μ and σ^2 can then be estimated using the Method of Moments as shown in Eqs. (5.6)-(5.7).

$$\mu = \frac{1}{T}\sum_{i=1}^{T} y_i \tag{5.6}$$

$$\sigma^2 = \frac{1}{T-1}\sum_{i=1}^{T} (y_i - \mu)^2 \tag{5.7}$$

While a Gaussian distribution is the most general form of a distribution, they are not capable of handling distributions with skewness. A four-parameter Beta distribution is a more robust form of a distribution that, while still capable of handling a non-skewed distribution such, can capture skewness as well. As such, for the given data set in Eq. (5.4), a Beta distribution of the form shown in Eq. (5.8) can be assumed.

$$f_y(y;a,b,\alpha,\beta) = \frac{1}{B(\alpha,\beta)} \frac{(y-a)^{\alpha-1}(b-y)^{\beta-1}}{(b-a)^{\alpha+\beta-1}} \tag{5.8}$$

The *a* and *b* parameters in Eq. (5.8) represent the lower and upper bound for the distribution. As such, given a reasonably well populated data set (*n* > 1,000), *a* and *b* can be defined as shown in Eq. (5.9) and (5.10).

$$a = \min[\, y_1, \ldots, y_T \,] \tag{5.9}$$

$$b = \max[\, y_1, \ldots, y_T \,] \tag{5.10}$$

Given two parameter values, the other two parameters can be estimated using the Method of Moments as shown in Eqs. (5.11) and (5.12).

$$\alpha = \frac{\bar{y} - a}{b - a}\left[\frac{\left(\frac{\bar{y} - a}{b - a}\right) - \left(1 - \frac{\bar{y} - a}{b - a}\right)}{\frac{s^2}{(b - a)^2}}\right] \tag{5.11}$$

$$\beta = \left(1 - \frac{\bar{y} - a}{b - a}\right)\left[\frac{\left(\frac{\bar{y} - a}{b - a}\right) - \left(1 - \frac{\bar{y} - a}{b - a}\right)}{\frac{s^2}{(b - a)^2}} - 1\right] \tag{5.12}$$

where:

$$\bar{y} = \frac{1}{n}\sum_{i=1}^{n} y_i \tag{5.13}$$

$$s^2 = \frac{1}{n}\sum_{i=1}^{n} (y_i - \mu)^2 \tag{5.14}$$

5.1.2 Analytical Methods

As mentioned in Section 5.1, calculating the probabilistic response of a system to uncertain parameters is very sensitive to the number of uncertain parameters that are input into the problem. In a subset of the uncertainty quantification field-- reliability-- the metric of interest is the probability of failure (P_f) of a system, where failure is defined as the violation of a particular set of constraints, as mentioned in Section 5.1.1. The evaluation of this probability of failure is paramount to the quantification of the uncertainty present in the modeling problem. To determine the probability of failure, a limit state function *g(x)* is first defined where a value of *g(x)* less than zero indicates a failure of the design. Using Eq. (5.15) the probability of failure of the system can be evaluated through the *n*-dimensional integration of the joint PDF of all uncertain variables, $\{x_1, x_2, \dots, x_n\}$.

$$P_f = \Pr[g_x(x_1,...,x_n) \le 0] \int_{g_x(x_1,...,x_n)} ... \int f_x(x_1,...,x_n) dx_1 ... dx \qquad (5.15)$$

Evaluation of the integral shown in Eq. (5.15) is difficult in most modeling problems as there is no closed-form expression available for the joint-pdf of all *n* variables, $f_x(x_1,..,x_n)$, or the limit state function $g_x(x)$. As such, most analytical methods will concentrate upon representing the limit state function through some sort of surrogate expression, and use that surrogate to evaluate the probability of failure for the system. This, however, will only provide the probability of failure and not a probability distribution function of any output parameters. To remedy this, additional methods exist to evaluate an expression for $f_x(x)$ in closed form to provide a distribution

of an output parameter of interest, $f_y(y)$ where $y = f(x)$. These methods each quantify the system response in different ways to produce varying levels of accuracy with different levels of computational effort (65). These methods will be introduced in this section and their relative merit and applicability within a complete uncertainty quantification framework will be discussed.

FORM and SORM

As mentioned before, many analytical methods attempt to approximate the limit state function $g(x)$ so that closed-form evaluation of Eq. (5.15) is possible. The First Order Reliability Method (FORM) and Second Order Reliability Method (SORM) approximate this function through the use of first- and second-order Taylor series respectively (66). For FORM, this approximation is represented by Eq. (5.16) where $g_x(x)$ is the limit-state to be approximated, n is the number of variables in the problem, and c_i are a set of constants to be solved for.

$$g_x(x) = c_0 + \sum_{i=1}^{n} c_i x_i \tag{5.16}$$

The SORM method utilizes a similar approximation to Eq. (5.16), but with a quadratic term included as well. The question then becomes what values of the design variable vector should this approximation be formed around. In reliability analysis, the safety-index approach is used to find the most probable point (MPP) of failure, and this point is used as the basis point for the approximation of the limit-state function. In general terms, any such point could be used to form the approximation around, but

with the possibility of increased error due to the linear or quadratic nature of the approximation. In addition, different approximation methods can be used to form a surrogate for either the joint pdf or the limit state function.

After constructing an approximation of the limit-state function, the *n*-dimensional integral shown in Eq. (5.15) can then be evaluated to solve for the probability of failure. This provides a numeric value for the probability that the output of the system violates any of the set constraints, much in a similar way as the sampling methods. However, these methods are unable to provide a distribution of the output parameter of interest, but instead, only the probability that it falls above or below a prescribed value in the design space.

Fast Fourier Transforms (FFT):

Another method for the quantification of the uncertainty in an engineering modeling problem, and more specifically, the estimation of the probability of failure, is to compute and evaluate the cumulative distribution function of the limit-state function (or in the case of simple uncertainty quantification, the CDF of the joint probability distribution function). Similar to the joint pdf, though, this evaluation is often unavailable in closed-form, and can be very costly to compute. However, the Fast Fourier Transform (FFT) technique has been developed for an efficient evaluation of the reliability of a system by solving the convolution integral to estimate the limit-state

function of the problem. The applicability of this approach to engineering problems has been demonstrated in the literature for both structural reliability estimates (67) and numerical simulations schemes (68).

The Fast Fourier Transform technique first requires that the output of interest be approximated as a linear combination of intervening variables, as shown in Eq. (5.17).

$$f_y(y) = z_1 + z_2 + \ldots + z_n \tag{5.17}$$

In Eq. (5.17), *y* is the output response of interest, a function of variables $\{x_1 - x_n\}$ and z_i is an intervening variable defined to make the function approximation a linear combination of these variables. The intervening variables are functions of the original variables *x,* where $x \rightarrow \{x_1 - x_n\}$. The approximation of the function can take many forms ranging from a simple Taylor Series expansion to multi-point approximations such as response surface approximations or Two-Point Nonlinear Approximations (TANA). The accuracy of the Fast Fourier Transform is a function of how accurately these approximations of the output response of interest estimate the actual response of the model. In this work, weighted Stack Response Surface Methodology (w-StackRSM) discussed in Section 3.2 was utilized to approximate the output response subject to the uncertain input parameters. This approach was selected due to its relative efficiency and accuracy, the fact that it does not require gradients for the approximation, which are not analytically available in the simulation being used in this work, and the fact that the form of the surrogate is easily tailorable to exclude the interaction terms. As the

approximation for the output response must remain a linear combination of the intervening variables for the Fast Fourier Transform technique, interaction terms in a surrogate model could not be considered in the approximation.

After a linear approximation of the output value of interest is obtained, the probability distribution of the intervening variables must be obtained. Using the Chain Rule, the distributions of the intervening variables z_i can be obtained as shown in Eq. (5.18) where $z_i = f(x_j)$.

$$f_{z_i}(z_i) = \frac{dx_j}{dz_i} f_{x_j}(z_i) \tag{5.18}$$

As $f_y(y)$ is now a linear function of the intervening variables, its distribution can be solved for by the convolution of the intervening variables, as shown in Eq. (5.19).

$$f_y(y) = f_{z_1}(z_1) * f_{z_2}(z_2) * \ldots * f_{z_n}(z_n) \tag{5.19}$$

The convolution shown in Eq. (5.19) can be solved for by first applying a Fast Fourier Transform to both sides of the equation, as shown in Eq. (5.20).

$$FFT\left[f_y(y)\right] = FFT\left[f_{z_1}(z_1)\right] \cdot FFT\left[f_{z_2}(z_2)\right] \cdot \ldots \cdot FFT\left[f_{z_n}(z_n)\right] \tag{5.20}$$

Using the properties of Fourier Transforms, $FFT[f_y(y)]$ can be solved for as the product of the FFTs of each of the intervening variables. After performing the product shown in Eq. (5.20), the distribution of $f_y(y)$ can be obtained by taking the inverse

Fourier Transform of *FFT[$f_y(y)$].* In this work, the inverse Fourier Transform is done numerically, resulting in a discrete set of n_{int} values and probabilities. Using discrete statistics, the first and second moments of the data can be estimated as shown in Eqs. (5.21) and (5.22):

$$E[y] = \sum_{i=1}^{n_{\text{int}}} p_{\text{int}} x_{\text{int}} \tag{5.21}$$

$$Var[y] = \sum_{i=1}^{n_{\text{int}}} p_{\text{int}} (x_{\text{int}} - E[y])^2 \tag{5.22}$$

As such, a number distribution can be selected to fit the data to, as discussed in Section 5.1.1. In this work, two distributions were selected for demonstration--Gaussian and Beta distributions.

5.2. Model-Form Uncertainty Quantification

Many methods in the literature that quantify model-form uncertainty require the presence of experimental data points to quantify predictive uncertainty as well. An example of this is Bayesian Model Averaging (69), which will be discussed in further detail in Section 5.3, that uses the experimental data to develop maximum likelihood estimates for each of the models—quantifying the predictive uncertainty--and to approximate model probabilities using Bayes Theory—quantifying model-form uncertainty. However, this methodology is not applicable in its current form to problems without experimental data available. Many other methods in the literature

are also not applicable due to similar conflicts. The methods of Continuous Model Expansion explored by Drapert showed a reliance on experimental data points, as well as difficulty in handling asymmetric distributions of parametric uncertainties (70). Likewise, work done recently by Allaire and Willcox requires a maximum entropy representation of the modeling uncertainty, an extra step that could be cost-intensive for a high simulation-cost model (71). The common thread among these methods is that they use experimental data to quantify the model-form uncertainty and identify the best models. However, in the absence of experimental data, other metrics must be utilized to quantify this uncertainty.

5.2.1. Adjustment Factors Approach:

The adjustment factors approach was first demonstrated by Mosleh and Apostolakis as a method to utilize expert opinions in the absence of experimental data to quantify model-form uncertainty using an adaptation of Bayes' Theorem (72). The adjustment factors approach modifies the result of the best model—the model with the highest model probability among the model set being considered—by an adjustment factor to account for the uncertainty that exists in the selection of the best model: model-form uncertainty. The applicability of this approach to engineering problems has been demonstrated in the literature. Zio and Apostolakis used an adjustment factors approach to quantify the uncertainty in the selection of radioactive waste repository

models (73). In addition, Reinert and Apostolakis included an adjustment factors approach in the assessment of risk for decision-making processes (74).

Two derivatives of the adjustment factors approach exist in the literature. The derivations of the approaches employ the similar technique of quantifying the model-form uncertainty through the use of expert opinions regarding each individual model's accuracy relative to the other models. This is done through the assigning of model probabilities to each of the models, most commonly based upon expert opinions regarding the relative merit and accuracy of each individual model. In this approach, $Pr(M_i)$ represents the probability of model *i.* By definition, this is the probability that model *i* is the best model among the model set being considered: $M = \{M_1, M_2, \ldots, M_N\}$.

The model probabilities for each of the *N* individual models within the model set *M* remain bounded by the laws of probability theory. Thus, constraints are applied to the model probability values, as shown in Eq. (5.23).

$$\sum_{i=1}^{N} \Pr(M_i) = 1 \qquad \text{such that} \qquad 0 \le \Pr(M_i) \le 1 \tag{5.23}$$

Where the various derivations of the adjustment factor approach differ is with the form of the factor that is used to adjust the "best" model--specifically the distribution assigned to the factor. In the additive adjustment factors approach, the adjusted model, *y,* is formed by adding an additive adjustment factor, E_a^*, to the best model in the model set being considered, as shown in Eq. (5.24).

$$y = y^* + E_a^* \tag{5.24}$$

The response of the best model, y^*, is simply defined as the prediction of the model with the highest model probability. The additive adjustment factor, E_a^*, is assumed to be a normally distributed factor that represents the uncertainty in the selection of the most accurate model, the model-form uncertainty in the problem. By assuming a Gaussian form to this factor, the first and second moments of the additive adjustment factor can be calculated as shown in Eqs. (5.25)-(5.26).

$$E[E_a^*] = \sum_{i=1}^{N} \Pr(M_i)(y_i - y^*) \tag{5.25}$$

$$Var[E_a^*] = \sum_{i=1}^{N} \Pr(M_i)(y_i - E[y])^2 \tag{5.26}$$

Where y_i the prediction of model *i*. By definition, the models considered in the traditional formulation of the adjustment factors approach are assumed to be deterministic. As such, the expected value of the adjustment model, denoted as *E(y)*, can be calculated as shown to be the sum of the best models result and the expected value of the additive adjustment factor, as shown in Eq. (5.27).

$$E[y] = y^* + E[E_a^*] \tag{5.27}$$

Similarly, as each individual model is deterministic, the variance of the adjusted model *y* can be said to be equal to the variance of the additive adjustment factor, as shown in Eq. (5.28).

$$Var[y] = Var[E_a^*] \tag{5.28}$$

The first and second moments shown in Eqs. (5.27)-(5.28) now fully define a normally distributed adjusted model, *y*, that represents the uncertainty in the calculation of an output value as a result of model-form uncertainty. There exist additional derivations of the adjustment factors approach in the literature for different assumptions regarding the distribution of the adjustment factor itself (72). In the multiplicative adjustment factors approach, the adjustment factor E_m^* is assumed to be a lognormal random variable, as opposed to the normality assumption that was applied to the adjustment factor, E_a^*, in the additive adjustment factors approach. Thus, the adjusted model for the multiplicative is shown in Eq. (5.29).

$$y_m = y^* * E_m^* \tag{5.29}$$

Similar to the derivation of the additive adjustment factor, the multiplicative adjustment factors approach first calculates the first and second moments of the multiplicative adjustment factor, E_m^*, as shown in Eqs. (5.30) and (5.31).

$$E\left(\ln\left(E_m^*\right)\right) = \sum_{i=1}^{N} \Pr(M_i)\left(\ln\left(y_i\right) - \ln\left(y^*\right)\right) \tag{5.30}$$

$$Var\left(\ln\left(E_m^*\right)\right) = \sum_{i=1}^{N} \Pr(M_i)\left(\ln\left(y_i\right) - E\left(\ln\left(y\right)\right)\right)^2 \tag{5.31}$$

The key differences between the Eqs. (5.25)-(5.26) and Eqs. (5.30)-(5.31) are that in the multiplicative adjustment factors approach, that the model outputs are lognormally transformed before calculating their moments, to account for the lognormal assumption regarding the adjusted model. The model probabilities in Eqs. (5.30) and (5.31), are assigned with the same constraints that are set upon the additive

adjustment factors approach. Once the expected value of the multiplicative adjustment factor is known (Eq. (5.30)), the expected value of the adjusted model, y_m, can be found using Eq. (5.32) as the sum of the lognormally transformed best model result and multiplicative adjustment factor.

$$E\left(\ln\left(y_m\right)\right) = \ln\left(y^*\right) + E\left(\ln\left(E_m^*\right)\right) \tag{5.32}$$

Finally, similar to the additive adjustment factors approach, the variance of the adjusted model, y_m, can be shown to be equal to the variance of the multiplicative adjustment factor (Eq. (5.33)).

$$Var\left(\ln\left(y_m\right)\right) = Var\left(\ln\left(E_m^*\right)\right) \tag{5.33}$$

However, in the absence of any data suggesting else wise, a normally distributed adjustment factor is used in this research.

While the traditional adjustment factors approaches are capable of quantifying model-form uncertainty without experimental data points, they are incapable, in the presented form, of quantifying or even handling parametric uncertainties within each of the individual models. This incapability is due to the assumption made in the derivation that each of the individual models in the adjustment factors approach be deterministic. However, if the adjustment factors approach shown above was to be re-derived with the assumption that each individual model be stochastic in nature with an assigned form, the approach could be adapted to handle parametric uncertainty.

5.2.2. Probabilistic Adjustment Factors Approach:

The probabilistic adjustment factors approach is an adaptation of the traditional adjustment factors approach derived to handle stochastic models. While this approach does not quantify the parametric uncertainty within each model, it can stochastic models provided that the output quantity of interest in the models is represented through a probability density function. In the probabilistic adjustment factors approach, similar to the traditional adjustment factors approach, a distribution is assumed for each of the individual models, as well as the adjustment factor itself. In general, there are no restrictions on the form of this distribution other than that it be defined. However, similar to the additive adjustment factors approach detailed before, each of the individual models will initially be assumed to be normally distributed, as shown in Eq. (5.34).

$$f_{y,i}(y) = norm(\mu_i, \sigma_i^2) \forall i = 1...N \tag{5.34}$$

Model probabilities are then applied to each of the models shown in Eq. (5.34) such that the constraints in Eq. (5.23) are still satisfied, identical to the methods used in the traditional adjustment factors approaches. The adjusted model for the probabilistic adjustment factors approach can then be computed as shown in Eq. (5.35).

$$y = E[y^*] + E_a^* \tag{5.35}$$

Eq. (5.35) is similar to Eq. (5.25) with the exception that since each model, including the best model y^* is stochastic, that the expected value of y^* is what is operated on rather than the deterministic model result. Calculating the first and second

moments of the additive adjustment factor E_a^* is also slightly different for this new approach, as the approach had to be re-derived to handle the stochastic model set. The calculation of these two moments can be seen in Eqs. (5.36)-(5.37).

$$E[E_a^*] = \sum_{i=1}^{N} \Pr(M_i)(E[y_i] - E[y^*]) \tag{5.36}$$

$$Var[E_a^*] = \sum_{i=1}^{N} \Pr(M_i)(E[y_i] - E[y])^2 \tag{5.37}$$

After calculating the first and second moments of the additive adjustment factor, the expected value and variance of the adjusted model can then be calculated as shown in Eqs. (5.38) and (5.39).

$$E[y] = E[y^*] + E[E_a^*] \tag{5.38}$$

$$Var[y] = Var[E_a^*] + \sum_{i=1}^{N} \Pr(M_i)(Var[y_i])^2 \tag{5.39}$$

While the representation for the expected value of the adjusted model remains relatively unchanged from the traditional to the probabilistic adjustment factors approach, there is a noticeable difference in the formulation of the equation for the variance of the model. The variance computed in Eq. (5.39) is shown to be a sum of two terms. The first term represents the variance in the adjusted model that is due to the variance between each of the individual models--between-model variance--which arises as a result of the different assumptions that are used within each model. The second term in the equation represents the variance in the adjusted model due to variances within each of the individual models--the within-model variance. As such, the first term

in Eq. (5.39) can be thought of as representing the model-form uncertainty within the problem while the second term represents the parametric uncertainties inherent to each of the individual models.

The above approach was derived with the assumption that the parametric uncertainty within each individual model be represented by a Gaussian distribution. However, as mentioned, the approach can be applied to any number of predefined distributions for outputs of the models. To demonstrate an additional, more robust distribution, and to broaden the scope of output responses that can be represented, the probabilistic adjustment factors approach was also derived for models with a Beta distribution in the following.

Similar to the assumption with Gaussian models, it is first assumed that the distribution of the output response of interest for each individual model can be represented with a Beta distribution as shown in Eq. (5.40).

$$f_{y,i}(y) = beta(a_i, b_i, \alpha_i, \beta_i) \forall i = 1...N \tag{5.40}$$

The adjusted model can then be developed by adding a parameter with a beta distribution, E_{β}^{*}, to the expected value of the best model y^{*} as shown in Eq. (5.41).

$$y = E[y^{*}] + E_{\beta}^{*} \tag{5.41}$$

While the Gaussian form demonstrated before only requires two parameters to be estimated, the beta-distributed form requires the estimation of four parameters.

However, due to the definition of the *a* and *b* parameters as the upper and lower bounds to the distribution, the limit parameters of the adjusted model *y* can be computed as the weighted values of the individual model bounds, as shown in Eqs. (5.42) and (5.43).

$$a = \sum_{i=1}^{N} \Pr(M_i) a_i \tag{5.42}$$

$$b = \sum_{i=1}^{N} \Pr(M_i) b_i \tag{5.43}$$

As two parameters are already defined in the adjusted model *y*, only two moments of the model are then needed to estimate the two shape parameters in the adjustment model, α and β. Thus, the same approach that was used to derive the moments for the Gaussian form can be used for the beta form. The derivation of these two moments is shown in Eqs. (5.44) and (5.45) where the calculation of the first and second moments of the adjustment factor are shown in Eqs. (5.46) and (5.47).

$$E[y] = E[y^*] + E[E_\beta^*] \tag{5.44}$$

$$E[y^2] = E[E_\beta^{*2}] + \sum_{i=1}^{N} \Pr(M_i) E[y_i^2] \tag{5.45}$$

$$E[E_\beta^*] = \sum_{i=1}^{N} \Pr(M_i) \left(E[y_i] - E[y^*] \right) \tag{5.46}$$

$$E[E_\beta^{*2}] = \sum_{i=1}^{N} \Pr(M_i) \left(E[y_i] - E[y] \right)^2 \tag{5.47}$$

After obtaining the first and second moments of the adjusted model *y* using the probabilistic adjustment factors approach, the two remaining parameters to define the

adjusted model, α and β , must be determined. Using the Method of Moments, the shape parameters of any Beta distribution can be approximated from the first and second statistical moments of the distribution, as shown in Eqs. (5.48) and (5.49).

$$\alpha = \frac{\left(\frac{E[y]-a}{b-a}\right)^2\left(1-\frac{E[y]-a}{b-a}\right)}{\frac{E[y^2]}{(b-a)^2}} - \frac{E[y]-a}{b-a} \tag{5.48}$$

$$\beta = \frac{\left(\frac{E[y]-a}{b-a}\right)\left(1-\frac{E[y]-a}{b-a}\right)^2}{\frac{E[y^2]}{(b-a)^2}} + \frac{E[y]-a}{b-a} - 1 \tag{5.49}$$

As such, the four parameters of the adjusted model *y* are defined by Eqs. (5.42)-(5.43) and Eqs. (5.48)-(5.49).

The probabilistic adjustment factors approach provides a method that—given the parametric uncertainty within each model is first quantified and represented as a pdf of some output response of interest—can quantify both the parametric and model-form uncertainties in the estimation of a particular output response of interest. As such, a parametric uncertainty quantification method that is capable of producing a pdf representation of an output parameter of interest must be coupled with the probabilistic adjustment factors approach to quantify both forms of uncertainty. In this work, the Fast Fourier Transform approach detailed in Section 5.1.2 is utilized to quantify the parametric uncertainty. The FFT implementation requires a surrogate

model of the output response of interest. For this work, the weighted Stack Response Surface Method that was discussed in Section 3.2 was utilized.

The traditional and probabilistic adjustment factors approaches discussed thus far provide robust methodologies for the quantification of the model-form uncertainties given model probabilities, primarily elicited through expert opinion. As these model probabilities are an integral part of the model-form UQ process, great care must be given to ensure that they do not falsely represent the data. Model probabilities can only be refined through the introduction of additional data. This data can either take the form of additional expert opinion—which still suffers from the infallibility associated with the initial model probability predictions—or addition experimental data introduced into the problem. As mentioned prior, obtaining experimental data points can be a cost-intensive and even restrictive process, especially early the in the design stage where multiple configurations of parameters are being evaluated in quick succession. Thus, it would be beneficial to know the sensitivity of the adjusted model to the individual model probabilities. In this regard, two primary pieces of information could be obtained:

1. By looking at the sensitivity of the adjusted model to the model probability set as a whole, it could be determined what the effect of introducing additional data into the problem—for the purpose of refining the individual model probabilities—would have on

the overall variance in the prediction of the output response of interest given by the adjusted model.

2. On another level, determining the sensitivity of the adjusted model response to each individual model probability would provide an estimate of the individual models within the model set that contribute most significantly to the overall variance in the adjusted model. As such, if additional data was unable to be obtained, the models with the highest sensitivity would indicate the models that, if refined or improved, would have the greatest effect of the overall variance in the adjusted model.

To estimate the sensitivities listed above, the Modified Adjustment Factors Approach was developed in this work.

5.2.3. Modified Adjustment Factors Approach:

The model probabilities, $Pr(M_i)$, assigned to each model are initially based on expert opinion, or an incomplete set of preliminary data, which introduces an additional layer of uncertainty into the output distribution, *y*. As such, it would be beneficial to know the sensitivity of the adjusted model's response to the model probability set as a whole, as a high sensitivity would denote the potential for a reduction in model-form uncertainty through the introduction of additional data into the problem. To

approximate this sensitivity, first the values for each the model probabilities, $Pr(M_i)$, are treated as uncertain variables with a defined normal distribution (Eq. 5.50):

$$\Pr(M_i) = norm(\Pr(M_i)_{\exp}, \sigma_i^2) \forall i = 1,..., N \tag{5.50}$$

where $Pr(M_i)_{exp}$ represents the original model probability based on the expert opinion and σ_i is the standard deviation applied to the model probability distributions as defined in Eq. (5.51).

$$\sigma_i = \min\left[0.05, 0.25 * \Pr(M_i)_{\exp}\right] \tag{5.51}$$

The variance defined in Eq. (5.51) is developed as an artificial metric to explore the design space with respect to the model probabilities. As a result of the definition in Eq. (5.50), there are now distributions of model probabilities for each of the *N* models. These model probability distributions are then independently sampled using Monte Carlo Sampling to obtain a set model probability values. Before these sampled values are used, though, they must be renormalized to maintain the constraints set forth in Eq. (5.23). After normalization, the sampled values are then used in a adjustment factors approach, either traditional or probabilistic, to obtain a modified adjusted model, referred to as y_{adj}^{j} . This process of sampling the model probability distributions is then repeated *p* times, resulting in a set of adjusted models: $\{y_{adj}^{1}, y_{adj}^{2}, \ldots y_{adj}^{p}\}$, with each adjusted model representing the result of a different set of model probabilities. These individual adjusted models are then sampled using Markov Chain Monte Carlo Sampling and *m* samples. Using the *m* samples of the *j* adjusted models, a new aggregate

adjusted model, y_{mafa}, can then be constructed by fitting the data set to the same distribution defined in the adjustment factors approach, as shown in Section 5.1.1.

After completing the Modified Adjustment Factors Approach, two adjusted models now exist that represent the model-form uncertainty in the problem of interest: *y*, which uses the deterministic model probability values obtained from expert opinions and y_{maf}, which represents the potential variance in the prediction of the adjusted model as a result of perturbations of $Pr(M_i)$. A metric must now be implemented that measures the similarity of the two models. The Bhattacharyya distance is a metric developed to measure the geometric similarity between two distinct distributions (Eq. 5.52) (75).

$$BC\left(f_{x_1}, f_{x_2}\right) = \int_{-\infty}^{\infty} f_{x_1}(x)^{0.5} f_{x_2}(x)^{0.5} dx \qquad (5.52)$$

In Eq. (5.52), $f_{x_1}(x)$ and $f_{x_2}(x)$ represent the distributions of the two models of interest, *y* and y_{mafa} respectively. The Bhattacharyya distance is a bounded value between *0* and *1* where a value of *1* implies that the two models of interest are identically distributed. As such, a value of the Bhattacharyya distance close to *1* implies a greater similarity between the two models being considered whereas a lower value implies that there is a greater variance between the models. Thus, for the given problem, a critical value for the Bhattacharyya number can be defined. This critical value is a function of the cost of obtaining additional data. For problems where additional data is at a high cost, one would want to ensure that introducing additional

data would result in a significant reduction in the variance of the adjusted model, meaning that the critical value for the Bhattacharyya number would be lower. However, a value for the Bhattacharyya number less than the critical value would indicate that, should additional data be introduced into the problem and used to update the model probabilities, that the variance in the output response predicted by the adjusted model can be significantly reduced. While the opportunity for reduction in model-form uncertainty is indicated by this approach, it cannot guarantee a reduction. In cases where all models were inaccurate with respect to the true physical scenario, the model-form uncertainty might actually be increased due to the discrepancy

While the approach detailed above identifies whether or not a significant reduction of variance in the adjusted model could theoretically be obtained through the introduction of additional data, it does not identify the models that contribute most significantly to the variance in the adjusted model. To identify the contribution of each model to the overall variance, the approach detailed above can be modified slightly. Instead of treating each of the N model probabilities as being stochastic in nature, as shown in Eq. (5.50), each model probability is considered individually while holding the other $N-1$ model probabilities to be held constant at their prior model probability values. The rest of the approach is followed as before, resulting in a Bhattacharyya number for each of the N individual models. Now, instead of comparing the value of the Bhattacharyya number to a defined threshold value, they are compared relative to one another, analogous to sensitivities. The models with the highest Bhattacharyya number,

i.e. greatest sensitivity, is thus identified as the model that contributes most significantly to the variation in the output response predicted through the adjusted model. As such, if additional data was unable to be obtained, that the models with the highest sensitivities can be identified as models to refine for potential reduction in the overall variance of the adjusted model.

5.3. Predictive Uncertainty Quantification

The quantification of predictive uncertainty is commonly associated with the field of model validation and verification (V&V). Oberkampf and Roy provided an in-depth overview of methods used both in academic and in industry for V&V approaches (76). These approaches are generally intrusive methods that adjust and change model parameters and formulations to better match the experimental data points provided to the system. There are two primary problems with this approach in regards to this work:

1. The methods discussed in Oberkampf and Roy assume access to the source code of every model considered in the analysis, which is not available in many cases, such as those explored in Chapter 8. As such, in situations where direct access to the source code is not available—such as "black-box" models where only the input parameters and output responses are known—only non-intrusive methods can be considered. This results in a situation in that the predictive uncertainty can only be quantified, not

necessarily reduced, and to reduce to the predictive uncertainty would require a change of the model itself.

2. Validating a model against a set of experimental data points is analogous to fitting a curve to a set of data points in that it will guarantee good performance of the model at and near the design points used in the validation process, but provides no guarantee of the performance outside of those regions. As it is impossible to validate models with all possible permutations of designs, there exists an unknown predictive uncertainty associated with each model and each design point that should be quantified to obtain an accurate estimate of the complete uncertainty in the model itself.

As such, for the problems of interest in this work, it is not the goal to minimize the predictive uncertainty associated with the model—which would require an intrusive approach. Instead, it is the goal to merely quantify the predictive uncertainty of the model, which allows the use of non-intrusive approaches. This work categorizes non-intrusive methods into two general categories: Bayesian approaches and artificial uncertainty approaches. Artificial uncertainty approaches, in general, aim to induce a greater level of uncertainty in the response of a model as a function of observed data points, analogous to a correction factor of sorts. This artificial uncertainty is different from that used in prior model-form uncertainty approaches such as the adjustment factors approach in that instead of representing the uncertainty associated with the selection of the "best" model, this factor represents the predictive uncertainty

associated with a particular model. In applications to aerospace design, this approach has most often been seen with respect to surrogate models. Papila and Haftka used a noise function derived from the residual errors of points within surrogate models used in the design of the High-Speed Civilian Transport (HSCT) to represent the predictive uncertainty associated with a particular model of interest (77). This work was expanded upon by Hosder et.al to include variable complexity modeling into the construction of the artificial factor for HCST surrogates (78). Much work in the field of artificial predictive uncertainty representation has concentrated on quantifying the predictive uncertainty associated with the surrogate models, which could be extrapolated to black-box models, but was not developed with such models in mind.

As opposed to artificial predictive uncertainty representations, work done using Bayesian approaches for the quantification of predictive uncertainty in engineering problems has been more plentiful. Zhang and Mahadevan have shown for multiple problems the use of Bayesian networks to update the stochastic response of a model of interest, given experimental data points, for both full scale experiments (79) and lower-order experimental data (80). Rebba et.al later expanded on this methodology to use Bayesian networks for error estimates by isolating the source of the predictive error to input data error, discretization error, output measurement error, and model-form error, but for an intrusive model (81). Bayesian networks have been shown to be a robust technique for quantifying this error; and for cases where intrusive models are available, at isolating its sources as well. As these approaches quantify the predictive uncertainty,

as well as are capable of handling parametric uncertainties, all which is left is to couple them with an approach to handle model-form uncertainty. One such approach for coupling the Bayesian network approach to quantifying predictive uncertainties with a model integration technique to quantify model-form uncertainties is Bayesian Model Averaging.

5.3.1. Bayesian Model Averaging:

Bayesian Model Averaging (BMA) is a methodology that quantifies both the model-form uncertainty addressed in Section 5.2, as well as the predictive uncertainty associate with each model. This approach was first proposed in theory by Leamer in 1978 (69). Since then, it has gone through minor changes in both the way that the data points are used to calculate posterior model distributions (i.e. quantify predictive uncertainty) and update model probabilities (i.e. quantify model-form uncertainty). BMA is a broad approach with numerous applications. The approach that is adapted in this work begins with the introduction of an empirical data set $D = \{d_1,\ldots,d_m\}$ to the problem of interest (normally considered a set of experimental data points), and then consists of two primary steps:

1. Update the individual model predictions to include the predictive uncertainty associated with each models prediction of the points included in the data set *D* using a Maximum Likelihood Estimate.

2. Update the model probabilities by means of the model likelihoods evaluated given the data set *D* using Bayes Theorem and a Maximum Likelihood Estimate for the model likelihoods.

The adjusted model *Pr(y|D)* can then be shown to be the product of each of the *N* models' predictive distribution $Pr(y|M_i, D)$ and posterior model probability $Pr(M_i|D)$, as shown in Eq. (5.53).

$$\Pr(y \mid D) = \sum_{i=1}^{N} \Pr(y \mid M_i, D) \Pr(M_i \mid D) \tag{5.53}$$

Updating Model Predictions:

Initially, each model in the model set $M=\{M_1,M_2,\ldots,M_N\}$ is assumed to be either deterministic or stochastic with respect to only parametric uncertainties. It is then necessary to account for the predictive uncertainty associated with each particular model in the model set. This is done by modifying the result of a particular model at a set of parameters X_k, denoted $f_i(X_k)$, as shown in Eq. (5.54).

$$y_{i_k} = f_i(X_k) + \varepsilon_{i_k} \tag{5.54}$$

Where y_{ik} represents the prediction of model *i* at parameter set X_k and ε_{ik} is the value of the random error term for model *i* at that parameter set. ε_{ik} is assumed to be an independent and identically distributed normal random variable, as shown in Eq. (5.55).

$$\varepsilon_{i_k} = Norm(0, \sigma_i^2) \tag{5.55}$$

In Eq. (5.55), the random error term is assumed to have a mean value of *0* to represent an unbiased model response. The predictive uncertainty is assumed to be represented by the variance term in Eq. (5.55), σ_i^2. If model *i* is deterministic, then the predictive distribution of the output response *y* made by model *i* can be shown in Eq. (5.56).

$$\Pr(y \mid M_i, D) = Norm(f_i(X_k), \sigma_i^2) \tag{5.56}$$

However, if model *i* is stochastic, then the predictive distribution must be computed using Eq. (5.57).

$$\Pr(y \mid M_i, D) = \int_{\theta_i} \Pr(\theta_i \mid M_i) \Pr(y \mid \theta_i, X_k, M_i, D) d\theta_i \tag{5.57}$$

In Eq. (5.57), $Pr(\theta_i|M_i)$ is a joint pdf of the uncertainties in random parameter set θ_i and $Pr(y|\theta_i, X_k, M_i, D)$ is the predictive distribution of response *y* estimated by model *i* with random parameter set θ_i. A closed form expression for $Pr(y|\theta_i, M_i, D)$ cannot be obtained and instead must be approximated using an approach such as the Fast Fourier Transform approach detailed earlier in Section 5.1.2.

Looking back at the case shown in Eq. (5.56), if model *i* is deterministic, the predictive uncertainty can easily be estimated through the representation shown above, provided that the variance term, σ_i^2, can be solved for analytically. This is done using a Maximum Likelihood Estimate which determines the value of σ_i^2 that maximizes the likelihood of observing the data set *D* in the model prediction, $r(D|M_i)$ (8). To do this, it

is first assumed that each of the data points in the observed data set are independent of each other, allowing the representation of $Pr(D|M_i)$ shown in Eq. (5.58).

$$\Pr(D \mid M_i) = \Pr(d_1,...,d_m \mid \sigma_i) = \prod_{k=1}^{m} \Pr(d_k \mid \sigma_i) \tag{5.58}$$

As it is assumed that the distribution of *y* can be represented, in general, by Eq. (5.56), the distributions $Pr(d_k|\sigma_i)$ shown in Eq. (5.58) can be represented as a function of σ_i as shown in Eq. (5.59).

$$\Pr(d_k \mid \sigma_i) = \frac{1}{\sqrt{2\pi\sigma_i^2}} \exp\left(-\frac{(d_k - f_i(X_k))^2}{2\sigma_i^2} \right) \tag{5.59}$$

Substituting the expression for $Pr(d_k|\sigma_i)$ shown in Eq. (5.59) into Eq. (5.58) yields:

$$\Pr(D \mid M_i) = \prod_{k=1}^{m} \Pr(d_k \mid \sigma_i) = \left(\frac{1}{2\pi\sigma_i^2} \right)^{\frac{m}{2}} \exp\left(-\frac{\sum_{k=1}^{m} (d_k - f_i(X_k))^2}{2\sigma_i^2} \right) \tag{5.60}$$

Because the above equation is considered to be a function of only one variable, σ_i^2, the maximum likelihood value of the variable of interest can be solved by differentiating the logarithm of the likelihood function, $Pr(D|M_i)$, and setting it equal to *0,* which yields:

$$\sigma_{i,MLE}^2 = \frac{\sum_{k=1}^{m} (d_k - f_i(X_k))^2}{m} \tag{5.61}$$

Eq. (5.59) provides the maximum likelihood estimator for the variance in Eq. (5.54) which is shown to be a function of only the observed data points d_k and the model predictions of the data points, $f_i(X_k)$.

Updating Model Probabilities:

Bayesian Model Averaging usually assumes equal probability among all models, providing an unbiased initial estimator (Eq. (5.62)). This approach stand in contrast to the prior adjustment factor approaches which used potentially biased expert opinion to assign the model probabilities. The reason a Bayesian approach is applied here is that in the prior adjustment factor case, additional data was unavailable to use to update the probability predictions while in this case, the data set will be used to update the unbiased model probability predictions.

$$\Pr(M_i) = \frac{1}{N} \tag{5.62}$$

By introducing the data set *D* into the problem, Bayes' Theorem can be applied and the posterior model probabilities given data set *D* can be solved for each model using Eq. (5.63), which is a direct interpretation of Bayes Theorem.

$$\Pr(M_i \mid D) = \frac{\Pr(M_i) \times \Pr(D \mid M_i)}{\sum_{j=1}^{N} \Pr(M_j) \times \Pr(D \mid M_j)} \tag{5.63}$$

In Eq. (5.63), $\Pr(M_i)$ represents the probability of model M_i prior to the observation of experimental data, as defined by Eq. (5.62), and $\Pr(D|M_i)$ represents the

likelihood of model M_i given an experimental data set, *D,* the derivation of which was shown in prior section in Eq. (5.60).

The model probability updating process is then repeated for each of the additional data points to provide updated model probabilities for the Bayesian Model Averaging Approach. These posterior model probabilities can then be combined with the posterior predictive distributions defined in Eq. (5.56) or (5.57), depending upon the presence or absence of parametric uncertainties, to construct the distribution of the adjusted model *y*.

Retaining every model in the Bayesian Model Averaging approach can become burdensome and cost restrictive when used in the design process. As such, metrics exist to mathematically eliminate models from consideration when they are deemed to have minimal effect upon the adjusted model *y*. To determine models eligible for elimination from consideration, a Bayes' Factor B_i is defined for each model as a function of the models' posterior model probabilities (Eq. (5.64)).

$$B_i = \frac{\max[\Pr(M_i \mid D)] \forall i = 1,...,N}{\Pr(M_i \mid D)} \tag{5.64}$$

The Bayes' Factor represents the potential impact that a particular model would have on the adjusted model's estimate of the output response. A model with a large Bayes factor, such as a value of *100*, would be considered to have a negligible effect on the adjusted model, regardless of its divergence from the "best" model in the model set.

As such, a critical Bayes' Factor can be defined in the analysis approach where models that have Bayes' Factors that rise above that number can be eliminated from consideration without a significant effect on the adjusted model itself. The critical Bayes' Factor value would be defined as a function of the relative cost of running a particular model in the model set. As such, if the cost of evaluating a model is low, a higher critical Bayes' Factor could be used than if the computational cost associated with the models was significant. In this work, a critical Bayes' Factor of *10* will be used for all problems.

The applicability of Bayesian Model Averaging approaches have been shown for multiple problems in the literature. Draper proposed a standard Bayesian solution to the problem of fitting general mathematic models to structural uncertainties for Continuous Model Expansion (82). Hoeting later published a baseline methodology for the development of posterior distributions for Bayesian Model Averaging approaches which was the basis used in the development of this section (83). Wasserman later reviewed the methods in the literature for the evaluation of posteriors looking at both their relative accuracies and efficiencies (84). Droguett and Mosleh developed an approach to handle different forms of data to be input into the Bayesian methodology, such as single points, interval bounds, probability density functions, and qualitative inputs (51). Concurrently, Ando developed a Bayesian predictive criteria as a function of each model's posterior model probability for the purpose of down-selecting from a large model set to a smaller (85). Vrugt et.al later proposed using Markov Chain Monte Carlo

sampling to evaluate the posterior distributions under uncertain variables (Eq. (5.57)) (86).

Only recently, though, have Bayesian Model Averaging approaches been applied to aerospace engineering problems. Park et.al also developed a Bayesian approach to quantify the model-form and predictive uncertainty among the difference among multiple material models and experimental data sets in the simulation of laser peening of an aircraft lug (8). Riley and Grandhi quantified the model-form and predictive uncertainty in the calculation of the flutter velocity of the AGARD 445.6 wing using Bayesian Model Averaging (9). Swiler et.al also championed the potential of Bayesian Model Averaging for handling model-form uncertainty in aerospace application, but stopped short of demonstrating its applicability (87).

In this work, the Bayesian Model Averaging approach is adapted and implemented in situations where experimental data is available to allow for quantification of model-form, predictive, and parametric (if applicable) uncertainties. This methodology provides an approach for the complete quantification of uncertainties in the presence of full available data—parametric uncertainty representations, multiple models, and experimental data. In the absence of this full available data, the approaches detailed in the earlier sections of this chapter must be utilized to quantify the uncertainty from as many sources as possible given the available data. Examples of

the applications of these approaches will be demonstrated in the following three chapters.

6. Spring-Mass Demonstration Problem

To demonstrate the application of some of the uncertainty quantification techniques discussed in Chapter *5*, a simple nonlinear spring-mass system (shown in Figure 6.1) with model-form and parametric uncertainties will be considered and analyzed. This problem was originally demonstrated as a benchmark problem for model-form uncertainty quantification by Park *et.al* (8), who drew upon the work of He to develop the problem (88).

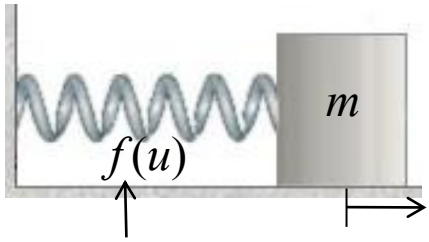

Figure 6.1: Single DOF Spring-Mass System

6.1. Problem Definition:

The free vibration of the mass in the single degree of freedom system shown in Figure 6.1 can be described by the governing equation shown in Eq. (6.1).

$$m\ddot{u} + f(u) = 0 \tag{6.1}$$

Where *m* is the mass of the block, *u* is the displacement of the mass for the equilibrium point, and *f(u)* is the spring force, a nonlinear function of the displacement of the mass. For different spring-mass systems, there are different models to represent the spring force functions, as shown in Eqs. (6.2)-(6.4) (88):

$$f_1(u) = \varepsilon u^{1/3} \tag{6.2}$$

$$f_2(u) = au + bu^3 \tag{6.3}$$

$$f_3(u) = cu + \frac{du}{\sqrt{1+u^2}} \tag{6.4}$$

Where the constants applied to Eqs. (6.2)-(6.4) can be seen in Table 6.1:

Table 6.1: *Parameter Values*

Parameter	*Value*
ε	*0.65 [N/cm$^{1/3}$]*
a	*1 [N/cm]*
b	*-0.35 [N/cm^3]*
c	*1 [N/cm]*
d	*-0.5 [N]*

Plotting the three forcing functions defined in Eqs. (6.2)-(6.4) with the parameters listed in Table 6.1 yields the three forces as a function of the displacement of the mass, shown in Figure 6.2.

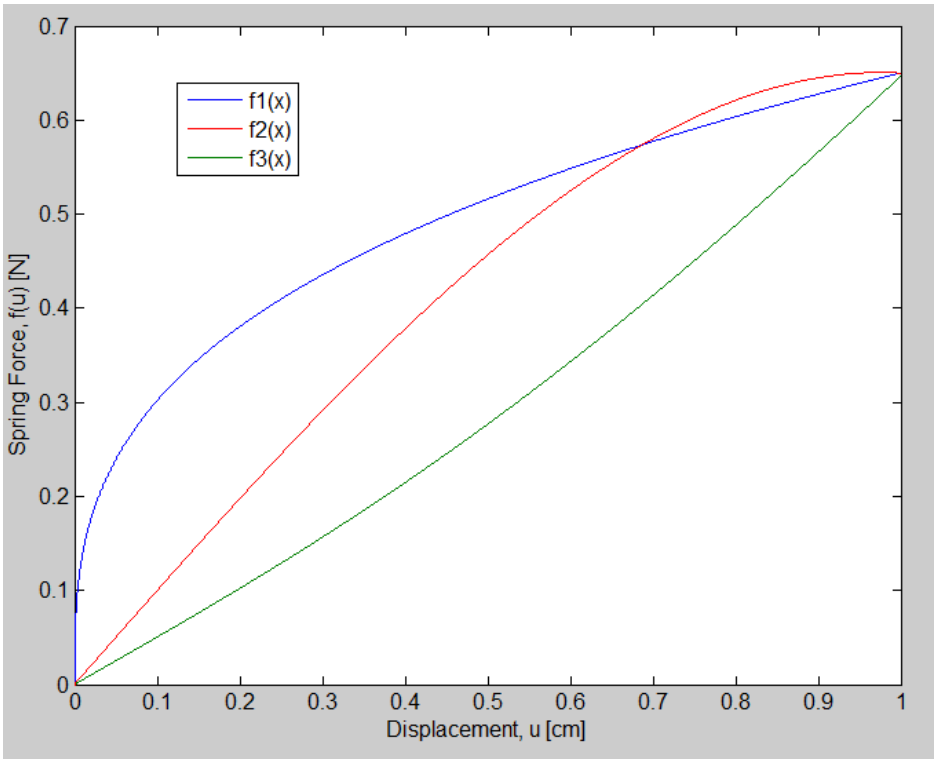

Figure 6.2: Plot of Spring Forcing Functions

Given a set of initial conditions shown in Table 6.2, ODE solver can be used to solve for the natural frequency of the spring-mass system for each of the models. The results of these analyses are shown in Table 6.3.

Table 6.2: *Initial Conditions*

Condition	*Value*
m	*1 [kg]*
u(0)	*1 [cm]*
u'(0)	*0 [cm/s]*

Table 6.3: *Solution Results*

Model	*Frequency [rad/s]*
$f_1(x)$	*0.864*
$f_2(x)$	*0.859*
$f_3(x)$	*0.808*

6.2. Quantification of Model-Form Uncertainty:

Given the three different models shown in Eqs. (6.2)-(6.4), there exists a degree of model-form uncertainty in selecting the model that best captures the physics being modeled in the problem. To quantify the model-form uncertainty in this problem, the Adjustment Factors Approach detailed in Section 5.2.1 will be utilized. The first step in this approach is to assign model probabilities to the constitutive models of interest. In the absence of any experimental data, this is done through the elicitation of expert opinions. For this problem, the values of the model probabilities used in Park *et.al* will be used and are shown in Table 6.4 (8).

Table 6.4: *Model Probabilities*

Model	$P(M_i)$
$f_1(x)$	*0.30*
$f_2(x)$	*0.50*
$f_3(x)$	*0.20*

After assigning the model probabilities as shown in Table 6.4, the appropriate form of the Adjustment Factors Approach must be applied. In the absence of any information regarding the output distribution forms of the models within the model set, a Gaussian form will be assumed, and thus, the Additive Adjustment Factors Approach will be utilized. The first step is to calculated the expected value of the adjustment factor E_a^* using Eq. (5.25), as shown in Eq. (6.5):

$$E[E_a^*] = 0.3(0.864 - 0.859) + 0.5(0.859 - 0.859) + 0.2(0.808 - 0.859)$$
$$E[E_a^*] = -0.009 \tag{6.5}$$

From this result, the expected value of the adjusted model can be calculated using Eq. (5.27):

$$E[y] = 0.859 - 0.009 = 0.850 \tag{6.6}$$

After calculating the expected value of the adjusted model, the variance of the adjustment factor can be solved for using Eq. (5.26):

$$Var[E_a^*] = 0.3(0.864 - 0.85)^2 + 0.5(0.859 - 0.85)^2 + 0.2(0.808 - 0.850)^2$$
$$Var[E_a^*] = 0.021 \tag{6.7}$$

Eq. (5.28) shows that due to the deterministic nature of each of the models, the adjusted model's variance is equation to the adjustment factor's variance, shown in Eq. (6.7). As such, the adjusted model *y* can be shown in Eq. (6.8) and Figure 6.3.

$$\omega = Norm(0.850, 0.021) \tag{6.8}$$

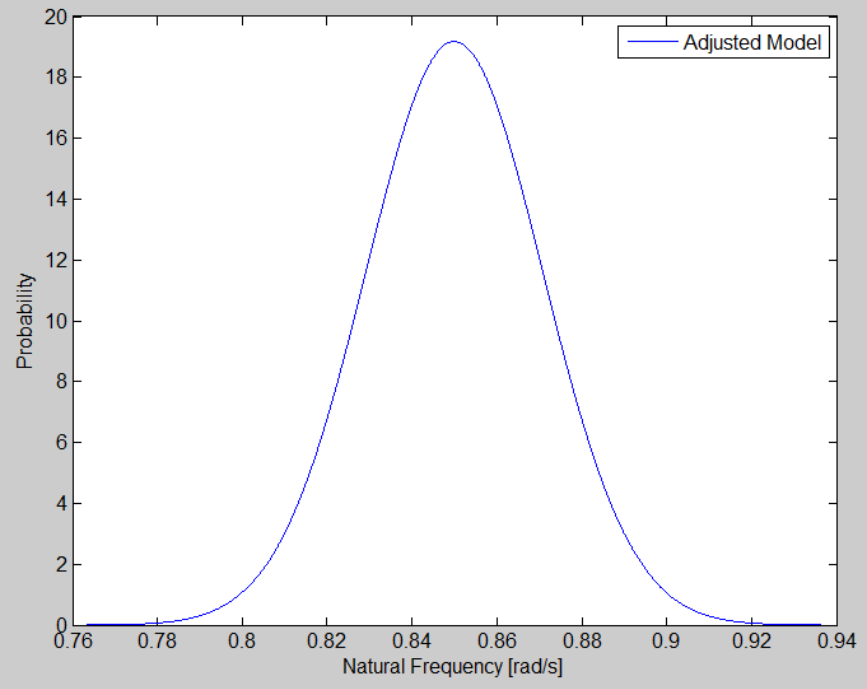

Figure 6.3: Adjusted Model w/ Model-Form Uncertainty

The distribution shown in Figure 6.3 represents the model-form uncertainty that exists in the estimation of the natural frequency of the system as a result of the multiple models that exist to represent its behavior and the inability of the designer to know with complete certainty the "best" model of the behavior among the models that are considered. At this point in the design process, one of two questions might arise:

1. How can the variance observed in the adjusted model be reduced?
2. What model(s) contribute most significantly to the variance observed in the adjusted model?

The answer to the two questions posed above can be obtained through the use of the Modified Adjustment Factors Approach. The Modified Adjustment Factors Approach, introduced in Section 5.2.2, has two stages to approximate the sensitivity of the adjusted model developed through an adjustment factors approach (Eq. (6.8)) to the individual model probabilities that were assigned in the problem (Table 6.4). The first stage of the approach determines the sensitivity of the adjusted model to the model probability set as a whole. The magnitude of this sensitivity is related to the Bhattacharyya number between the adjusted models using the traditional Adjustment Factors Approach and the Modified Adjustment Factors Approach (Table 6.5).

Table 6.5: *Modified Adjustment Factors Approach Results*

	Mean [rad/s]	***Standard Dev.***
Additive AFA	*0.8500*	*0.0208*
Modified AFA	*0.8501*	*0.0209*
Model Disagreement	*0.011%*	*0.481%*
Bhattacharyya Number:		***0.99991***

It is observed in Table 6.5 that the adjusted models obtained through the additive Adjustment Factors Approach and the Modified Adjustment Factors Approach are very similar with a Bhattacharyya number greater than the threshold value of *0.99.* This result indicates that the adjusted model shown in Eq. (6.8) is not particularly

sensitive to the model probabilities assigned in Table 6.4. As such, even with the addition of new data to refine the model probability distributions, the expected decrease in variance would be minimal. Of course, this statement is a relative statement, as in theory, it would be possible to reduce the model-form uncertainty to *0* if one model were shown to match an infinite experimental data set with no associated experimental error. However, in practice, one cannot obtain this result. As such, in this problem, with the introduction of new data, a minimal decrease in the variance of the adjusted model is expected.

While the first stage identified that the adjusted model is not particularly sensitive to the individual model probabilities assigned in the approach, the sensitivity of the adjusted models to the individual models themselves remains to be estimated. The Modified Adjustment Factors Approach approximates these sensitivities by individually redefining each model's model probability stochastically, obtaining a Bhattacharyya Number for each model. Relative to one another, the model with the lowest Bhattacharyya Number can then be seen to have the highest sensitivity to the adjusted model. Running this approach on the problem of interest yields the results shown in Table 6.6.

Table 6.6: *Modified Adjustment Factors Approach Results for Individual Models*

	Mean [rad/s]	***SD***	***Bhattacharyya No.***
Additive AFA	*0.8500*	*0.0208*	---
Modified AFA, $f_1(x)$	*0.8500*	*0.0211*	*0.99949*
Modified AFA, $f_2(x)$	*0.8499*	*0.0211*	*0.99946*
Modified AFA, $f_3(x)$	*0.8501*	*0.0209*	*0.99991*

Two features of the Bhattacharyya Numbers shown in Table 6.6 are of note. The first feature is that all three Bhattacharyya Numbers are very high, close to *1*. This effect is the coupling of two measures:

1. The sensitivity of the adjusted model to the model probability set as a whole was small (Table 6.5), implying that the sensitivity of the adjusted model to each individual model probability should remain relatively small.

2. The sensitivity of the adjusted model to each model as a whole is relatively small, and similar among each of the three models considered.

Given the results in Table 6.6, it is apparent that, given the problem and available data, the model-form uncertainty cannot be reduced by a significant amount without the introduction of significant amounts of data or refinement of the models.

6.3. Quantification of Parametric Uncertainty:

To demonstrate the potential of the methods developed in this work of handling uncertainties from multiple sources, uncertain input parameters are included in this analysis. For the problem of interest, Park and Grandhi looked at exploring the parametric uncertainty associated with the initial displacement by considering it to be a random input parameter with a value described by Eq. (6.9) (89).

$$u(0) = Norm(1.0[cm], 0.04[cm^2]) \tag{6.9}$$

With the given representation of the parametric uncertainty in each of the three models, the uncertainty within each model in predicting the natural frequency of the system can be solved for using the Fast Fourier Transform / weighted-Stack Response Surface Method approach detailed in Section 5.1.2. To implement this approach, a surrogate model of the natural frequency predicted by each of the models as a function of the uncertain input parameter must be constructed. Using a third order polynomial regression approximation, as shown in Eq. (6.10), the β coefficients in the approximations can be solved for using the weighted Stack Response Surface Method (w-StackRSM) with *16* data points and *4* folds in the data (*k=4)*. The *16* data points are

obtained through a Latin Hypercube Sampling of the distribution function shown in Eq. (6.9).

$$\omega_{f_i} = f_i(\bar{x}) = \beta_{0,i} + \beta_{1,i}x_1 + \beta_{2,i}x_1^2 + \beta_{3,i}x_1^3 \tag{6.10}$$

The β coefficients obtained through this approach are seen in Table 6.7:

Table 6.7: *Surrogate Models*

	β_1	β_2	β_3	β_4
$f_1(x)$	*0.4395*	*0.5962*	*-0.2098*	*0.0372*
$f_2(x)$	*1.0327*	*-0.1178*	*0.0195*	*-0.0756*
$f_3(x)$	*0.8759*	*0.6814*	*-0.5835*	*0.1634*

After obtaining the β coefficients in the surrogate models (Table 6.7), the Fast Fourier Transform technique can be implemented to estimate the output distribution of the natural frequency of the system for each of the models. In the absence of any known information regarding the output form of each of the models, a Gaussian form shall be assumed for the numerical evaluation of the distribution of the natural frequency. This approach, detailed in Section 5.1.2, was repeated for each of the three models, yielding the results shown in Table 6.8. Additionally, the results for the FFT / w-StackRSM approach were compared to results obtained through Monte Carlo Sampling (*n=100,000)* as a measure of validation for the approach. The comparison of these two approaches can be seen in Table 6.8.

Table 6.8: *Parametric UQ Results*

	FFT w/ w-StackRSM		***Monte Carlo***	
	μ	σ^2	μ	σ^2
$f_1(x)$	*0.8697*	*0.0053*	*0.8713*	*0.0040*
$f_2(x)$	*0.8511*	*0.0059*	*0.8504*	*0.0042*
$f_3(x)$	*0.8014*	*0.0047*	*0.7859*	*0.0037*

It can be seen in Table 6.8 that the FFT / w-StackRSM approach captures the stochastic behavior of the natural frequency of the system for each of the three models reasonable well when compared to the "true" results of the exhaustive Monte Carlo Sampling technique. It should be noted that the FFT / w-Stack RSM approach was able to yield these results with only *16* evaluations of the model while the Monte Carlo Sampling technique utilized *100,000* evaluations. For a simple problem such as this, this savings in number of function evaluations might be not necessary or even beneficial. However, for problems with larger simulations times, this reduction is necessary for evaluation of the parametric uncertainties.

6.4. Quantification of Parametric and Model-Form Uncertainties:

The prior two sections have detailed approaches for the quantification of model-form and parametric uncertainties individually. This section deals with the quantification of the two forms of uncertainty concurrently using the Probabilistic Adjustment Factors Approach that was detailed in Section 5.2.2. This approach,

integrates the probabilistic response of each of the individual models shown in Table 6.8 into the probabilistic adjustment factor using the model probabilities defined in Table 6.4. Using this data, an adjusted model can be developed using the Probabilistic Adjustment Factors Approach that captures both the model-form and parametric uncertainties present in the problem. To apply this approach, it is first noted that each of the three output response predictions shown in Table 6.8 are equivalent to Eq. (5.34) defining three normally distributed outputs. Looking at the model probabilities shown in Table 6.4, it can be seen that model *2* has the highest model probability, *0.50*, and thus is represented as y^* in Eq. (5.35) with an expected value of *0.8511*. As such, by applying Eq. (5.36), the expected value of the adjustment factor E_a^* can be computed as shown in Eq. (6.11):

$$E[E_a^*] = 0.3(0.8697 - 0.8511) + 0.5(0.8511 - 0.8511) + 0.2(0.8014 - 0.8511)$$
$$E[E_a^*] = -0.0076 \quad (6.11)$$

With the expected value of the adjustment factor computed, the expected value of the adjusted model *y* can be obtained through the application of Eq. (5.38):

$$E[y] = 0.8511 - 0.0076 = 0.8435 \quad (6.12)$$

Next, the variance of the adjustment factor must be computed using Eq. (5.37):

$$Var[E_a^*] = 0.3(0.8697 - 0.8435)^2 + 0.5(0.8511 - 0.8435)^2 + 0.2(0.8014 - 0.8435)^2$$
$$Var[E_a^*] = 0.0006 \quad (6.13)$$

The variance of the adjusted model can then be calculated trhough Eq. (5.39):

$$Var[y] = 0.0006 + 0.2(0.8014 - 0.8435)^2 + 0.3(0.0053) + 0.5(0.0059) + 0.2(0.0047)$$
$$Var[E_a^*] = 0.0061 \quad (6.14)$$

Eqs. (6.12) and (6.14) define the first and second moments of the normally distributed adjusted model *y*, which represents the uncertainty involved in the prediction of the natural frequency ω, as shown in Eq. (6.15) and Figure 6.4.

$$\omega_{pafa} = Norm(0.8435, 0.0304) \quad (6.15)$$

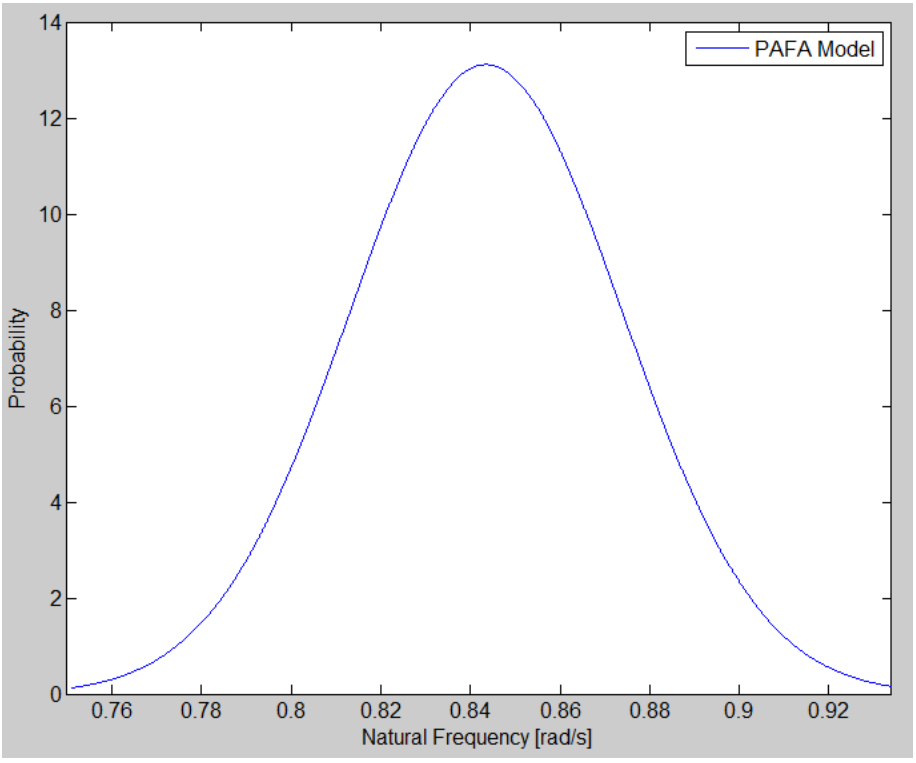

Figure 6.4: Adjusted PAFA Model w/ Model-Form and Parametric Uncertainties

It can be seen by comparing that the adjusted model in Eq. (6.15) is greater than the variance seen in the adjusted model capturing only the model-form uncertainty (Eq. (6.8)) and the models capturing only parametric uncertainties (Table 6.7). This increase in variance is a result of the fact that by ignoring one of the possible sources of uncertainty, an under-conservative design can result. In problems with reliability and safety in mind, under-conservative designs are far more dangerous than over-conservative designs due to the over-estimation of system safety that can accompany under-conservative predictions.

Looking at the variance observed in Eq. (6.15), it is observed that in this problem, the model-form uncertainty contributes more to the overall variance in the prediction of the natural frequency than the parametric uncertainty does. This is concluded because the variance observed in the adjusted model obtained using the Adjustment Factors Approach (*0.0208*) is approximately four times the variance observed in each of the models considering only parametric uncertainties (~*0.005*). Thus, if only the parametric uncertainty in the "best" model (distribution shown in red) was considered as the stochastic response of the system, it would result in a dramatically under-conservative, and potentially dangerous, result when compared to the PAFA result (distribution shown in blue), as shown in Figure 6.5. It can be observed, then, that for the spring-mass problem of interest, the contribution from model-form uncertainty is greater than the contribution from simply parametric uncertainty. This conclusion can be noted by

observing the relative variances of the two adjusted models shown in Figure 6.5. The adjusted model only considering the parametric uncertainty—shown in red—has a variance significantly smaller than the adjusted model that considers both model-form and parametric uncertainties—shown in blue.

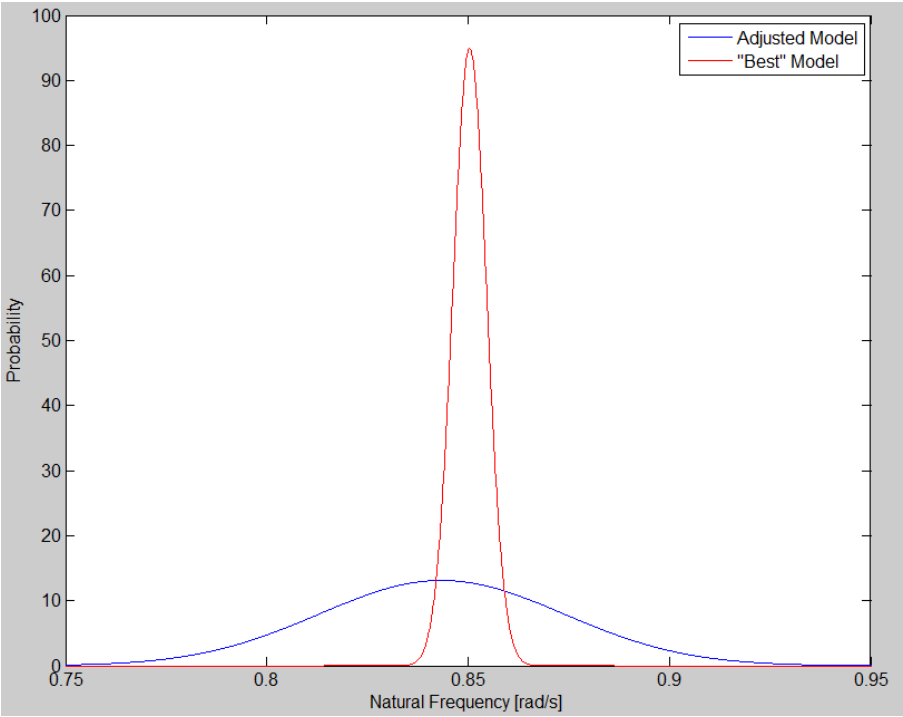

Figure 6.5: Comparison of "Best" Model and PAFA Adjusted Model

7. Flutter of Two Degree of Freedom Airfoil Subject to Unsteady Aerodynamics

7.1. Problem Definition:

To demonstrate the application of the uncertainty quantification tools developed in this work, they will first be applied to solve a simple aeroelastic analysis problem—the determination of the flutter velocity of a 2 degree of freedom (pitching and plunging) airfoil subject to unsteady aerodynamics (Fig. 7.1).

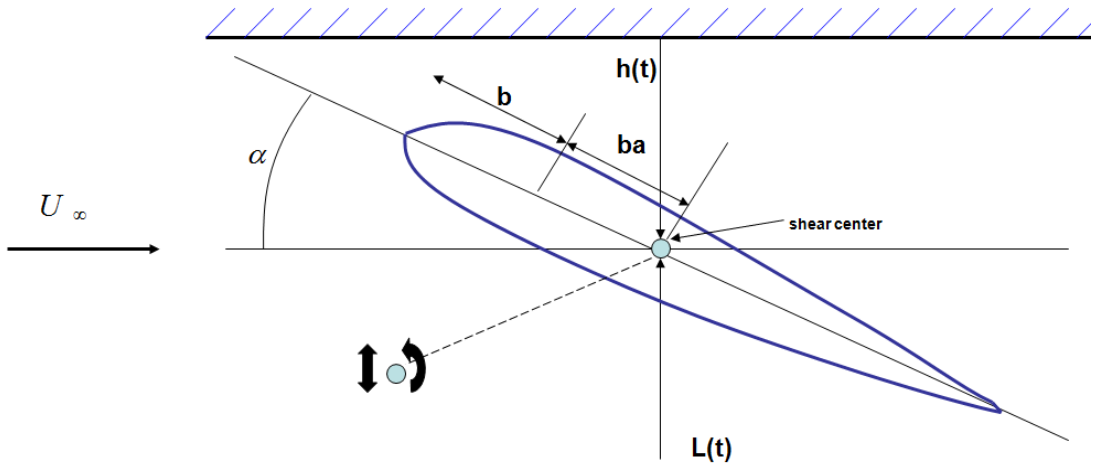

Figure 7.1: 2-DOF Airfoil

As this work includes the presence of parametric uncertainties, not all parameters in this model are considered deterministic. To represent the uncertainty associated with the structural components of the airfoil, the pitching and plunging frequencies of the airfoil are assumed to be stochastic parameters that are represented by the distributions shown in Eqs. (7.1) and (7.2).

$$\omega_h = Norm(0.869, 0.043) \tag{7.1}$$

$$\omega_\theta = Norm(1.552, 0.078) \tag{7.2}$$

The other parameters in the system are assumed to be deterministic in nature and are shown in Table 7.1.

Table 7.1: *Parameter Values*

Parameter	*Value*
μ	*40*
b	*30 [in]*
$\bar{r}_\theta$	*0.489*
m	*269*

Where μ is the reduced mass of the system, b is the semi-chord, $\bar{r}_\theta$ is the radius for pitching motion, and m is the mass of the system. All other parameters not listed in Table 7.1 are assumed to be equal to *0*. As such, for this two degree of freedom system, the equations of motion can be shown in Eq. (7.3).

$$\begin{bmatrix} \overline{A} & \overline{B} \\ \overline{D} & \overline{E} \end{bmatrix} = \begin{Bmatrix} h \\ b \\ \theta \end{Bmatrix} \tag{7.3}$$

where:

$$\overline{A} = \mu\left(1 - \Omega\left(\frac{\varpi_h^2}{\varpi_\theta^2}\right)\right) + L_h \tag{7.4}$$

$$\overline{B} = \mu\bar{x}_\theta + L_\alpha - L_h(0.5 + a) \tag{7.5}$$

$$\overline{D} = \mu\bar{x}_\theta + M_h - L_h(0.5 + a) \tag{7.6}$$

$$\overline{E} = \mu\bar{r}_\theta^2(1 - \Omega) - M_h(0.5 + a) + M_\alpha - L_\alpha(0.5 + a) + L_h(0.5 + a)^2 \tag{7.7}$$

Of note from Eqs. (7.4)-(7.7) are the lift terms denoted L_h and L_α. As shown in Eqs. (7.8) and (7.9), these two terms are a function of Theodorsen's Circulation Function, denoted *C(k)*, and the reduced frequency *k*, defined in Eq. (7.10).

$$L_h = 1 - \frac{i(2C(k))}{k} \tag{7.8}$$

$$L_\alpha = \frac{1}{2} - \frac{i(1 + 2C(k))}{k} - \frac{2C(k)}{k^2} \tag{7.9}$$

$$k = \frac{\omega b}{U_\infty} \tag{7.10}$$

Upon selection of an appropriate Theodorsen's Circulation Function, the eigenvalue of the equations of motion shown in Eq. (7.3) can be solved along a spectrum of *k* values and the flutter velocity of the airfoil can be determined using the Vg solution method.

7.2. Uncertainty Definition

The parametric uncertainties within the problem of interest were defined in Eqs. (7.1) and (7.2). Predictive uncertainty is inherent to a model due to the nature of the model-formulation process. In his problem, the source of model-form uncertainty originates with the formulation of Theodersen's Circulation Function that is used in the analysis of the system. Theodorsen's Circulation Function is a complex function that controls the relative phasing and amplitude of the lift and pitching moments with respect to the airfoil motion. While an empirically correct representation of the function exists (Eq (7.15), (it should be noted that Eq. (7.13) is mathematically the same as Eq. (7.15) but can differ slightly depending on the evaluation of the Bessel functions) multiple lower-order approximations exist and have been used in prior solution approaches to approximate Theodorsen's Function as a function of *k* over the range of *k*-values experienced by the system (Eqs. (7.11)-(7.16)):

$$C_1(k) = 1 - \frac{0.165k}{k - 0.0455i} - \frac{0.355k}{k - 0.3i} \tag{7.11}$$

$$C_2(k) = \frac{0.01365 + 0.2808ik - 0.5k^2}{0.01365 + 0.3455ik - k^2} \tag{7.12}$$

$$C_3(k) = \frac{J_1 - J_{oy}i}{J_1 - J_{oy}i + J_o - J_{1y}i} \tag{7.13}$$

$$C_4(k) = \frac{(1+10.61ik)(1+1.774ik)}{(1+13.51ik)(1+2.745ik)} \tag{7.14}$$

$$C_5(k) = \frac{H_1^{(2)}(k)}{H_1^{(2)}(k) + iH_0^{(2)}(k)} \tag{7.15}$$

$$C_6(k) = \frac{0.015 + 0.3ik - 0.5k^2}{0.015 + 0.35ik - k^2} \tag{7.16}$$

It can be seen that the real and imaginary parts of these six surrogate models vary over an average operating range of *k*'s, as shown in Figures 7.2 and 7.3.

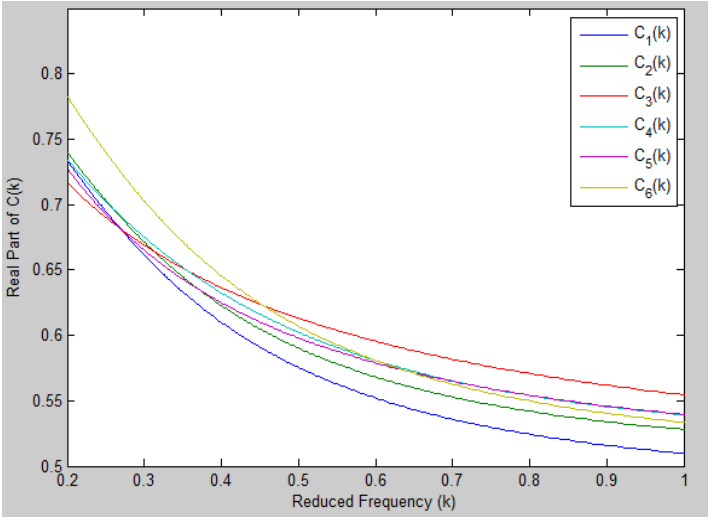

Figure 7.2: Real Component of C(k) for 6 Models

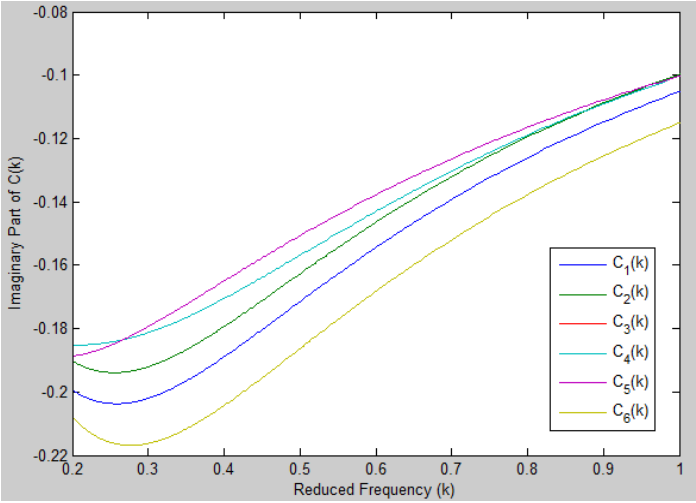

Figure 7.3: Imaginary Components of C(k) for 6 Models

It is assumed for the purpose of this demonstration problem that the "best" model among the model set *M* is not clear along the entire spectrum of *k* values. Thus, there is a degree of model-form uncertainty in the selection of which model is best. As such, all three forms of uncertainty introduced in Chapter 4 are present in the problem of interest: the parametric uncertainty associated with the value of the pitching and plunging frequencies of the airfoil, the model-form uncertainty associated with the selection of the proper Theodorsen's Circulation Function to use in the flutter solution technique, and the predictive uncertainty associated with the assumptions that were made to develop the equations of motion of the system represented in Eq. (7.3).

7.3. Quantification of Model-Form Uncertainty

The first analysis that will be done is the quantification of the model-form uncertainty associated with the selection of the proper Theodorsen's Circulation Function to use in the flutter analysis. The model-form uncertainty associated with the

model selection process will be done using the Adjustment Factors Approach detailed in Section 5.2.1. In this approach, each of the six models are first run to determine the flutter velocity prediction of the airfoil for each of the models of interest. The parameters that were used in this problem are shown in Table 7.1. As the two parameters shown in Eqs. (7.1) and (7.2) were initially assigned to be stochastic in nature, they must be represented as deterministic in this initial analysis. This is done by simply considering the two stochastic parameters to be equal to their expected values for this analysis.

After defining the input variables to the problem, the solution approach detailed in Eqs. (7.3)-(7.10) can be performed for each of the six Theodorsen's Circulation Functions denoted in Eqs. (7.11)-(7.16), solving for the flutter velocity of the airfoil using each of the six model individually (the Matlab code for this analysis is included in Appendix A to this dissertation). This approach yields the results shown in the second column of Table 7.2.

Table 7.2: *Flutter Velocities and Model Probabilities for 6 Models*

	V_f [ft/s]	$P(M_i)$
$f_1(x)$	163.32	0.20
$f_2(x)$	163.61	0.10
$f_3(x)$	163.33	0.25
$f_4(x)$	163.70	0.10
$f_5(x)$	163.49	0.30
$f_6(x)$	164.19	0.05

To apply the adjustment factors approach, model probabilities must first be assigned to each model considered in the analysis. In the absence of experimental or historical data, this is done using expert opinions regarding the relative accuracy and merit of each model being considered. In this analysis, the model probabilities are assigned as a function of the complexity of the form of the Theodorsen's Circulation Function, as shown in the third column of Table 7.2. The effect of the assigning of these particular model probabilities will be explored in the subsequent analysis.

After assigning the model probabilities, an adjusted model to represent the potential variance in the flutter velocity of the airfoil as a result of the model-form uncertainty in the problem can be developed. Using the additive adjustment factors

approach detailed in Eqs. (5.22)-(5.26), an adjusted model is developed and presented in Eq. (7.17) and Figure 7.4.

$$y_{add} = Norm(163.48, 0.207) \tag{7.17}$$

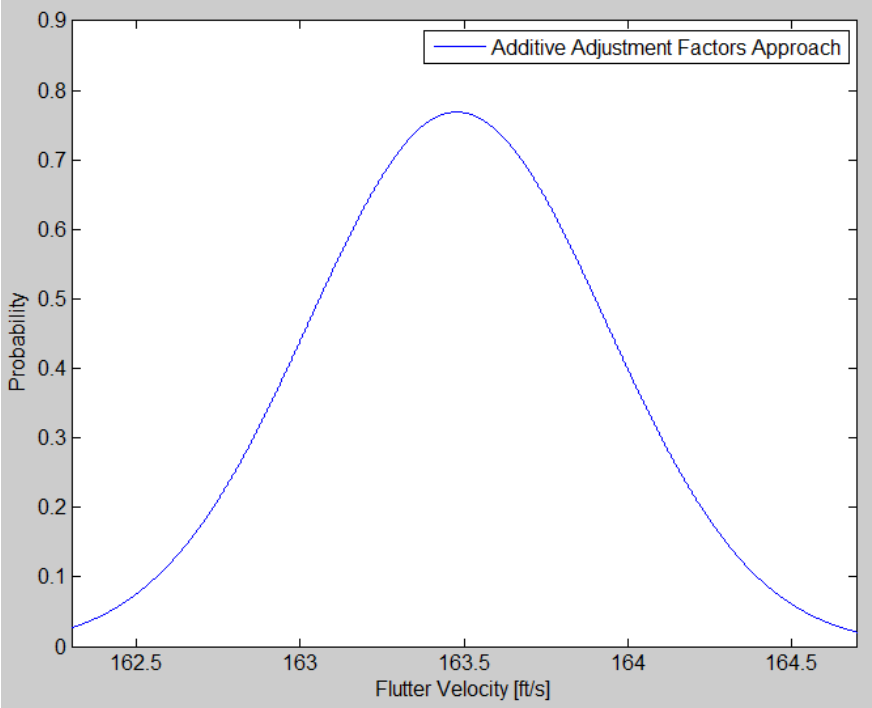

Figure 7.4: *PDF of Adjusted Model, y_{add}*

It can be seen in Figure 7.4 that although each of the individual component models in this analysis are deterministic, that when the model-form uncertainty in the selection of the "best" model is considered that a stochastic representation of the flutter velocity of the airfoil is obtained. After completing an analysis such as this, multiple questions arise. First, as the model probabilities that were assigned to each of the individual models were done so using an imprecise and non-empirical method—

expert opinions—is the adjusted model shown in Eq. (7.17) highly sensitive to the values selected, and if so, which models in particular contribute most significantly to this variance? Additionally, if the variance that is observed in Eq. (7.17) is considered too large for the problem of interest, can it be reduced through the introduction of additional data?

The answers to the questions proposed above are addressed by the Modified Adjustment Factors Approach detailed in Section 5.2.3. First, the sensitivity of the adjusted model to the individual model probabilities is to be estimated. To do this, the model probabilities for each of the six models of interest are redefined as stochastic parameters as shown in Eqs. (5.49) and (5.50). This information is then propagated through the problem using the Modified Adjustment Factors Approach to develop an adjusted model as a function of these redefined model probabilities, shown in Table 7.3.

Table 7.3: *Modified Adjustment Factors Approach Results*

	Mean [ft/s]	***Standard Dev.***
Additive AFA	*163.48*	*0.207*
Modified AFA	*163.49*	*0.252*
Model Disagreement	*0.06%*	*21.7%*
Bhattacharyya Number:		***0.9892***

As the Bhattacharyya number between the two models is smaller than the critical value of *0.990* used in this work, this indicates that the problem is sensitive to the individual model probabilities that were assigned in Table 7.2. However, since the value is barely below the threshold, a large reduction in the model-form uncertainty in the problem is not to be expected, as the adjusted model is not particularly sensitive to the model probabilities assigned to its constituent models, which is clear by looking at the two distributions plotted in Figure 7.5.

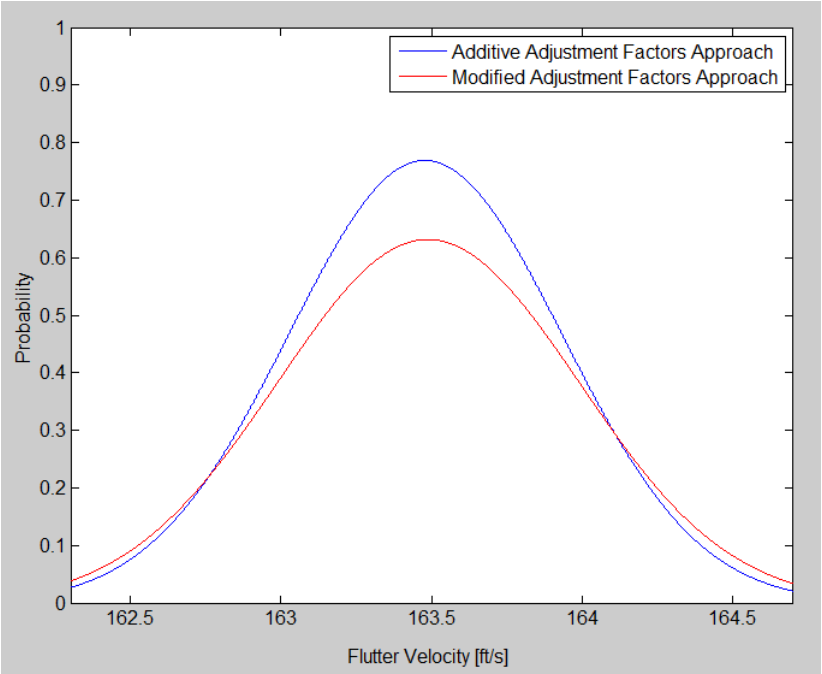

Figure 7.5: *Additive and Modified AFA Models*

As a result, the model-form uncertainty in the problem should be able to be reduced significantly through the introduction of additional data, which will be

discussed in Section 7.4. In addition, it would be of interest to know which of the models contribute most significantly to the amount of model-form uncertainty observed in the adjusted model. To obtain this information, the Modified Adjustment Factors Approach is applied to the problem defining only one model probability at a time as stochastic, as detailed in Section 5.2.3. By repeating the process detailed above and isolating each model individually, six different Bhattacharyya numbers can be determined, each representing the approximate sensitivity of the adjusted model to the model probability of a particular model. The results for this analysis can be seen in Table 6.4.

Table 7.4: *Individual Sensitivities Through MAFA*

Model	Bhattacharyya Number
$f_1(x)$	*0.9874*
$f_2(x)$	*0.9773*
$f_3(x)$	*0.9733*
$f_4(x)$	*0.9809*
$f_5(x)$	*0.9866*
$f_6(x)$	*0.9581*

From Table 7.4, the sensitivity of the adjusted model to the individual models can be shown to be related to the inverse of the Bhattacharyya number. This implies that, at the current set of model probabilities, model *6* has the greatest impact on the adjusted model while model *1* has the smallest effect. If additional data was unable to be obtained, then this approach says that relative to the other models, improvement in

model *6* would result in the greatest decrease in the amount of model-form uncertainty in the problem.

A qualitative statement regarding the magnitude of the improvement to be expected cannot be made though. Instead, only qualitative conclusions can be drawn from this approach regarding the rank and magnitude of the model sensitivities. For instance, if the Bhattacharyya Number for model *6* had been *0.5* as opposed to *0.9581* then it could be said that model *6* had a much more significant effect on the adjusted model than the other five models. However, the value of *0.5* would not necessarily indicate that the model was incorrect, as this information cannot be drawn without the availability of experimental or validation data. Instead, a significantly divergent value when compared to the other models would indicate a high potential for inaccuracy and that further consideration should be given to the model.

7.4. Quantification of Model-Form and Predictive Uncertainties

As discussed in the previous section, due to the results of the Modified Adjustment Factors Approach applied to all models being less than the critical value for the problem of interest, a significant reduction of the model-form uncertainty in the prediction of the flutter velocity for this problem can be expected with the introduction of additional data. For the parameters defined in Table 7.1 and the expected values of

the distributions defined in Eqs. (7.1) and (7.2), wind tunnel data exists in the literature for the flutter velocity of the airfoil (90). By introducing experimental data into the problem, the predictive uncertainty associated with the modeling of the flutter velocity of the airfoil can be quantified using the Bayesian Model Averaging scheme detailed in Section 5.3.1. Additionally, the data can be used to update the model probabilities using Bayes' Theorem, reducing the amount of model-form uncertainty present in the problem as well.

The first step in the Bayesian Model Averaging approach is to update the model prediction to include the predictive uncertainty in representing the physical data provided in data set *D*. In this case, data set *D* consists of a single flutter point at the specified parameters with a flutter velocity of *163.4 [ft/s]* (90). This is done using the Maximum Likelihood Estimator derived in Section 5.3.1. As such, the predictive variance of each model, σ_i^2, can be calculated through Eq. (5.59), there results of which are shown in Table 7.5.

Table 7.5: *Predictive Distributions of Models*

Model	μ	σ_i^2
$f_1(x)$	*163.32*	*0.0061*
$f_2(x)$	*163.61*	*0.0441*
$f_3(x)$	*163.33*	*0.0049*
$f_4(x)$	*163.70*	*0.0900*
$f_5(x)$	*163.49*	*0.0081*
$f_6(x)$	*164.19*	*0.6241*

After defining the predictive distributions of the models of interest, the next step in the Bayesian Model Averaging approach is to determine the posterior model probabilities of each model. While approaches such as the Adjustment Factors Approach utilized expert opinions to develop a prior model probability, Bayesian Model Averaging assumes uniform prior model probabilities in the absence of data. As such, all six model probabilities are assumed to be *0.166*, as shown in Table 7.5. Bayes' Theorem is then applied, as shown in Eq. (5.61) to determine the posterior model probabilities for each model of interest.

Table 7.6: *Posterior Model Probabilities*

	$P(M_i)_{prior}$	$P(M_i)_{post}$	*Bayes' Factor*
$f_1(x)$	*0.1666*	*0.2645*	*1.143*
$f_2(x)$	*0.1666*	*0.1008*	*2.999*
$f_3(x)$	*0.1666*	*0.3023*	*1*
$f_4(x)$	*0.1666*	*0.0705*	*4.288*
$f_5(x)$	*0.1666*	*0.2351*	*1.286*
$f_6(x)$	*0.1666*	*0.0268*	*11.280*

From Table 7.6, two conclusions can be drawn. It is clear that model *3* has the highest model probability. This conclusion speaks well for the approach because, although it was assumed that the "best" model was not known going into the analysis, it is known the $f_3(x)$ is the proper representation of Theodorsen's Circulation Function. Secondly, the Bayes' Factor for model *6* is greater than the critical Bayes' Factor value established in Section 5.3.1. As such, model *6* can be excluded from the Bayesian Model Averaging approach. However, to maintain the model probability constraints established in Eq. (5.21), the remaining five posterior model probabilities must be renormalized, as shown in Table 7.7.

Table 7.7: *Updated Posterior Model Probabilities*

	$P(M_i)_{post}$	$P(M_i)_{post,updated}$
$f_1(x)$	*0.2645*	*0.2718*
$f_2(x)$	*0.1008*	*0.1036*
$f_3(x)$	*0.3023*	*0.3106*
$f_4(x)$	*0.0705*	*0.0724*
$f_5(x)$	*0.2351*	*0.2416*

After updating the model probabilities, the Bayesian Model Averaging approach shown in Eq. (5.51) can be applied, resulting in the adjusted model shown in Eq. (7.18).

$$y_{bma} = Norm(163.424, 0.063) \tag{7.18}$$

The adjusted model obtained using the Bayesian Model Averaging approach—quantifying predictive uncertainty and reducing the model-form uncertainty—can be compared to the model-form uncertainty quantification technique utilized in the adjustment factors approach (Eq. (7.18)), as shown in Table 7.8 and Figure 7.6.

Table 7.8: *Adjusted Models from Two Approaches*

	Mean [ft/s]	*Standard Dev.*
AFA	*163.481*	*0.207*
BMA	*163.424*	*0.063*

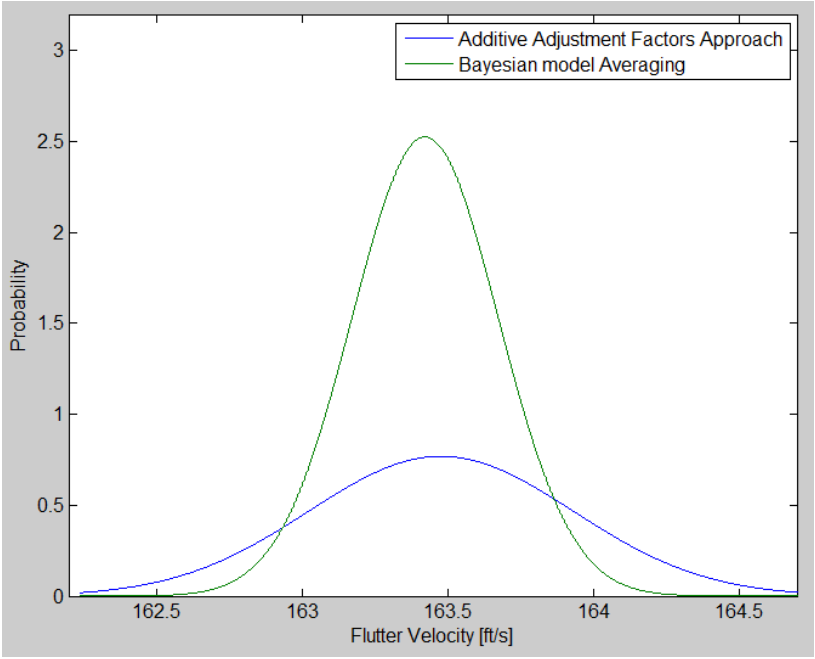

Figure 7.6: *PDFs for AFA and BMA Adjusted Models*

Figure 7.6 illustrates that by introducing the additional knowledge of the experimental data through the Bayesian Model Averaging approach, two primary changes in the adjusted model (shown in green) are noted. First, the mean of the adjusted model is shifted slightly lower, from *163.481 [ft/s]* to *163.424 [ft/s]*. This reduction in the mean of the adjusted model is due to the fact that since experimental data was introduced into the problem, the predictive uncertainty within the problem could begin to be quantified. As such, the mean value of the adjusted distribution begins to approach the value shown in the experimental data set, *163.40 [ft/s]*. The second change observed in the adjusted model from the adjustment factors approach to the Bayesian Model Averaging approach is the reduction in the variance of the adjusted model from *0.207* to *0.063.* This reduction in variance is due to the fact that the model-form uncertainty in the problem was able to be reduced by the introduction of

additional data to update the model probabilities. This potential for reduction in model-form uncertainty was indicated by the Modified Adjustment Factors Approach result, where the Bhattacharyya number below the critical value indicated that the adjusted model was sensitive to the model probabilities assigned to the problem.

7.5. Quantification of Model-Form and Parametric Uncertainties

In Section 7.3, the model-form uncertainty problem associated with the selection of the appropriate approximation to Theodorsen's Circulation Function was addressed. In this approach, all parameters were considered to be deterministic in nature, include the two frequency parameters which shown in Eqs. (7.1) and (7.2). As such, both parametric and model-form uncertainties are to quantified. This will be done using the Probabilistic Adjustment Factors Approach that was introduced in Section 5.2.2.

To utilize the Probabilistic Adjustment Factors Approach, the parametric uncertainty within each model must first be quantified using the Fast Fourier Transform approach, as mentioned in Section 5.1.2. In the FFT approach, a third order response surface was constructed to estimate the flutter velocity of the airfoil for each of the models as shown in Eq. (7.19).

$$v_{f_i} = f_i(\bar{x}) = \beta_{0,i} + \beta_{1,i}x_1 + \beta_{2,i}x_1^2 + \beta_{3,i}x_1^3 + \beta_{4,i}x_2 + \beta_{5,i}x_2^2 + \beta_{6,i}x_2^3 \qquad (7.19)$$

Where x_1 represents the plunging frequency (ω_h) and x_2 represents the pitching frequency (ω_ϑ). The approximation shown in Eq. (7.19) is then constructed for each of the six approximations to Theodorsen's Circulation Function by performing a basic design of experiments within the design space at $\mu \pm n\sigma$ perturbations of the parametrically uncertain variables, obtaining a total of twenty data points. The weighted Stack Response Surface Method approach (Section 3.3) was then applied to the data set with *25* samples to obtain estimates the seven β-values to approximate the output response (flutter velocity) of the model. After obtaining the β-values for each of the six models, the FFT approach was applied, using the chain rule to convert the *x*-space distributions into *z*-space, as shown in Eq. (5.19), to solve for the distribution of the flutter velocity of the airfoil predicted by each respective model. To validate the results of this FFT approach, as well as the approximations being used to represent the behavior of the system, the results for each of the six models is compared to a brute-force Monte Carlo evaluation of the flutter distribution with 250,000 simulations as shown in Table 7.9.

Table 7.9: *Parametric UQ Results*

	FFT w/ w-StackRSM		***Monte Carlo***	
	μ	σ	μ	σ
$f_1(x)$	*163.59*	*4.24*	*163.79*	*4.18*
$f_2(x)$	*163.87*	*4.49*	*164.00*	*4.19*
$f_3(x)$	*162.22*	*5.53*	*162.35*	*5.64*
$f_4(x)$	*163.84*	*4.26*	*164.08*	*4.23*
$f_5(x)$	*164.04*	*4.41*	*163.88*	*4.26*
$f_6(x)$	*164.23*	*4.05*	*164.56*	*3.99*

It can be seen in Table 7.9 that the distributions predicted by the FFTs match very closely with those determined through rigorous Monte Carlo simulation. It should be noted that the values for the FFT / w-StackRSM approach were obtained with only twenty-five simulations while the Monte Carlo approach required 250,000 simulations.

As the parametric uncertainty within each model can now be approximated as a distribution function of the output response of interest, the probabilistic adjustment factors approach can then be applied. The first step in this approach is to assign the model probabilities to each of the six models being considered. These model probabilities are determined from expert opinion regarding the relative accuracy of each model, and are the same that was used with the traditional adjustment factors approach shown in Table 7.2.

After assigning the model probabilities, it can be seen that Model *5* is shown to have the highest model probability, and is thus assumed to be the "best" model (y^*) in this analysis. By applying Eqs. (5.34)-(5.37) to each of the two sets of models shown in Table 7.9, two different adjusted models for the flutter velocity can be solved for—one using the FFT approximations and one using the Monte Carlo Results. These two models are shown below in Table 7.10 and plotted on Figure 7.7.

Table 7.10: *PAFA Results*

	Mean [ft/s]	*Standard Dev.*
FFT	*163.38*	*5.64*
MC	*163.53*	*5.31*

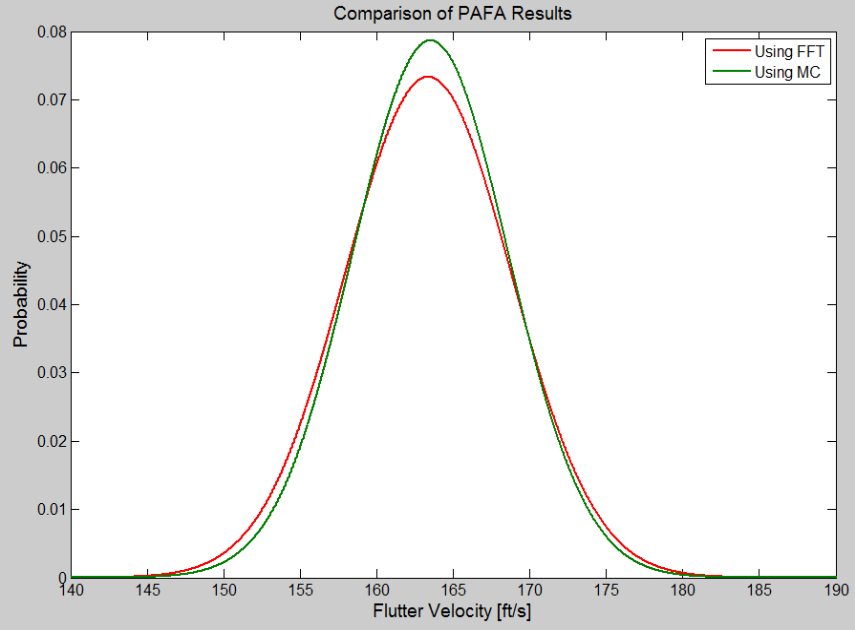

Figure 7.7. *PAFA Results for Two Parametric UQ Approaches*

It can be seen in Table 7.10. and Figure 7.7 that both parametric uncertainty quantification techniques, when propagated through the probabilistic adjustment factors approach, produced similar adjusted models for the flutter velocity of the airfoil of interest. This result implies that utilizing Fast Fourier Transforms to quantify the parametric uncertainties in a problem such as this is viable when coupling this method with the probabilistic adjustment factors approach. The methodology developed in this work results in an adjusted model (shown in red in Figure 7.7) that quantifies both the

parametric uncertainty associated with the pitching and plunging frequencies used in the flutter analysis as well as the model-form uncertainty associated with the selection of the proper Theordorsen's Circulation Function approximation to use in the analysis.

Looking at a histogram of the Monte Carlo results for a particular model of interest, it can be seen that the Gaussian distribution assumption assigned to the output response results in a discrepancy between the "true" data represented by the Monte Carlo data points and the assumed response represented by the distribution (the blue line in Figure 7.8). To address this discrepancy, the methodology was repeated with a beta distribution assumed as the form of the responses for each of the models. It can be seen in the red line on Figure 7.8 that assuming the form of a beta distribution resulted in a much more accurate representation of the response of the system.

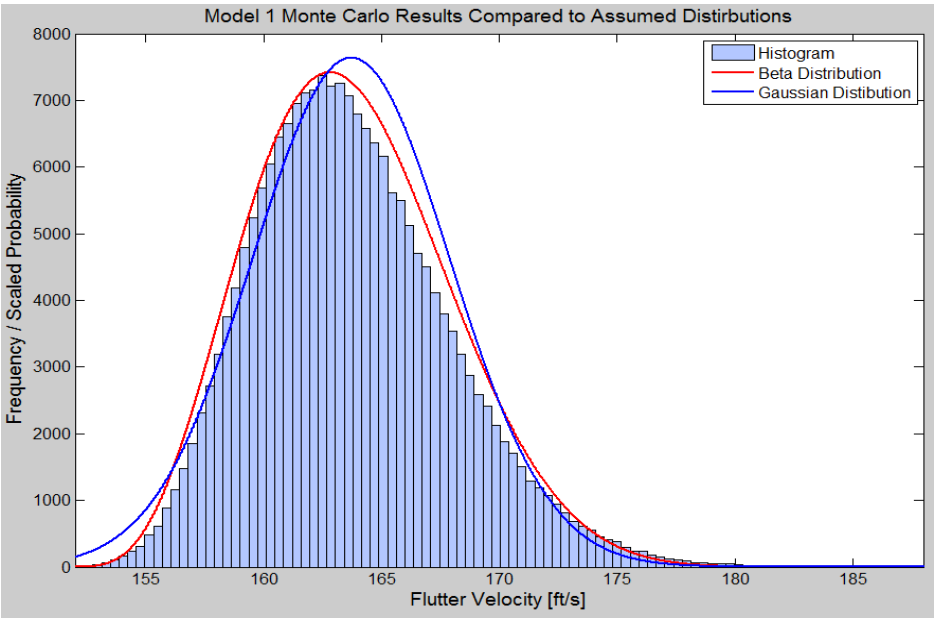

Figure 7.8. *Fits of Distributions to Monte Carlo Results*

Using the Beta distribution assumption for the output of the data, the flutter velocity of each of the models could be estimated using both the numerical data from the inverse Fourier Transform and the Monte Carlo data points, as was done prior for the Gaussian assumption. The results for these two approaches are shown in Table 7.11.

Table 7.11. *Parametric UQ Results (Assumed Beta Distribution)*

	FFT w/ RSM				***Monte Carlo (n=250,000)***			
	l	*u*	*α*	*β*	*l*	*u*	*α*	*β*
$f_1(x)$	*150.85*	*187.52*	*5.19*	*10.63*	*151.66*	*188.43*	*5.28*	*10.80*
$f_2(x)$	*151.22*	*188.00*	*5.44*	*10.56*	*151.80*	*188.63*	*5.35*	*10.78*
$f_3(x)$	*142.80*	*189.74*	*7.03*	*10.04*	*141.20*	*189.94*	*7.52*	*9.81*
$f_4(x)$	*151.12*	*188.64*	*5.50*	*11.11*	*151.71*	*188.76*	*5.37*	*10.70*
$f_5(x)$	*151.40*	*188.94*	*5.28*	*10.72*	*151.49*	*188.68*	*5.32*	*10.65*
$f_6(x)$	*153.23*	*189.66*	*5.42*	*11.74*	*152.82*	*188.56*	*5.47*	*11.18*

It can be seen in Table 7.11 that as with the Gaussian assumption, the Fast Fourier Transform technique provides an accurate representation of the response of the system at a dramatically reduced computational cost. Similar to before, the probabilistic adjustment factors approach was then applied to both sets of models, obtaining two adjusted models--one for the FFT technique and one using the Monte Carlo data--shown in Table 7.12 and Figure 7.9.

Table 7.12: *PAFA Results (Beta Assumption)*

	FFT (RSM)	Monte Carlo
l	149.19	149.07
u	188.77	188.94
α	5.59	5.77
β	10.23	10.14

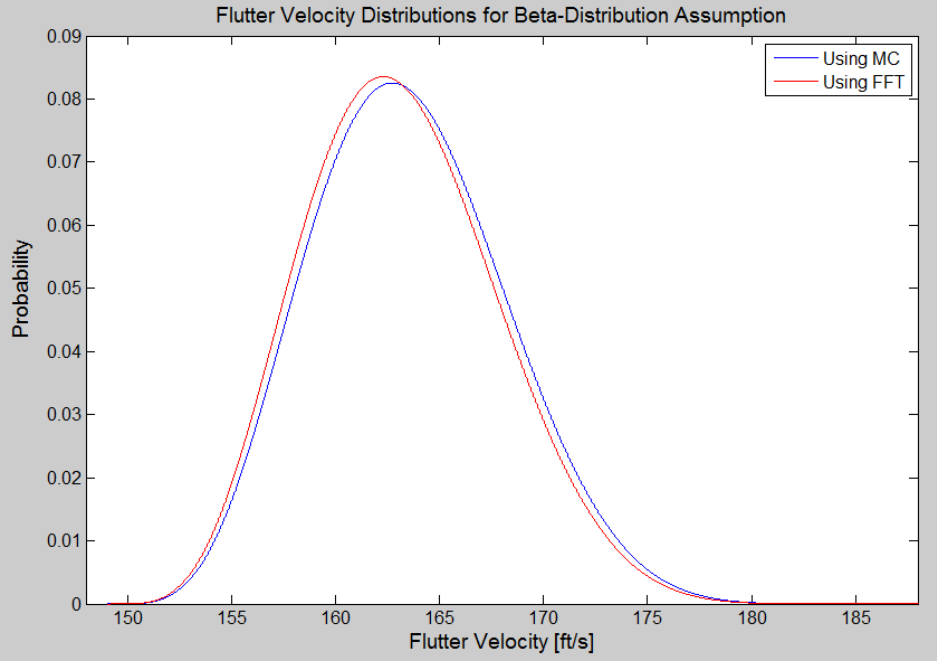

Figure 7.9. *PAFA Results for Beta Distributions*

Once again, Table 7.12 and Figure 7.9 show the distribution of the flutter velocity of the airfoil that is due to both the parametric and model-form uncertainty associated with the computational prediction of its value. Comparing the results of the two approaches for parametric uncertainty quantification, it can be seen that the Fast

Fourier Transform technique produces results very close to those produced by the exhaustive Monte Carlo sampling approach. In addition, by comparing the results shown through the FFT technique with looking simply at the results of the "best" model, $f_5(x)$, which only include the parametric uncertainty in the problem, it can be seen that ignoring the model-form uncertainty in this problem results in an overly-conservative representation of the flutter velocity (Figure 7.10).

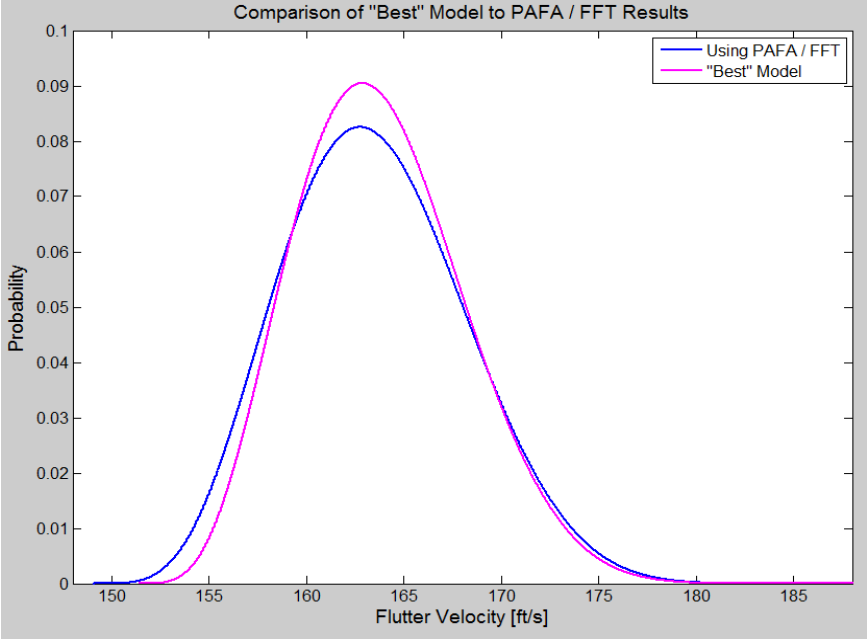

Figure 7.10. *Comparison of PAFA / FFT to "Best" Model*

This example demonstrated a methodology developed to quantify the model-form and parametric uncertainties that arose from the use of six aerodynamic models and two parametrically uncertain variables in the evaluation of the flutter velocity of a two degree of freedom airfoil subject to unsteady aerodynamics. The approach

demonstrated yields a single PDF of an output response of interest that represents the uncertainty in its prediction due to these uncertainties. The form of this PDF was shown to be applied for any number of distributions, although only Gaussian and Beta distributions were demonstrated in the example.

7.6. Quantification of Complete Uncertainties

In the prior four sections, different methods and approaches have been presented to quantify different subsets of the three forms of uncertainty, depending on the amount of data available in the analysis. In this final section, all three forms of uncertainty—model-form, parametric, and predictive—will be quantified for the problem of interest. These uncertainties will be quantified using the Bayesian Model Averaging approach detailed in Section 5.3.1. For this approach, the parametric uncertainty within each of the six models must be quantified. This has been done for the models of interest in Section 7.4 using the Fast Fourier Transform technique and the weighted Stack Response Surface Method approximation approach, and the results of which are presented in the first two columns of Table 7.9.

After quantifying the parametric uncertainty in each of the models, the next step in the approach is to calculate the posterior distribution of each model given the data set *D.* As mentioned in Section 7.5, the data set *D* consists of an experimental data point run at the expected value of all parameters with a value of *163.4 [ft/s]*. Inputting

this data into the expression shown in Eq. (5.55), the posterior model distributions for each of the six models can be computed through a numerical integration technique with an assumed Gaussian form.

Table 7.13: *Posterior Distributions*

	FFT w/ w-StackRSM	
	μ	σ
$f_1(x)$	*163.57*	*4.25*
$f_2(x)$	*163.81*	*4.51*
$f_3(x)$	*162.74*	*5.54*
$f_4(x)$	*163.80*	*4.27*
$f_5(x)$	*163.94*	*4.43*
$f_6(x)$	*164.03*	*4.45*

It can be seen by comparing the results of Table 7.13 to Table 7.9 that for this problem, the parametric uncertainty associated with each model dominates and renders the predictive uncertainty associated with each model nearly moot. This result is to be expected, as each model among the model set being considered predicts the results shown in the experimental data reasonable well—within about 1%—while the parametric uncertainty associated with each model comprises about 3-5% error. After developing the predictive distributions for each of the models, quantifying both the parametric and predictive uncertainties with the models, the next step in the approach is to calculate the posterior model probabilities for each model, as shown in Table 7.14.

Table 7.14: *Posterior Model Probabilities*

	$P(M_i)_{prior}$	$P(M_i)_{post}$	*Bayes' Factor*
$f_1(x)$	*0.1666*	*0.2714*	*1.044*
$f_2(x)$	*0.1666*	*0.1118*	*2.535*
$f_3(x)$	*0.1666*	*0.2834*	*1*
$f_4(x)$	*0.1666*	*0.0744*	*3.809*
$f_5(x)$	*0.1666*	*0.2336*	*1.213*
$f_6(x)$	*0.1666*	*0.0254*	*11.157*

It should be noted from Table 7.14 that although this process remains the same as the process detailed in the earlier Bayesian Model Averaging approach, that the posterior model probabilities for the models will not be identical to those shown in Table 7.6 due to the presence of parametric uncertainties as well. It can be noted from Table 7.14, though, that very similar results to those seen in Table 7.14 are observed. Model *3* remains the model with the highest model probability, although by a lesser margin this time. This decrease in margin is due to the fact that the parametric uncertainty associated with model *3* is slightly larger than the other five models considered. It can also be observed that, as with the case in Section 6.4, model *6* has a Bayes' Factor value greater than the critical value of *10*. As such, it can be concluded that the model has minimal effect on the adjusted model to be constructed due to inaccuracies within the model, and as such, can be eliminated at this time from consideration. As with the prior case, though, it is necessarily to renormalize the

posterior model probabilities after elimination of the model to maintain the constraints set forth in Eq. (5.21), as shown in Table 7.15.

Table 7.15: *Updated Posterior Model Probabilities*

	$P(M_i)_{post}$	$P(M_i)_{post,updated}$
$f_1(x)$	*0.2714*	*0.2789*
$f_2(x)$	*0.1118*	*0.1147*
$f_3(x)$	*0.2834*	*0.2909*
$f_4(x)$	*0.0744*	*0.0763*
$f_5(x)$	*0.2336*	*0.2397*

Using the posterior predictions shown in Table 7.13 with the posterior model probabilities in Table 7.15, the adjusted model can be solved for using Bayesian Model Averaging, as shown in Eq. (7.20).

$$y_{bma} = Norm(163.611, 4.643) \tag{7.20}$$

The distribution shown in Eq. (7.20) represents the uncertainty in the calculation of the flutter velocity of the airfoil due to the parametric, model-form, and predictive uncertainties associated with the computational modeling process. As such, by looking at the approaches shown in the sections of this chapter, it can be seen that depending upon the availability of input data—experimental data points, input variable distributions, or multiple models—the uncertainty in the prediction of the flutter

velocity of the airfoil can be solved by quantifying the uncertainty from as many of the potention sources as possible.

8. Full Flutter Simulations using Three Aeroelasticity Packages

8.1. AGARD Wing Background

To demonstrate the applicability of the modeling uncertainty framework on a full scale aeroelasticity problem, the design and analysis of an AGARD Standard 445.6 Weakened Wing will be observed. The AGARD Standard 445.6 Weakened Wing is a tapered wing with a quarter-chord weep angle of *45* degrees, an aspect ratio of *1.65*, and a taper ratio of *0.*66. The profile of the wing is a semispan model with a NACA 65A004 airfoil (91). The wing has a span of *2.50 [ft]* with a planform shape seen in Figure 8.1, and natural frequencies shown in Table 8.1.

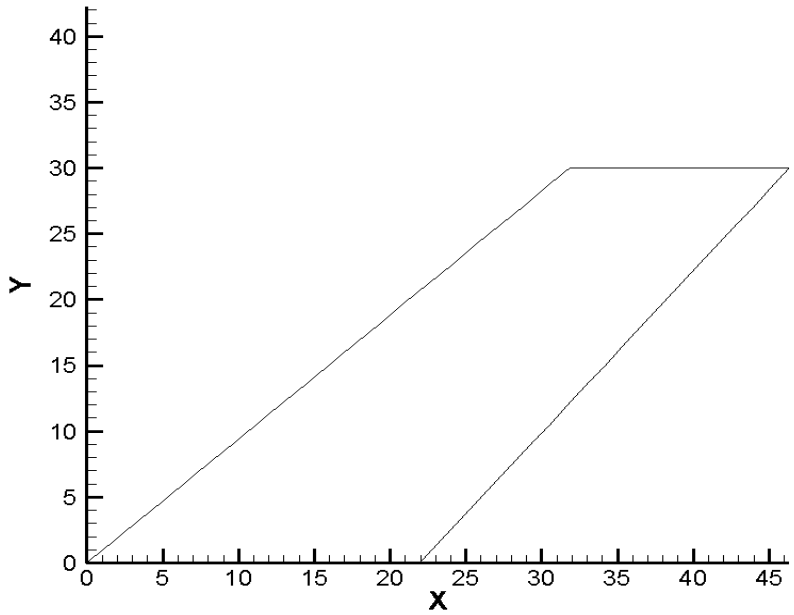

Figure 8.1: *Planform view of AGARD 445.6 Wing*

Table 8.1: *Experimental Natural Frequencies of AGARD 445.6 Wing*

	Experimental Frequency [Hz][91]	***Mode Shape***
Mode 1	*9.60*	*1st Bending*
Mode 2	*38.10*	*1st Torsion*
Mode 3	*50.70*	*2nd Bending*
Mode 4	*98.50*	*2nd Torsion*

The initial wing design was constructed and tested in NASA Langley's Transonic Dynamics Tunnel in 1963 using various wing models and angles of attack. One such popular configuration was the weakened wing model which was constructed of laminated mahogany with holes bored throughout the structure to artificially reduce the frequency of the wing, inducing a lower flutter velocity (20).

The aeroelastic flutter behavior of the weakened AGARD 445.6 wing has been explored and addressed in great detail in the literature in both the experimental and simulation field. Yates explored the transonic flutter of the airfoil through experimental measures by developing wind tunnel data for a model with both standard atmospheric and Freon-flow conditions (92). Initial studies in CFD simulation by Rausch (93) and Lee-Rausch (94) using Euler methods experienced errors in the prediction of flutter conditions when compared to experimental data. Lee-Rausch et al then studied the wing using an unsteady Navier-Stokes code (CFL3D) to further investigate the initial discrepancies that were found between the Euler investigations and the experimental data (95). It was found that both the Euler and Navier-Stokes codes initially experienced much greater success at predicting the flutter boundary of the wing in the upper transonic regime (M=0.96) than in the transonic / supersonic border region (M=1.141). Further analysis by Liu et al demonstrated the capture of the transonic flutter dip phenomenon through the use of a coupled CFD-CSD method (96).

8.2. Model Definition and Parameters

To quantify the complete uncertainty in the prediction of the flutter behavior of the AGARD 445.6 wing, models of the wing were constructed in the three aeroelasticity packages listed in Section 2.3.2-2.3.4: ZONA6, ZTAIC (CAPTSD), and ZEUS. As mentioned in Section 2.3, each of these aeroelastic modeling packages requires a representation of

the structural components of the wing using FEM. Before applying the parametric uncertainties to the problem of interest, the structural model to be used in these three codes was validated at the expected values of all structural parameters. An overview of these deterministic parameters can be seen below in Table 8.2.

Table 8.2: *Deterministic Structural and Aerodynamic Parameters of Three Aeroelastic Models Considered*

Panel Span	*2.50 [ft]*
Aspect Ratio	*1.6525*
Streamwise Semichord	*0.9165 [ft]*
Wing Mass	*0.1276 [slugs]*
Sweep Angle	*45˚*
Mach Number	*0.95*

To determine the structural response of the wing, a Nastran model of the AGARD wing structure was first constructed (Figure 8.2) that could be validated against the experimental data published by Yates, and then be used with the modeling packages identified above to perform the aeroelastic analysis. The Nastran model was constructed with *10* chord-wise elements and *20* span-wise elements for a total of 200 CQUAD4 elements using the model parameters set forth by Kolonay (97). Table 8.3 below shows the comparison of the frequencies observed in the Nastran structural model to the experimental data points published by Yates (92).

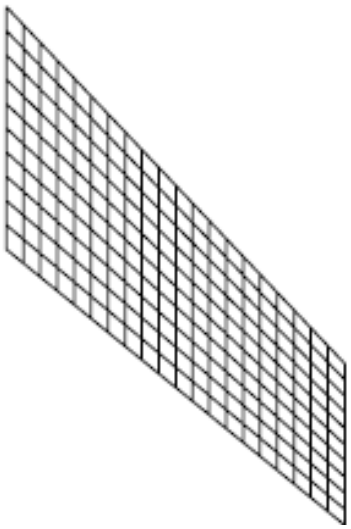

Figure 8.2: *Nastran Model of AGARD 445.6 Wing*

Table 8.3: *Frequency Comparison of Structural Model of AGARD 445.6 Weakened Wing*

	Nastran Model	***Experimental*** [92]	***Mode Shape***
Mode 1 [Hz]	9.60	*9.60*	*1st Bending*
Mode 2 [Hz]	36.77	*38.10*	*1st Torsion*
Mode 3 [Hz]	49.93	*50.70*	*2nd Bending*
Mode 4 [Hz]	88.71	*98.50*	*2nd Torsion*

It can be seen in Table 8.3 that the structural model's dynamic response demonstrates an acceptable level of agreement with the published experimental results. Although the higher frequencies, such as the third and fourth frequencies, show approximately 2-10% disagreement, the contribution of these frequencies to the aerodynamic flutter phenomenon is less than the lower frequencies. In addition, as will

be shown in the analysis, the first and second mode shapes are the primary modes contributing to the aerodynamic flutter, so agreement between the model and the physical scenario for these two frequencies is most critical.

In the wind tunnel tests conducted by Yates at NASA Langley (92), the results were presented in terms of the flutter velocity coefficient (Eq. (8.1)):

$$v_f = \frac{U_\infty}{b_s \omega_\alpha \sqrt{\mu}} \tag{8.1}$$

Where in Eq. (8.1), U_∞ refers to the free stream velocity of the flow at the flutter of the wing, b_s is the semispan root of the wing, ω_α is the first torsional frequency of the wing, and μ is the relative density of the wing, calculated as shown in Eq. (8.2):

$$\mu = \frac{m}{\rho V} \tag{8.2}$$

In Eq. (8.2), m is defined as the mass of the wing, ρ is the free stream density of the fluid medium at the flutter speed, U, and V is the volume of a conical frustrum with the streamwise root chord as a lower base diameter, the streamwise tip chord as the upper base diameter, and the span of the wing panel as the height. As a general frame of reference, in the original wind tunnel studies, the flutter speed coefficients observed ranged from about *0.3* to *1.1* depending upon the particular parameters used in the analysis.

Now that the structural model has been proven valid and the output response of interest has been clearly defined, the uncertainties can be formally introduced into the problem. For this analysis, three different aeroelastic packages were used to estimate the flutter velocity coefficient, representing three different models. The selection of the most appropriate or accurate model among the model set represents the model-form uncertainty in the problem. Wind tunnel data is available in the literature for the baseline parameters that are run in this analysis, allowing for the quantification of predictive uncertainty as well. Finally, the mass of the wing in the analysis will be considered stochastic to represent possible changes in the fuel state contained within the wing, as well as to demonstrate the capability of the approach to quantify parametric uncertainties as well. The mass is treated as a Gaussian variable and is defined in Eq. (8.3).

$$m = Norm(0.1276, 0.0128) \tag{8.3}$$

8.3. Simulation Results

For a baseline set of values, the three models discussed above were run at the expected value of the mass of the wing and the parameters defined in Table 8.2, yielding the results shown in Table 8.4.

Table 8.4: *Deterministic Results of 3 Simulation Models*

Solver	V_f
ZONA6 Linear Method	0.3460
ZTAIC (CAPTSD)	0.3170
ZEUS g-Method	0.3086

It is observed at the given parameters that while there is approximately 10% disagreement between the models' prediction for the flutter velocity coefficient, V_f, the results seem consistent with the expectations regarding their assumptions. The linear solver, ZONA6, produces the highest estimate of the flutter velocity coefficient while the more advanced, non-linear approaches produce a lower estimate of the value. It can be noted, as well, that the ZONA6 code is not intended for use within the transonic regime. However, the simulation model is included within this analysis. This is done intentionally to determine if the approaches developed in this work can identify an erroneous model, as the definitions of the boundaries within which models are valid are not necessarily clear for many application problems.

After ensuring the relative accuracy of each of the three models, a number of evaluations of the models must be performed to construct the surrogate that will be used in the parametric uncertainty quantification approach. In this problem, twelve simulations are to be run of each model, varying the mass of the wing, to construct the surrogate model relating the change in the flutter velocity coefficient as a function of

the change in the variable. The value of the parameter to run these twelve simulations was determined using a Latin Hypercube Sampling of the parameter distribution defined in Eq. (8.3).

8.4. Quantification of Complete Uncertainty

The first step in the complete uncertainty quantification process is to quantify the parametric uncertainty inherent to each of the three models. In this approach, the parametric uncertainty is quantified using the Fast Fourier Transform / weighted-Stack Response Surface Methodology approach that was detailed in Section 5.1.2. For this problem with one uncertain variable, a third order surrogate was used (Eq. (8.4)) and the twelve points that were sampled using Latin Hypercube Sampling (as mentioned in the prior section) are used to populate the surrogate and estimate the four β coefficients using w-StackRSM with $k = 4$.

$$v_{f_i} = f_i(\bar{x}) = \beta_{0,i} + \beta_{1,i} x_1 + \beta_{2,i} x_1^2 + \beta_{3,i} x_1^3 \tag{8.4}$$

The trained surrogate model is then used in the Fast Fourier Transform approach to estimate the pdf of the output response of interest—in this case, the flutter coefficient of the wing. As mentioned in Section 5.1.2, for the numerical integration technique utilized in this work to be implemented, an *a priori* distribution form must be assumed to the output response. By the Central Limit Theorem, in the absence of any data suggesting otherwise, a Gaussian distribution is assumed. Thus, the numerical

integration results for each of the three models are then fit to Gaussian distributions, producing the results shown in Table 8.5.

Table 8.5: *Distributions Due to Parametric Uncertainties*

	FFT w/ w-StackRSM	
	μ	σ
ZONA6	*0.3451*	*0.0281*
ZTAIC	*0.3173*	*0.0127*
ZEUS	*0.3094*	*0.0145*

The distributions defined in Table 8.5 represent the parametric uncertainties associated with each of the three models. The next step in the complete uncertainty quantification process is to quantify both the model-form and predictive uncertainty using the Bayesian Model Averaging approach. For this to be done, experimental data must be introduced into the problem. From Yates' wind tunnel experiments, the flutter velocity coefficient at the parameters defined in Table 8.1 for the wing was *0.3059*. With this experimental data set *D*, consisting of only one point in this case, the predictive uncertainty in each model can be quantified through the numerical evaluation of Eq. (5.55), resulting in the distributions shown in Table 8.6.

Table 8.6: *Model Predictive Distributions*

	μ	σ
ZONA6	*0.3451*	*0.0481*
ZTAIC	*0.3173*	*0.0171*
ZEUS	*0.3094*	*0.0149*

Looking at the results in Table 8.6, two points become apparent. First, it is clear that the predictive uncertainty associated with each of the models has an effect on the variance of the predictive distributions on each of the models when the results in Table 8.6 are compared to those of Table 8.5. Secondly, it can be seen that the models that show greater disagreement from the data point obtained at *0.3059* experience a larger increase in model variance when the predictive uncertainty is quantified. This result is to be expected, as the predictive uncertainty represents the potential of a model to accurately predict the true physical results. If the true physical results are shown to be different from the predictions of the model, it is then expected that the variance in those predictions, the predictive uncertainty associated with the model, would increase.

After obtaining the predictive distributions for each of the models, the model probabilities of each model must be calculated to complete the Bayesian Model Averaging approach. Using Bayes' Theorem as shown in Eq. (5.61), the posterior model probabilities for each of the three models can be calculated as shown in Table 8.7.

Table 8.7: *Posterior Model Probabilities*

	$P(M_i)_{prior}$	$P(M_i)_{post}$	*Bayes' Factor*
ZONA6	*0.3333*	*0.1179*	*4.3328*
ZTAIC	*0.3333*	*0.3714*	*1.3880*
ZEUS	*0.3333*	*0.5107*	*1*

Looking at the posterior model probabilities in Table 8.7, it can be seen that the ZEUS model has the highest posterior model probability, an expected result as this model is considered the highest fidelity among the models considered. Additionally, looking at the Bayes' Factor for each of the three models shown in Table 8.7, it can be seen that the *ZONA6* model has the largest Bayes' Factor of *6.*46, but it is not greater than the critical value of *10* defined earlier in this work. Although the deterministic result from the *ZONA6* model is divergent from the other values, the parametric uncertainties associated with the model results prohibits the elimination of the model from just one experimental data point. Extending the results, if additional points were to be observed in the future near the current data point of *0.3059*, the trends observed in Table 8.7 would continue and the Bayes' Factor for the ZAERO6 model would continue to increase.

With the posterior model probabilities shown in Table 8.7, the adjusted model for the flutter velocity coefficient the contains the parametric, model-form, and

predictive uncertainties associated with the estimation of its value can be obtained using Eq. (5.51) and is shown in Eq. (8.5) and Figure 8.3.

$$v_{f,bma} = Norm(0.315, 0.023) \tag{8.5}$$

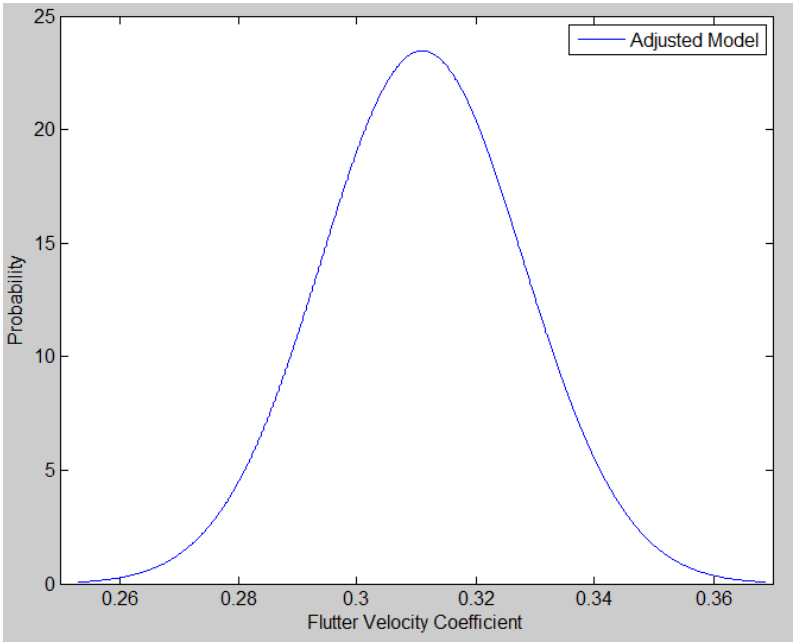

Figure 8.3: *Adjusted Model of Flutter Velocity Coefficient*

The amount of uncertainty in the prediction of the flutter velocity coefficient for the AGARD 445.6 at the parameter set listed in Table 8.1 can be seen in the figure above. This uncertainty is a complete representation of the uncertainty in the modeling process, including both the uncertainty in the selection of the most appropriate model to evaluate to the output response of interest, as well as the uncertainty associated with each model's relative ability to predict the true physical scenario of interest. If the adjusted model obtained through this approach was to be compared to an approach ignorant of model-form and predictive uncertainty, such as simply selecting the model

representing the parametric uncertainty in the ZEUS model, it can be seen that an under-conservative design results (Figure 8.4).

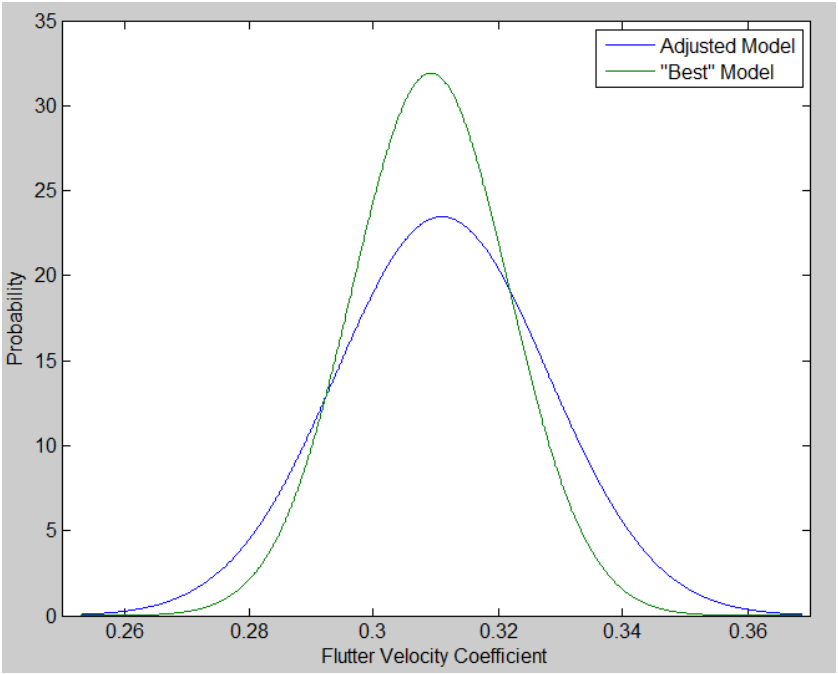

Figure 8.4: *Comparison of Adjusted Model to "Best" Model*

This under-conservative design is the result of ignoring multiple potential sources of uncertainty in the computational modeling process. As with any reliability engineering problem, under-conservative designs are dangerous as they can give a false sense of confidence regarding a particular output response. When handling a response as critical and potentially catastrophic as the flutter of an aircraft, this can be incredibly reckless and dangerous. It has been shown in this example, though, that be systematically considering all possible models and data available to the designer, the

uncertainty from all possible sources can be considered, resulting in a more accurate and representative distribution of uncertainty.

9. Summary

This work developed and demonstrated methods for the complete quantification of uncertainty from all sources for the application to aeroelastic analyses. Aeroelasticity is a complex, multi-disciplinary field that draws upon background from the fields of structures, aerodynamics, control theory, and dynamics to analyze the coupling between the inertial, aerodynamic, and elastic forces on an air vehicle. As a result of the complexities in the analyses within each of the individual disciplines, and with their couplings, there is a great deal of uncertainty associated with both the simulation and modeling of aeroelastic responses and phenomena. Chapter 4 showed how these uncertainties could be thought of as originating from three sources: parametric, model-form, or predictive uncertainty. While it is important to be able to quantify, and if possible, minimize these uncertainties, methods that can be used to quantify uncertainties from one source are not necessarily applicable to the other two sources. As mentioned, much of the research in uncertainty quantification in aeroelasticity has focused upon quantifying the parametric uncertainty with aeroelastic modeling tools and packages. Such an approach ignores two potential forms of uncertainty, and as shown in Section 7.4, can result in an under-conservative representation of the potential uncertainty in the problem.

This work addresses the two often ignored sources of uncertainty, as well as parametric uncertainties, by developing and demonstrating methods for the quantification of uncertainties from all sources in aeroelastic simulation problems, as shown in Chapter 5. While the methods developed in this work are not limited to aeroelastic problems, they are demonstrated and validated on such. While the quantification of the uncertainties from all three potential sources is the optimal goal of an approach, this goal is not always feasible depending upon the information available for the problem of interest. For instance, as mentioned in Section 4.3, the quantification of the predictive uncertainty in a model is impossible without data regarding the true physical scenario of interest—often some form of experimental data. As such, in instances where complete information is unavailable, methods must exist to quantify as much of the uncertainty as possible. Chapter 5 detailed multiple methods developed in this work for the quantification of different forms of uncertainty given different sets of available information to the designer.

Section 2.3 detailed the extensive computational cost that can be associated with the aeroelastic analysis of a design using different simulation packages. As uncertainty quantification is often a process that is heavily limited by the simulation time of the respective models, it is imperative to minimize the computational time required to develop these accurate stochastic measures. Chapter 3 detailed a novel surrogate modeling technique, the weighted Stack Response Surface Methodology, to

be coupled with the parametric uncertainty quantification techniques discussed in Section 5.1.2 to yield surrogate models with improved accuracies at no additional computational cost. For the validation cases demonstrated in Section 3.3, a *3-6%* improvement in residual error was observed when compared to the established least-squares response surface methodology. This surrogate modeling method was then utilized to quantify the parametric uncertainty associated with each of the models using a Fast Fourier Transform technique, detailed in Section 5.1.2.

Finally, the applicability of the uncertainty quantification tools developed in this work was demonstrated on three different problems of interest: a simple closed-form spring-mass problem, a two degree of freedom airfoil subject to unsteady aerodynamics, and the flutter simulation of the AGARD 445.6 wing using commercial aeroelastic packages. For the closed-form spring-mass system and the airfoil problem, many possible permutations of available data were explored to demonstrate the capability of the different approaches at efficiently and accurately quantifying the sources of uncertainty and identifying the sources contributing most significantly to those uncertainties. For the AGARD 445.6 simulation problem, the Bayesian approach for the quantification of uncertainties from all sources was demonstrated by coupling the results of the individual models with published experimental data to develop a complete representation of the uncertainty associated with the estimation of the flutter velocity coefficient for the wing.

9.1. Research Contributions

As mentioned in the introduction, there are four primary and novel research contributions in this work. First, as discussed in Section 3.3, the weighted Stack Response Surface (w-StackRSM) method was developed in this work as an improved and efficient surrogate modeling technique for situations where an *a priori* surrogate model must be assumed, such as Fast Fourier Transforms. The w-StackRSM approach utilizes *k*-fold sampling measures to partition the complete data set into smaller, independent data sets. Using these smaller data sets, multiple independent models can be developed and cross-validated using the traditional least-squares response surface method, resulting in *k* different models and residual errors. Then, by weighing each of the component models inversely with respect to their residual errors, a weighted response surface model can be developed that is shown to have a *3-6%* reduced residual error when compared to simply using least-squares RSM on the complete data set.

The second research contribution of this work was the development of the Probabilistic Adjustment Factors Approach (PAFA). This approach utilizes the framework of an existing approach, the Adjustment Factors Approach (73), which was originally developed to quantify the model-form uncertainty among deterministic models. By redefining each of the constituent models as stochastic with a specified

distribution on an output response of interest, the Adjustment Factors Approach was re-derived for different possible distribution assumptions to develop an approach that was capable of quantifying both the model-form and parametric uncertainties in the modeling process without the necessity for experimental data points. While this approach is applicable for distributions of any form, it does require an *a priori* assumption regarding the distribution form itself. In Section 5.2.2, the derivation of this approach for both Gaussian and Beta distribution assumptions was demonstrated.

The third research contribution of this work was the development of the Modified Adjustment Factors Approach (MAFA). This approach approximates the sensitivity of an adjusted model developed using either the traditional Adjustment Factors Approach or the Probabilistic Adjustment Factors Approach to the individual model probabilities that are assigned to each of the models using expert opinions. The MAFA has two different stages to its application. The first stage approximates the sensitivity of the adjusted model to the model probability set as a whole. This sensitivity, quantified through a Bhattacharyya metric, estimates the potential reduction in model-form uncertainty that could be experienced through the refinement of the model probability values assigned to each of the models—likely done through the introduction of additional data or knowledge into the problem. If additional data or knowledge is unable to be introduced due to limitations on experimental data sets, then the second stage of the MAFA approximates the sensitivity of the adjusted model to each of the individual models utilized. The models with the highest sensitivity can then

be identified as models that contribute most significantly to the variance in the adjusted model. As such, if a model has a significantly higher sensitivity than the majority of the model set, this approach identifies that model as being potentially erroneous or misused, and that further analysis or attention should be given to the particular model of interest.

The final research contribution of this work is the adaptation of the Bayesian Model Averaging (BMA) approach to aerospace engineering applications. As mentioned in Section 5.3.1, BMA has been used in the last *10* years for forecasting models in the fields of economics, geology, and meteorology by combining multiple historical models into a singular predictive model of future events. This same approach is applied in this work to utilize the results of individual constituent models of aeroelastic responses to develop a composite prediction of the expected uncertainty that can be associated with the true physical response that is being modeled. BMA, through the use of Bayes' Theorem and Maximum Likelihood Estimators enables to the quantification of uncertainty from all three potential sources, provided that experimental data is available. This approach does so through two steps: first developing the predictive distribution of each of the constituent models to include the predictive uncertainty associated with the model itself and then using the data set, and Bayes' Theorem, to develop posterior model probabilities of the constituent models that are determined empirically through the capability of the individual models to capture the physics represented in the given data set. By coupling this approach with methods to quantify

the parametric uncertainties within each of the models (FFT / w-StackRSM approach), the BMA approach can be utilized to quantify the complete uncertainty in a problem where the full amount of information is made available to the designer.

10. References

1. Acar, E., Kale, A., Haftka, R.T., and Stroud, W.J. "Structurally Safety Measures for Airplanes." *AIAA Journal of Aircraft*, Vol. 43, 2006, pp. 30-38.

2. Lincoln, J.W. "Method for Computation of Structural Failiure Probability for an Aircraft." Wright-Patterson Air Force Base. Dayton, OH. Technical Report, 1980. ASD-TR-80-5035.

3. Wirsching, P.H. "Literature Review on Mechanical Reliability and Probabilistic Design." NASA Langley Research Center. Hampton, VA. NASA Contractor Report, 1992. No. 189159.

4. Long, M.W. and Narciso, J.D. "Probabilistic Design Methodology for Composite Aircraft Structures." Federal Aviation Administration, 1999. FAA Final Report. DOD/FAA/AR-99/2.

5. Riley, M.E. and Grandhi, R.V. "Efficient Surrogate Modeling Using a Weighted-Stack Response Surface Methodology (w-StackRSM)." *Structural and Multidisciplinary Optimization*, Vol. 89, No. 25-26, 2011, pp. 889-896.

6. Riley, M.E. and Grandhi, R.V. "A Method for Quantification of Model-Form and Parametric Uncertainties in Physics-Based Simulations." *AIAA Journal*, 2011. (sumbitted).

7. Riley, M.E., Grandhi, R.V., and Kolonay, R. "Quantification of Modeling Uncertainty in Aeroelastic Analyses." *AIAA Journal of Aircraft*, Vol 48, No. 3, 2011.

8. Park, I., Amarchinta, H.K., and Grandhi, R.V. "A Bayesian Approach for Quantification of Model Uncertainty." *Reliability Engineering and System Safety*, Vol. 95, 2010. pp. 777-785.

9. Riley, M.E. and Grandhi, R.V. "Quantification of Model-Form and Predictive Uncertainty for Multi-Physics Simulation." *Computers and Structures*, Vol. 89, 2011. pp. 1206-1213.

10. Collar, A.R. "Aeroelastic Problems at High Speed." *Journal of the Royal Aeronuatical Society*, Vol. 51, No. 1, 1947.

11. Collar, A.R. "The Expanding Domain of Aeroelasticity." *Journal of the Royal Aeronautical Society*, Vol. L, August 1946. pp. 616-636.

12. Wright, J.R. and Cooper, J.E. *Introduction to Aircraft Aeroelasticity and Loads*. John Wiley & Sons: West Sussex, England. 2007.

13. Collar, A.R. "The First Fifty Years of Aeroelasticity." *Aerospace Engineering*. February 1978, pp. 12-20.

14. Garrick, I.E. and Reid, W.H. "Historical Development of Aircraft Flutter." *AIAA Journal of Aircraft,* Vol. 18, No. 11, 1981. pp. 897-912.

15. Bisplinghoff, R.L., Ashley, H., and Halfman, R.L. *Aeroelasticity*. Dover Publications Inc.: Mineloa, NY. 1996.

16. Singh, S.N. and Brenner, M. "Limit Cycle Oscillations and Orbital Stability in Aeroelastic Systems wih Torsional Nonlinearity." *Journal of Nonlinear Dynamics*, Vol. 31, 2003. pp. 435-450.

17. Hassig, H.J. "An Approximate True Damping Solution of the Flutter Equation by Determinant Iteration." *AIAA Journal of Aircraft*, Vol. 8, 1971. pp. 885-889.

18. Clancy, L.J. *Aerodynamics*. Pitman Publishing: London, England. 1975.

19. Dowell, E.H. *A Modern Course in Aeroelasticity.* Kluwer Academic: Dordrecht, Pays-Bas. 1995.

20. Yates, E.C., Land, N.S., and Foughner, J.T. "Measure and Calculated Subsonic and Transonic Flutter Characterisitics of a 45 Degree Sweptback Wing Planform in Air and in Freon-12 in the Langley Transonic Dynamic Tunnel." NASA Langley, Virginia. NASA Technical Note, 1963. D-1616.

21. Theodorsen, T. *General Theory of Aerodynamic Instability and the Mechanism of Flutter.* N.A.C.A. 1935. Report 496.

22. NASTRAN User's Manual . Santa Ana, CA : MSC Software Corporation, 2005 r3.

23. ZAERO Applications Manual Vol.1. s.l. : Zona Tech, 2008, Version 8.3.

24. ZEUS User's Manual. Scottsdale, AZ : ZONA Technology, 2009.

25. Kleijnen, J.P.C. *Statistical Tools for Simulation Practitioners*. Marcel Dekker: New York. 1978.

26. Sobeiszczanski-Sobieski, J. and Haftka, R.T. "Multidisciplinary Aerospace Design Optimization: Survey of Recent Developments." *Structural Optimization*, Vol. 14, 1997. pp. 1-23.

27. Smith, M. *Neural Networks for Statistical Modeling*. Nostrand Reinhold: New York. 1993.

28. Sacks, J., Welch, W.J., Mitchell, T.J., and Wynn, H.P. "Design and Analysis of Computer Experiments." *Statistical Science*, Vol. 4, 1989. pp. 409-435.

29. Box, G.E.P, Hunter, W.G., and Hunter, J.S. *Statistics for Experimenters.* John Wiley & Sons: New York. 1978.

30. Simpson, T.W., Pepinski, J., Koch, P.N., and Allen, J.K. "On the Use of Statistics in Design and the Implications for Deterministic Computer Experiments." *ASME, Design Theory and Methodology - DTM'97*. Sacramento, CA . 1997. DETC97/DTM-3881.

31. Papila, N., Shyy, W., Griffin, L.W., and Domey, D.J. "Shape Optimization of Supersonic Turbines using Response Surface and Neural Network Methods." *Journal of Propulsion and Power*, Vol. 18, 2001. pp. 509-518.

32. Stander, N., Roux, W., Giger, M., Redhe, M., Federova, N., and Haarhoff, J. "A Comparison of Meta-Modeling Techniques for Crashworthiness Optimization." *AIAA, 10th AIAA/ISSMO Multidisciplinary Analysis and Optimization Conference*. Albany, NY. 2004. AIAA-2004-4489.

33. Queipo, N.V., Haftka, R.T., Shyy, W., Goel, T., Vaidyanathan, R., and Tucker, P.K. "Surrogate-Based Analysis and Optimization." *Progress in Aerospace Sciences*, Vol. 41, 2005. pp. 1-28.

34. Allaire, D.L., Willcox, K.E., and Toupet, O. "A Bayesian-Based Approach to Multifidelity Multidisciplinary Design Optimization." *13th AIAA/ISSMO Multidisciplinary Analysis and Optimization Conference*. Fort Worth, TX . 2010. AIAA 2010-9183.

35. Zerpa, L, Queipo, N.V., Pintos, S., and Salager, J. "An Optimization Methodology of Alkaline-Surfactant-Polymer Flodding Processes Using Field Scale Numerical Simulations and Multiple Surrogates." *Journal of Petroleum Science and Engeineering*, Vol. 47, 2005. pp. 197-208.

36. Goel, T., Haftka, R.T., Shyy, W., and Queipo, N.V. "Ensemble of Surrogates." *Structural and Multidisciplinary Optimization*, Vol. 33, 2007. pp. 199-216.

37. Glaz, B., Goel, T., Liu, L., Friedman, P.P., and Haftka, R.T. "Multiple-Surrogate Approach to Helicopter Rotor Blade Vibration Reduction." *AIAA Journal*, Vol. 47, No. 1, 2009. pp. 271-282.

38. Das, P.K. and Zheng, Y. "Cumulative Formation of Response Surface and its Use in Reliability." *Probabilistic Engineering Mechanics*, Vol. 15, 2002. pp. 309-315.

39. Mulani, S., Pankaj, J., Jing, L., Kapania, R., and Shin, Y. "Optimal Design of Unitized Structures Using Response Surface Approaches." *AIAA Journal of Aircraft*, Vol. 47, No. 6, 2010. pp. 1898-1906.

40. Box, G.E.P. and Wilson, K.B. "On the Experimental Attainment of Optimum Conditions.", *Journal of Royal Statistics Society*, Vol. 13, 1951. pp. 1-45.

41. Bucher, C.G. and Bourgund, U. "A Fast and Efficient Response Surface Approach for Structural Reliability Problems." *Structural Safety*, Vol. 7, No. 1, 1990. pp. 57-66.

42. Kaymaz, I. and McMahon, C.A. "A Response Surface Method Based on Weighted Regression for Structural Reliability and Analysis." *Probabilistic Engineering Mechanics*, Vol. 20, 2005. pp. 11-17.

43. Geisser, S. "The Predictive Sample Reuse Method with Applications." *Journal of the American Statistical Society Association*, Vol. 70, 1975. pp. 320-328.

44. Duda, R.O., Hart, P.E., and Strork, D.G. *Patter Classification*. Wiley: New York. 2001.

45. Tracey, B., Wolpert, D., and Alonso, J.A. "Using Supervised Learning to Improve Monte Carlo Integral Estimation." *52nd AIAA/ASME/ASCE/AHS/ASC Structures, Structural Dynamics, and Materials Conference*. Denver, CO. 2011. AIAA-2011-1843.

46. Jin, R., Chen, W., and Simpson, T.W. "Comparitive Studies of Metamodeling Techniques under Multiple Modeling Criteria." *Structural and Multidisciplinary Optimization*, Vol. 23, 2011. pp. 1-13.

47. Kennedy, M.C. and O'Hagan, A. Bayesian Calibration of Computer Models. *Journal of the Royal Statistical Society*, Vol. 63, No. 3, 2001. pp. 425-464.

48. Pate-Cornell, M.E. "Uncertainties in Risk Analysis: Six Levels of Treatment." *Reliability and System Safety*, Vol. 54, 1996. pp. 95-111.

49. Hacking, J. *The Emergence of Probability*. University Press: Cambridge, U.K. 1975.

50. Chernoff, H. and Moses, L.E. *Elementary Decision Theory*. Wiley: New York. 1959.

51. Droguett, E L and Mosleh, A. "Bayesian Methodology for Model Uncertainty Using Model Performance Data." *Risk Analysis*, Vol. 28, No. 5, 2008. pp. 1457-1476.

52. Pettit, C.L. "Uncertainty Quantification in Aeroelasticity: Recent Results and Research Challenges." *Journal of Aircraft*, Vol. 41, No. 5, 2004. pp. 1217-1229.

53. Cheng, J., Cai, C.S., Xiao, R.C., and Chen, S.R. "Flutter Reliability Analysis of Suspension Bridges." *Journal of Wind Engineering*, Vol. 93, 2005. pp. 757-775.

54. Kurdi, M., Lindsley, N., Beran, P. "Uncertainty Quantification of the Goland Wing's Flutter Boundary." *AIAA Atmospheric Flight Mechanics Conference and Exhibit.* Hilton Head, SC. 2007.

55. Beran, P.S., Pettit, C.L., and Millman, D.R. "Uncertainty Quantification of Limit-Cycle Oscilattions." *Journal of Computational Physics*, Vol. 217, No. 1, 2007. pp. 217-247.

56. Witteveen, J. and Bijl, H. "A TVD Uncertainty Quantification Method with Bounded Error Applied to Transonic Airfoil Flutter."*Communications in Computational Physics.* Vol. 6, No. 2, 2009. pp. 406-432.

57. Chen, W., Baghdasaryan, L. Buranathiti, T., and Cao, J. "Model Validation via Uncertainty Propagation and Data Transformations." *AIAA Journal* Vol. 42, No. 7, 2004. pp. 1406-1415.

58. Bae, H.R., Grandhi, R.V., and Canfield, R.A. "An Approximation Approach for Uncertainty Quantification Using Evidence Theory." *Reliability Engineering and System Safety,* Vol. 86, 2004 pp. 215-225.

59. Metropolis, N. and Ulam, S. "The Monte Carlo Method." *Journal of the American Statistical Association*, Vol. 44, 1949 pp. 335-341.

60. McKay, M.D., Beckman, R.J., and Conover, W.J. "A Comparison of Three Methods for Selecting Values of Input Variables in the Analysis of the Output from a Computer Code." *Technometrics*, Vol. 21, No. 2, 1979. pp. 239-245.

61. Metropolis, N, Rosenbluth, A.W., Rosenbluth, M.N., Teller, A.H., and Teller, E. "Equations of State Calculations by Fast Computing Machine." *Journal of Chemical Physics*, Vol. 21, 1953. pp. 1087-1091.

62. Tierney, L. "Markov Chains for Exploring Posterior Distributions." *Annual of Statistics*, Vol. 22, 1994. pp. 1701-1762.

63. Richardson, S., and Spiegelhalter, D.J. Gilks. *Markov Chain Monte Carlo in Practice*. Chapman & Hall : London. 1995.

64. Gilks, W.R. *Full Conditional Distributions*. Chapman & Hall : London. 1995.

65. Choi, S.K., Grandhi, R.V., and Canfield, R.A. *Reliability-based Structural Design*. Springer-Verlag: London, England. 2007.

66. "Integration of Probabilistic Methods into the Design Process." Society of Automotive Engineers. 1997. Aerospace Information Report 5080.

67. Penmetsa, R.C. and Grandhi, R.V. "Structural Failure Probability Prediction Using Fast Fourier Transformations for High Accuracy." *Journal of Finite Elements in Analysis and Design*, Vol. 39, nos. 5-6, 2003. pp. 473-478.

68. Kim, J.W. and Lee, D.J. "Optimized Compact Finite Difference Schemes with Maximum Resolution." *AIAA Journal*, Vol. 34, No. 5, 1996. pp. 887-894.

69. Leamer, E.E. S*pecification Searches: Ad hoc Inference with No Experimental Data*. Wiley & Sons: New York. 1978.

70. Draper, D. "Model Uncertainty in "Stochastic" and "Deterministic" Systems." P*roceedings of the 12th International Workshop on Statistical Modeling,* 1997*.* Biel/Bienne, Switzerland. pp. 43-59.

71. Allaire, D. and Willcox, K. "Surrogate Modeling for Uncertainty Assessment with Application to Aviate Environmental System Models." *AIAA Journal*. 2010. (accepted for publication).

72. Mosleh, A., and Apostolakis, G. "The Assessment of Probability Distributions from Expert Opinions with an Application to Seismic Fragility Curves." *Risk Analysis*, Vol. 6, No. 4, 1986. pp. 447-461.

73. Zio, E., and Apostolakis, G. "Two Methods for the Structural Assessment of Model Uncertainty by Experts in Performance Assessments of Radioactive Waste Repositories." *Reliability Engineering & System Safety*, Vol. 54, Nos. 2-3, 1996. pp. 225-241.

74. Reinert, J.M., and Apostolakis, G. "Including Model Uncertainty in Risk-Informed Decision Making." *Annals of Nuclear Energy*, Vol. 33, No. 4, 2006. pp. 354-369.

75. Bhattacharyya, A. "On a Measure of Divergence Between Two Statistical Populations Defined by Probability Distributions." *Bull. Calcutta Mathethmaics Society*, 1943. pp. 99-110.

76. Oberkampf, W.L. and Roy, C.J. *Verification and Validation in Scientific Computing*. Cambridge University Press : New York. 2010.

77. Papila, M. and Haftka, R.T. "Resposne Surface Approximations: Noise, Error Repair, and Modeling Errors." *AIAA Journal*, Vol. 38, No. 12, 2000. pp. 2336-2343.

78. Hosder, S., Watson, L.T., Grossman, B., Mason, W.H., Kim, H., Haftka, R.T., and Cox, S.E. "Polynomial Response Surface Approximations for the Multidisciplinary Design Optimization of a High Speed Civil Transport." *Optimization and Engineering*, Vol. 2, 2001. pp. 431-452.

79. Zhang, R., Mahadevan, S. "Model Uncertainty and Bayesian Updating in Reliability-based Inspection." *Structural Safety*, Vol. 22, 2000. pp. 145-160.

80. Zhang, R. and Mahadevan, S. "Bayesian Methodology for Reliability Model Acceptance." *Reliability Engineering and System Safety*, Vol. 80, 2003. pp. 95-103.

81. Rebba, R., Mahadevan, S., and Huang, S. "Validation and Error Estimation of Computational Models." *Reliability Engineering and System Safety,* Vol. 91, 2006. pp. 1390-1397.

82. Draper, D. "Assessment and Proagation of Model Uncertainty." *Journal of the Royal Statistical Society*, Vol. 57, No. 1, 1995. pp. 45-97.

83. Hoeting, J.A., Madigan, D., Raftery, A.E., Volinsky, C.T. "Bayesian Model Averaging: A Tutorial." *Statistical Science*, Vol. 14, No. 4, 1999. pp. 382-417.

84. Wasserman, L. "Bayesian Model Selection and Model Averaging." *Journal of Mathematical Psychology*, Vol. 44, 2000. pp. 92-107.

85. Ando, T. "Bayesian Model Averaging and Bayesian Predictive Information Criterior for Model Selection." *Journal of Japanese Statistical Society*, Vol. 38, No. 2, 2008. pp. 243-257.

86. Vrugt, J.A., Diks, C.G.H., and Clark, M.P. "Ensemble Bayesian Model Averaging Using Markov Chain Monte Carlo Sampling." *Environmental Fluid Mechanics*, Vol. 5, 2008. pp. 579-595.

87. Swiler, L.P., Urbina, A., and Williams, B.J. "Multiple Model Inference: Calibration, Selection, and Prediction with Multiple Models." *13th AIAA Non-Deterministic Approaches Conference*, Denver, CO. 2011. AIAA 2011-1844.

88. He, J.H. "Variational Approach for Nonlinear Oscillators." *Chaos Soluations and Fractals*, Vol. 34, No. 5, 2007. pp. 1430-1439.

89. Park, I. and Grandhi, R.V. "Quantifying Multiple Types of Uncertainty in Physics-based Simulation Using Bayesian model Averaging." *AIAA Journal*, Vol. 49, No. 5, 2011. pp. 1038-1045.

90. Rivera, J.A., Dansberry, B.E., Bennett, R.M., Durham, M.H., and Silva, W.A. "NACA 0012 Benchmark Model Experimental Flutter Results with Unsteady Pressure Distributions." *33rd AIAA/ASME/ASCE/AHS/ASC Structures, Structural Dynamics and Materials Conference.* Dallas, TX , 1992. Vol. 4, pp. 1898-1908.

91. Yates, E. Carson, Jr. "Preliminary Report on Candidates for AGARD Standard Aeroelastic Configurations for Dynamic Response." *Meeting of the AGARD Structures and Materials Panel*, Oberammergau, Germany. 1985. NASA TM 89142.

92. Yates Jr., E. Carson. "AGARD Standard Aeroelastic Configurations for Dynamic Response." NASA Langley Research Center, Hampton, VA. 1987. NASA Technical Memorandum.

93. Rausch, R.D, Batina, J.T., and Yang, H.T.Y. "Three Dimensional Time-Marching Aeroelastic Analyses Using an Unstructured Grid-Euler Method." AIAA, April, 1992. AIAA Paper No. 92-2506.

94. Lee-Rausch, E. M. and Batina, J.T. "Wing Flutter Boundary Predictions Using Unsteady Euler Method." AIAA, 1993. AIAA Paper No. 93-1422.

95. Lee-Rausch, E.M. and Batina, J.T. "Calculation of Agard Wing 445.6 Flutter Using Navier-Stokes Aerodynamics." *11th AIAA Applied Aerodynamics Conference*. Monetery, California, 1993. AIAA Paper No. 93-3476.

96. Liu, F., Cai, J., Zhu, Y., Tsai, H.M., and Wong, A.S.F. "Calculation of Wing Flutter by a Coupled Fluid-Structure Method." *AIAA Journal of Aircraft*, Vol. 38, No. 2, 2001. pp. 334-342.

97. Kolonay, R.M. "Unsteady Aeroelastic Optimization in the Transonic Regime." Purdue University, 1996. Ph.D. Dissertation.

Appendix A: 2 DOF Airfoil Matlab Solver (w/ parametric uncertainties):

```
%%   Establish Uncertain Database:
num_it = 1;
vf_hist1 = zeros(1,num_it);
vf_hist2 = zeros(1,num_it);
vf_hist3 = zeros(1,num_it);
vf_hist4 = zeros(1,num_it);
vf_hist5 = zeros(1,num_it);
vf_hist6 = zeros(1,num_it);

%   Define Problem Parameters
num_div=200;
invk_min=1;
invk_max=4;
size_div=(invk_max-invk_min)/num_div;
n=0;
tol=0.0001;

%   Define Certain Parameters:
wtheta=1.5524;      %[rad/sec]      1.5524
wh=0.8689;          %[rad/sec]      0.8689
b=30;               %[ft]           30
m=269;              %[slug/ft]      269
mu=40;              %               40
xthetabar=0;        %               0
rthetabar=0.4888;   %               0.7888
a=0;                %               0

%   Define Uncertain Parameters:
% wtheta_mean = 1.5524;
% wtheta_std = 0.0776;
%
% wh_mean = 0.8689;
% wh_std = 0.0434;

%%   Begin Uncertainty Loop:
for ii=1:num_it

    %  Redefine Uncertain Variables:
%     wtheta = normrnd(wtheta_mean,wtheta_std);
%     wh = normrnd(wh_mean,wh_std);

    %%   Begin Solution Loop 1
    for invk=invk_min:size_div:invk_max;
        n=n+1;

        k=1/invk;

        Ck=1-((0.165*k)/(k-0.0455*1i))-((0.355*k)/(k-0.3*1i));

        Lh=1-(1i*2*Ck)/k;
        La=1/2-(1i*(1+2*Ck))/k-(2*Ck)/(k^2);
```

```
        Mh=1/2;
        Ma=3/8-1i/k;

        x = wh^2/wtheta^2;
        temp = -Mh*(0.5+a) + Ma - La*(0.5+a) + Lh*(0.5+a)^2;

        quad = mu^2*x*rthetabar^2;

        linear = -mu^2*rthetabar^2 - mu^2*rthetabar^2*x - mu*x*temp -
...
            mu*rthetabar^2*Lh;

        con = mu^2*rthetabar^2 + mu*temp + mu*Lh*rthetabar^2 + Lh*temp
-(mu^2*xthetabar^2 + ...
            mu*xthetabar*Mh - 0.5*mu*xthetabar*Lh - a*mu*xthetabar*Lh +
mu*xthetabar*La + ...
            La*Mh - 0.5*Lh*La - a*Lh*La - 0.5*mu*xthetabar*Lh -
0.5*Lh*Mh + 0.25*Lh^2 + ...
            0.5*a*Lh^2 - mu*a*xthetabar*Lh - a*Lh*Mh + 0.5*a*Lh^2 +
a^2*Lh^2);

        eqn = [quad linear con];
        w = roots(eqn);
        w1=wtheta/sqrt(w(1,1));
        w2=wtheta/sqrt(w(2,1));

        w_real=zeros(2,1);
        w_real(1,1)=real(w1);
        w_real(2,1)=real(w2);
        if real(w1)<real(w2)
            wi=imag(w1);
        else
            wi=imag(w2);
        end
        w=min(w_real);

        wf=sqrt(wtheta/w);
        vf=wf*b/k;
        g=wi/(wtheta^2/w^2);

        if abs(g)-tol <= 0
            vfinal=vf;
            break
        end
    end  % Solution Routine 1

    vf_hist1(1,ii)=vf;
    n=0;

    %%   Begin Solution Loop 2
    for invk=invk_min:size_div:invk_max;
        n=n+1;
```

```
        k=1/invk;

        Ck=(0.01365+0.2808*1i*k-0.5*k^2)/(0.01365+0.3455*1i*k-k^2);

        Lh=1-(1i*2*Ck)/k;
        La=1/2-(1i*(1+2*Ck))/k-(2*Ck)/(k^2);

        Mh=1/2;
        Ma=3/8-1i/k;

        x = wh^2/wtheta^2;
        temp = -Mh*(0.5+a) + Ma - La*(0.5+a) + Lh*(0.5+a)^2;

        quad = mu^2*x*rthetabar^2;

        linear = -mu^2*rthetabar^2 - mu^2*rthetabar^2*x - mu*x*temp -
...
            mu*rthetabar^2*Lh;

        con = mu^2*rthetabar^2 + mu*temp + mu*Lh*rthetabar^2 + Lh*temp
-(mu^2*xthetabar^2 + ...
            mu*xthetabar*Mh - 0.5*mu*xthetabar*Lh - a*mu*xthetabar*Lh +
mu*xthetabar*La + ...
            La*Mh - 0.5*Lh*La - a*Lh*La - 0.5*mu*xthetabar*Lh -
0.5*Lh*Mh + 0.25*Lh^2 + ...
            0.5*a*Lh^2 - mu*a*xthetabar*Lh - a*Lh*Mh + 0.5*a*Lh^2 +
a^2*Lh^2);

        eqn = [quad linear con];
        w = roots(eqn);
        w1=wtheta/sqrt(w(1,1));
        w2=wtheta/sqrt(w(2,1));

        w_real=zeros(2,1);
        w_real(1,1)=real(w1);
        w_real(2,1)=real(w2);
        if real(w1)<real(w2)
            wi=imag(w1);
        else
            wi=imag(w2);
        end
        w=min(w_real);

        wf=sqrt(wtheta/w);
        vf=wf*b/k;
        g=wi/(wtheta^2/w^2);

        if abs(g)-tol <= 0
            vfinal=vf;
            break
        end
    end  % Solution Routine 2

    vf_hist2(1,ii)=vf;
```

```
    n=0;

    %%   Begin Solution Loop 3
    for invk=invk_min:size_div:invk_max;
        n=n+1;

        k=1/invk;

        Ck=(besselj(1,k)-1i*bessely(0,k))/(besselj(1,k)+besselj(0,k)-
1i*(bessely(0,k)+bessely(1,k)));

        Lh=1-(1i*2*Ck)/k;
        La=1/2-(1i*(1+2*Ck))/k-(2*Ck)/(k^2);

        Mh=1/2;
        Ma=3/8-1i/k;

        x = wh^2/wtheta^2;
        temp = -Mh*(0.5+a) + Ma - La*(0.5+a) + Lh*(0.5+a)^2;

        quad = mu^2*x*rthetabar^2;

        linear = -mu^2*rthetabar^2 - mu^2*rthetabar^2*x - mu*x*temp -
...
            mu*rthetabar^2*Lh;

        con = mu^2*rthetabar^2 + mu*temp + mu*Lh*rthetabar^2 + Lh*temp
-(mu^2*xthetabar^2 + ...
            mu*xthetabar*Mh - 0.5*mu*xthetabar*Lh - a*mu*xthetabar*Lh +
mu*xthetabar*La + ...
            La*Mh - 0.5*Lh*La - a*Lh*La - 0.5*mu*xthetabar*Lh -
0.5*Lh*Mh + 0.25*Lh^2 + ...
            0.5*a*Lh^2 - mu*a*xthetabar*Lh - a*Lh*Mh + 0.5*a*Lh^2 +
a^2*Lh^2);

        eqn = [quad linear con];
        w = roots(eqn);
        w1=wtheta/sqrt(w(1,1));
        w2=wtheta/sqrt(w(2,1));

        w_real=zeros(2,1);
        w_real(1,1)=real(w1);
        w_real(2,1)=real(w2);
        if real(w1)<real(w2)
            wi=imag(w1);
        else
            wi=imag(w2);
        end
        w=min(w_real);

        wf=sqrt(wtheta/w);
        vf=wf*b/k;
        g=wi/(wtheta^2/w^2);
```

```
        if abs(g)-tol <= 0
            vfinal=vf;
            break
        end
    end  % Solution Routine 3

    vf_hist3(1,ii)=vf;
    n=0;

    %%   Begin Solution Loop 4
    for invk=invk_min:size_div:invk_max;
        n=n+1;

        k=1/invk;


Ck=(1+10.61*1i*k)*(1+1.774*1i*k)/((1+13.51*1i*k)*(1+2.745*1i*k));

        Lh=1-(1i*2*Ck)/k;
        La=1/2-(1i*(1+2*Ck))/k-(2*Ck)/(k^2);

        Mh=1/2;
        Ma=3/8-1i/k;

        x = wh^2/wtheta^2;
        temp = -Mh*(0.5+a) + Ma - La*(0.5+a) + Lh*(0.5+a)^2;

        quad = mu^2*x*rthetabar^2;

        linear = -mu^2*rthetabar^2 - mu^2*rthetabar^2*x - mu*x*temp -
...
            mu*rthetabar^2*Lh;

        con = mu^2*rthetabar^2 + mu*temp + mu*Lh*rthetabar^2 + Lh*temp
-(mu^2*xthetabar^2 + ...
            mu*xthetabar*Mh - 0.5*mu*xthetabar*Lh - a*mu*xthetabar*Lh +
mu*xthetabar*La + ...
            La*Mh - 0.5*Lh*La - a*Lh*La - 0.5*mu*xthetabar*Lh -
0.5*Lh*Mh + 0.25*Lh^2 + ...
            0.5*a*Lh^2 - mu*a*xthetabar*Lh - a*Lh*Mh + 0.5*a*Lh^2 +
a^2*Lh^2);

        eqn = [quad linear con];
        w = roots(eqn);
        w1=wtheta/sqrt(w(1,1));
        w2=wtheta/sqrt(w(2,1));

        w_real=zeros(2,1);
        w_real(1,1)=real(w1);
        w_real(2,1)=real(w2);
        if real(w1)<real(w2)
            wi=imag(w1);
        else
            wi=imag(w2);
```

```
        end
        w=min(w_real);

        wf=sqrt(wtheta/w);
        vf=wf*b/k;
        g=wi/(wtheta^2/w^2);

        if abs(g)-tol <= 0
            vfinal=vf;
            break
        end
    end  % Solution Routine 4

    vf_hist4(1,ii)=vf;
    n=0;

    %%   Begin Solution Loop 5
    for invk=invk_min:size_div:invk_max;
        n=n+1;

        k=1/invk;

        Hankel_1=besselj(1,k)-1i*bessely(1,k);
        Hankel_0=besselj(0,k)-1i*bessely(0,k);
        Ck=Hankel_1/(Hankel_1+1i*Hankel_0);

        Lh=1-(1i*2*Ck)/k;
        La=1/2-(1i*(1+2*Ck))/k-(2*Ck)/(k^2);

        Mh=1/2;
        Ma=3/8-1i/k;

        x = wh^2/wtheta^2;
        temp = -Mh*(0.5+a) + Ma - La*(0.5+a) + Lh*(0.5+a)^2;

        quad = mu^2*x*rthetabar^2;

        linear = -mu^2*rthetabar^2 - mu^2*rthetabar^2*x - mu*x*temp -
...
            mu*rthetabar^2*Lh;

        con = mu^2*rthetabar^2 + mu*temp + mu*Lh*rthetabar^2 + Lh*temp
-(mu^2*xthetabar^2 + ...
            mu*xthetabar*Mh - 0.5*mu*xthetabar*Lh - a*mu*xthetabar*Lh +
mu*xthetabar*La + ...
            La*Mh - 0.5*Lh*La - a*Lh*La - 0.5*mu*xthetabar*Lh -
0.5*Lh*Mh + 0.25*Lh^2 + ...
            0.5*a*Lh^2 - mu*a*xthetabar*Lh - a*Lh*Mh + 0.5*a*Lh^2 +
a^2*Lh^2);

        eqn = [quad linear con];
        w = roots(eqn);
        w1=wtheta/sqrt(w(1,1));
        w2=wtheta/sqrt(w(2,1));
```

```
        w_real=zeros(2,1);
        w_real(1,1)=real(w1);
        w_real(2,1)=real(w2);
        if real(w1)<real(w2)
            wi=imag(w1);
        else
            wi=imag(w2);
        end
        w=min(w_real);

        wf=sqrt(wtheta/w);
        vf=wf*b/k;
        g=wi/(wtheta^2/w^2);

        if abs(g)-tol <= 0
            vfinal=vf;
            break
        end
    end  % Solution Routine 5

    vf_hist5(1,ii)=vf;
    n=0;

    %%   Begin Solution Loop 6
    for invk=invk_min:size_div:invk_max;
        n=n+1;

        k=1/invk;

        Ck=(0.015+0.3*1i*k-0.5*k^2)/(0.015+0.35*1i*k-k^2);

        Lh=1-(1i*2*Ck)/k;
        La=1/2-(1i*(1+2*Ck))/k-(2*Ck)/(k^2);

        Mh=1/2;
        Ma=3/8-1i/k;

        x = wh^2/wtheta^2;
        temp = -Mh*(0.5+a) + Ma - La*(0.5+a) + Lh*(0.5+a)^2;

        quad = mu^2*x*rthetabar^2;

        linear = -mu^2*rthetabar^2 - mu^2*rthetabar^2*x - mu*x*temp -
...
            mu*rthetabar^2*Lh;

        con = mu^2*rthetabar^2 + mu*temp + mu*Lh*rthetabar^2 + Lh*temp
-(mu^2*xthetabar^2 + ...
            mu*xthetabar*Mh - 0.5*mu*xthetabar*Lh - a*mu*xthetabar*Lh +
mu*xthetabar*La + ...
            La*Mh - 0.5*Lh*La - a*Lh*La - 0.5*mu*xthetabar*Lh -
0.5*Lh*Mh + 0.25*Lh^2 + ...
```

```
            0.5*a*Lh^2  -  mu*a*xthetabar*Lh  -  a*Lh*Mh  +  0.5*a*Lh^2  +
a^2*Lh^2);

        eqn = [quad linear con];
        w = roots(eqn);
        w1=wtheta/sqrt(w(1,1));
        w2=wtheta/sqrt(w(2,1));

        w_real=zeros(2,1);
        w_real(1,1)=real(w1);
        w_real(2,1)=real(w2);
        if real(w1)<real(w2)
            wi=imag(w1);
        else
            wi=imag(w2);
        end
        w=min(w_real);

        wf=sqrt(wtheta/w);
        vf=wf*b/k;
        g=wi/(wtheta^2/w^2);

        if abs(g)-tol <= 0
            vfinal=vf;
            break
        end
    end    % Solution Routine 6

    vf_hist6(1,ii)=vf;

end  % Uncertainty Routine


%%   Post-Processing of Data:

vf1_mean_tot=0;
vf1_std_tot=0;

vf2_mean_tot=0;
vf2_std_tot=0;

vf3_mean_tot=0;
vf3_std_tot=0;

vf4_mean_tot=0;
vf4_std_tot=0;

vf5_mean_tot=0;
vf5_std_tot=0;

vf6_mean_tot=0;
vf6_std_tot=0;

for jj=1:num_it
```

```
    vf1_mean_tot=vf1_mean_tot+vf_hist1(1,jj);
    vf2_mean_tot=vf2_mean_tot+vf_hist2(1,jj);
    vf3_mean_tot=vf3_mean_tot+vf_hist3(1,jj);
    vf4_mean_tot=vf4_mean_tot+vf_hist4(1,jj);
    vf5_mean_tot=vf5_mean_tot+vf_hist5(1,jj);
    vf6_mean_tot=vf6_mean_tot+vf_hist6(1,jj);
end

vf1_mean=vf1_mean_tot/num_it
vf2_mean=vf2_mean_tot/num_it
vf3_mean=vf3_mean_tot/num_it
vf4_mean=vf4_mean_tot/num_it
vf5_mean=vf5_mean_tot/num_it
vf6_mean=vf6_mean_tot/num_it

for kk=1:num_it
    vf1_std_tot=vf1_std_tot+(vf_hist1(1,kk)-vf1_mean)^2;
    vf2_std_tot=vf2_std_tot+(vf_hist2(1,kk)-vf2_mean)^2;
    vf3_std_tot=vf3_std_tot+(vf_hist3(1,kk)-vf3_mean)^2;
    vf4_std_tot=vf4_std_tot+(vf_hist4(1,kk)-vf4_mean)^2;
    vf5_std_tot=vf5_std_tot+(vf_hist5(1,kk)-vf5_mean)^2;
    vf6_std_tot=vf6_std_tot+(vf_hist6(1,kk)-vf6_mean)^2;
end

vf1_std=sqrt(vf1_std_tot/num_it)
vf2_std=sqrt(vf2_std_tot/num_it)
vf3_std=sqrt(vf3_std_tot/num_it)
vf4_std=sqrt(vf4_std_tot/num_it)
vf5_std=sqrt(vf5_std_tot/num_it)
vf6_std=sqrt(vf6_std_tot/num_it)
```